Report Title:

FABRICATION OF Pd/Pd-ALLOY FILMS BY SURFACTANT INDUCED ELECTROLESS PLATING FOR HYDROGEN SEPARATION FROM ADVANCED COAL GASIFICATION PROCESSES

Report Type: Final Technical Report

Reporting Period Start Date: 03/10/2008 End Date: 07/31/2012

Principal Author(s): Shamsuddin Ilias (PI)
Dhananjay Kumar (Co-PI)

Report Issue Date: February 15, 2013 DOE Award No.: DE-NT0001473

Report Number: DOE/NT/0001473

Name and Address of Submitting Organization:

North Carolina A&T State University
Department of Chemical, Biological and Bioengineering
Greensboro, NC 27411
E-mail: ilias@ncat.edu
Tel: (336) 285-3656 Fax: (336) 334-7417

DISCLAIMER

ABSTRACT

Dense Pd, Pd-Cu and Pd-Ag composite membranes on microporous stainless steel substrate (MPSS) were fabricated by a novel electroless plating (EP) process. In the conventional Pd-EP process, the oxidation-reduction reactions between Pd-complex and hydrazine result in an evolution of NH_3 and N_2 gas bubbles. When adhered to the substrate surface and in the pores, these gas bubbles hinder uniform Pd-film deposition which results in dendrite growth leading to poor film formation. This problem was addressed by introducing cationic surfactant in the electroless plating process known as surfactant induced electroless plating (SIEP). The unique features of this innovation provide control of Pd-deposition rate, and Pd-grain size distribution. The surfactant molecules play an important role in the EP process by tailoring grain size and the process of agglomeration by removing tiny gas bubbles through adsorption at the gas-liquid interface. As a result surfactant can tailor a nanocrystalline Pd, Cu and Ag deposition in the film resulting in reduced membrane film thickness. Also, it produces a uniform, agglomerated film structure. The Pd-Cu and Pd-Ag membranes on MPSS support were fabricated by sequential deposition using SIEP method. The pre- and post-annealing characterizations of these membranes (Pd, Pd-Cu and Pd-Ag on MPSS substrate) were carried out by SEM, EDX, XRD, and AFM studies. The SEM images show significant improvement of the membrane surface morphology, in terms of metal grain structures and grain agglomeration compared to the membranes fabricated by conventional EP process. The SEM images and helium gas-tightness studies indicate that dense and thinner films of Pd, Pd-Cu and Pd-Ag membranes can be produced with shorter deposition time using surfactant. H_2 Flux through the membranes fabricated by SIEP shows large improvement compared to those by CEP with comparable perm-selectivity.

Pd-MPSS composite membrane was subjected to test for long term performance and thermal cycling (573 - 723 - 573 K) at 15 psi pressure drop for 1200 hours. Pd membranes showed excellent hydrogen permeability and thermal stability during the operational period. Under thermal cycling (573 K - 873 K - 573 K), Pd-Cu-MPSS membrane was stable and retained hydrogen permeation characteristics for over three months of operation. From this limited study, we conclude that SIEP is viable method for fabrication of defect-free, robust Pd-alloy membranes for high-temperature H_2-separation applications.

TABLE OF CONTENTS

Title Page i

Disclaimer ii

Abstract iii

Table of Contents iv

List of Figure v

List of Tables viii

Introduction 1

Research Objectives 3

Materials and Methods 3

Results and Discussions 6

- Pd Membranes by CEP and SIEP 6
  - Microstructure analysis of Pd membranes 6
  - Permeability studies of Pd membranes 16
  - Long-term performance of Pd membranes 19
  - Post-process characterization of Pd membranes 21
- Pd-Cu Membranes by CEP and SIEP 23
  - Helium gas-tightness and film thickness analysis of Pd-Cu membranes 23
  - Microstructure analysis of Pd-Cu membranes 24
  - H_2-permselectivity studies of Pd-Cu membranes 38
- Pd-Ag Membranes by CEP and SIEP 43
  - Helium gas-tightness and film thickness analysis of Pd-Ag membranes 43
  - Microstructure analysis of Pd-Ag membranes 46
  - H_2-permselectivity studies of Pd-Ag membranes 61

Conclusions 66

Acknowledgments 67

References 67

LIST OF FIGURES

Figure 1. SEPM images of Pd membranes fabricated by CEP (top two images) and SIEP methods (bottom four images) at various magnifications.....8

Figure 2. Grain size distribution of Pd membrane fabricated by CEP (no DTAB) and SIEP (4×CMC DTAB). 10

Figure 3. SEM images of top surface of Pd membrane fabricated by SIEP method at pre- and post-HT (heat treatment) conditions. 11

Figure 4. AFM images of solid Pd surface aggregation onto typical MPSS substrate. 12

Figure 5. Typical EDS spectra of Pd membrane by SIEP shows the presence of polycrystalline Pd deposition. 13

Figure 6. XRD patterns of Pd membrane fabricated by SIEP method at pre-and post-heat treatment conditions. 14

Figure 7. EDS line scanning of Pd-film cross-section (scanning length 35 μm).....17

Figure 8. Hydrogen flux and H_2/N_2 selectivity data of Pd-membrane fabricated by SIEP and CEP methods.....18

Figure 9. H_2- and N_2-flux data of Pd1 and Pd2 membranes fabricated by SIEP method under thermal cycling at 15 psi trans-membrane pressure. 20

Figure 10. SEM images of Pd1 and Pd2 SIEP membranes after thermal cycling. 22

Figure 11. Helium gas-tightness of Pd-Cu membranes as a function film thickness fabricated by CEP and SIEP methods. 25

Figure 12. SEM images of Pd-Cu membrane film top surface fabricated by SIEP method.....26

Figure 13. Cu and Pd grain size distribution in Pd-Cu membrane fabricated by SIEP method with 4×CMC of DTAB surfactant. 27

Figure 14. SEM images of top surface of Pd-Cu membranes fabricated by CEP and SIEP methods at pre- and post-HT (heat treatment) conditions. 28

Figure 15. AFM images of solid Pd-Cu surface aggregation onto typical MPSS (SIEP and CEP). 31

Figure 16. Typical EDS spectrum of Pd-Cu membrane shows the presence of polycrystalline deposition of Pd and Cu particles. 33

Figure 17. Effect of heat treatment on XRD pattern of Pd-Cu membrane fabricated by SIEP method. 34

Figure 18. SEM images of Pd-Cu film cross-section: showing the locations of pores to study Pd and Cu metal distribution by EDS analysis starting from the pore mouth to deep inside (from Probe 1→Probe 4). 36

Figure 19. EDS line scanning of Pd-Cu film cross section (scanning length 25 μm, scanning direction from (a) → (b)). 37

Figure 20. Hydrogen flux and H_2/N_2 selectivity data of Pd-Cu membranes fabricated by SIEP and CEP methods (pre -HT). 39

Figure 21. Hydrogen flux and H_2/N_2 selectivity data of Pd-Cu membranes fabricated by SIEP and CEP methods (post -HT). 41

Figure 22. Arrhenius plots of H_2-permeability coefficients of Pd-Cu membranes fabricated by SIEP and CEP methods. 42

Figure 23. H_2 flux data of Pd-Cu MPSS membrane under thermal cycling fabricated by SIEP method. 45

Figure 24. Helium gas-tightness as a function of membrane thickness for Pd and Pd-Ag membranes fabricated using surfactant DTAB at concentration of 4×CMC. 48

Figure 25. SEM images of Pd-Ag film top surface showing agglomerated grain growth throughout the surface just beneath the apparent rough top surface. 49

Figure 26. Pd and Ag grain size distribution observed in Pd-Ag membrane fabricated by SIEP process with 4CMC DTAB. 51

Figure 27. SEM images of top surface of Pd-Ag membranes fabricated by SIEP method a pre- and post-HT (heat treatment) conditions at different resolution showing grain agglomeration. 52

Figure 28. AFM images of solid Pd-Ag surface aggregation onto typical MPSS surface with DTAB. 54

Figure 29. Typical EDS spectrum for Pd-Ag membrane shows the polycrystalline deposition of Pd and Ag particles. 55

Figure 30. Effect of heat treatment on XRD pattern of Pd-Ag membrane fabricated by SIEP process. 57

Figure 31. SEM images of Pg-Ag film from Pd-Ag membrane cross-section:

(a) showing the locations of EDS for metal deposition behavior analysis;
(b) Metal (Pd and Ag) distribution during deposition in the pores starting from
the pore mouth to the very deep inside (From Probe 1 →Probe 6). 59

Figure 32. EDS line scanning of Pd-Ag-film cross section [Scanning length
40 μm, scanning direction from (a) → (b)]. 60

Figure 33. Hydrogen flux data of Pd and Pd-Ag-MPSS membranes fabricated
by SIEP at different temperatures. 62

Figure 34. Hydrogen to nitrogen selectivity at different temperatures in Pd-Ag-MPSS
membrane fabricated by SIEP. 64

Figure 35. Arrhenius plot of H_2-permeability coefficients of (a) Pd-MPSS membrane
and (b) Pd-Ag-MPSS membrane. 65

LIST OF TABLES

Table 1. Chemical composition of cleaning solution 5

Table 2. Chemical composition of sensitization and activation solutions 5

Table 3. Chemical compositions and operating parameters of Pd-, Cu-, and Ag-baths 5

Table 4. Summary of Pd membranes characteristics fabricated by SIEP method 7

Table 5. Comparison of high angle XRD reflection peaks of Pd-film fabricated by SIEP method 15

Table 6. Permeation characteristics of Pd and Pd-Cu membranes fabricated by SIEP and CEP methods.....29

Table 7. Comparison of high angle XRD reflection peaks of Pd and Pd-Cu film fabricated by SIEP method 35

Table 8. Comparison of values of activation energy of different membranes fabricated by SIEP and CEP methods 44

Table 9. Summary of Pd and Pd-Ag membrane attributes fabricated by SIEP and CEP 47

Table 10. Comparison of high angle XRD reflection peaks of Pd- and Pd-Ag-film fabricated by SIEP process 58

INTRODUCTION

Dense metallic membranes, such as Pd and Pd-alloy membranes can selectively transport hydrogen (H_2). These metallic membranes consist of a dense perm-selective film and a support. The selective transport of H_2 is achieved via solution-diffusion of H_2 through the dense film. Hydrogen selectivity for these membranes is found to be from few hundreds to 70,000 [1]. The permeability of hydrogen varies on the thickness of the film and microstructure of the grain [2, 3]. The diffusivity of hydrogen in nanocrystalline Pd is higher than that of single crystal at low hydrogen concentrations [2]. Nanocrystalline palladium has almost 10 times higher diffusivity than conventional polycrystalline Pd [3]. In small nanocrystalline metal, at least 20 to 50 % of its atom located in the grain boundaries act as a network for faster diffusion.

H_2 permeability for a particular Pd-composite film is constant, which is a function of pressure and temperature. Consequently, high permeability will only result if the thickness of the film can be reduced at a constant temperature and trans-membrane pressure. But Pd and Pd-alloy membranes cannot be reduced in thickness beyond a certain degree because of the comparatively low mechanical strength of Pd [4]. As a result, H_2 flux through dense Pd membranes is small compared with those glass membranes. Hence, for high throughput of H_2, a very thin, nanocrystalline film microstructure is desirable. Additionally, these membranes require structural integrity and thermal stability for practical applications.

For H_2-separations at high temperatures, Pd-based membranes have been the focus of many studies [5-8]. However, hydrogen embrittlement of the Pd-layer is a problem with pure Pd membranes. It cannot be used for H_2-separation below 573 K due to the lattice expansion caused by dissolved hydrogen [1, 9-11]. Cracking of the Pd membrane under thermal stress due to the α to β Pd hydride phase transition, as well as poisoning and fouling due to the presence of sulfur or unsaturated carbon compounds in the operating gas stream, severely limits its use [1, 10, 11]. To alleviate these shortcomings, Pd-based membranes have been made from alloying with metals, such as silver, gold, nickel and copper [1, 10, 12]. By alloying Pd with selected metals, significant H_2-permeability enhancement can be achieved. For example, the $Pd_{77}Ag_{23}$ and $Pd_{60}Cu_{40}$ (wt. % composition) alloys show 73.4% and 6.3% increase in permeability respectively, over the pure Pd system [10, 12-19]. Alloy materials, such as copper or gold, are more resistant to sulfur compounds [10-12]. Specially, the Pd-Cu alloy film has enhanced thermal resistance without suffering any discernible physical changes [1, 9, 20, 21]. The H_2-

permeability of the Pd-Cu membrane passes through a maximum around 40 wt. % of Cu, while Pd-Ag membrane has maximum permeability at 23 wt% of Ag [9-12, 18]. In addition, $Pd_{60}Cu_{40}$ and $Pd_{77}Ag_{23}$ can withstand repeated temperature cycling with less distortion than pure Pd membrane [9, 22, 23].

In pursuit of defect free, thin and stable membranes, various techniques have been investigated over the past decades by numerous research groups. Of all the methods, electroless plating (EP) method for thin film deposition is regarded as the most suitable. Most often, the escaping gas produces pinholes in the deposited film in electroless deposition. Also in EP process, the resulting Pd-film is formed by columnar grain growth [24] and there is little control on the grain size distribution for the deposited film. Solueimanova et al., 2001 [25] suggested that the increase of osmotic pressure results in the decrease in Pd-grain size during the EP process. Ayturk et al., 2007 [26] applied agitation through internal rotation in EP solution bath as an external driving force to reduce mass transfer resistance.

In recent years Pd-Cu and Pd-Ag membranes on microporous stainless steel (MPSS) and ceramic supports have been fabricated by EP using sequential depositions of Pd and other metals with some variations of the deposition process [9, 14, 18, 21, 23, 27-36]. The major objective in these studies has been to improved membrane film performance in terms of H_2-perm-selectivity and structural integrity under thermal cycling in long-term operations.

Chen et al., 2002 [37] used surfactant in electroless deposition of nickel to increase reaction rate by preventing hydrogen bubble adsorption on the deposited surface. They actually observed a 20% increase in the deposition rate in presence of a suitable surfactant. This study established a quantitative and qualitative relationship between the effect of surfactants and the surface properties of the Ni-P plating layer, as well as corrosion resistance of the resulting Ni-P deposits.

The long-term performance of the Pd-composite membrane fabricated by the EP method is greatly affected by the crystallite distribution and microstructural characteristics of the film [38]. The oxidation-reduction reactions between the Pd-complex and hydrazine in the EP result in metallic deposition of Pd° on a solid surface by releasing NH_3 and N_2 gas bubbles. The gas bubbles adhering to the substrate surface and in the pores hinder uniform Pd-film deposition. To address this problem, we investigated the role of surfactant in a Pd EP bath and demonstrated

that surfactant induced EP (SIEP) can effectively tailor and control the Pd deposition rate, grain size and grain agglomeration on a MPSS substrate [39, 40].

RESEARCH OBJECTIVES

In this DOE project, we proposed to extend our patented SIEP method in fabricating Pd-Cu and Pd-Ag membranes on MPSS support for use in separation of hydrogen at elevated temperature and pressure. The major objectives of this investigative research were to:

- Develop processing technology for the deposition of continuous, thin, integral, stable films of Pd/Pd-alloy on microporous stainless steel planar substrate by surfactant induced electroless plating with suitable surfactant(s).
- Characterize the microstructure of the Pd-composite membrane by Scanning Electron Microscope (SEM), Transmission Electron Microscope (TEM) and X-Ray Diffraction (XRD) techniques.
- Conduct H_2-perm-selectivity tests using pure and mixed gases at elevated temperature and pressure.

MATERIALS AND METHODS

EP is a method of metal plating by autocatalytic deposition of a continuous film on a catalytic interface by the reaction of the corresponding metal ions and a chemical reducing agent [41, 42]. In this work, we used the Pd-, Ag- and Cu-EP baths as follows:

Pd-EP bath reactions [43]:

$$\left.\begin{aligned} &\text{Anodic Reaction:} && N_2H_4 + 4OH^- \rightarrow N_2\uparrow + 4H_2O + 4e^- \\ &\text{Cathodic Reaction:} && 2Pd\left[NH_3\right]_4^{2+} + 4e^- \rightarrow 2Pd^o + 8NH_3\uparrow \\ &\text{Overall Reaction:} && 2Pd\left[NH_3\right]_4^{2+} + N_2H_4 + 4OH^- \rightarrow 2Pd^o + N_2\uparrow + 8NH_3\uparrow + 4H_2O \end{aligned}\right\} \quad 1(a\text{-}c)$$

Ag-EP bath reactions [44]:

$$\left.\begin{aligned} &\text{Anodic Reaction:} && N_2H_4 + 4OH^- \rightarrow N_2\uparrow + 4H_2O + 4e^- \\ &\text{Cathodic Reaction:} && 4Ag\left[NH_3\right]_4^{+} + 4e^- \rightarrow 4Ag^o + 8NH_3\uparrow \\ &\text{Overall Reaction:} && 4Ag\left[NH_3\right]_4^{+} + N_2H_4 + 4OH^- \rightarrow 4Ag^o + N_2\uparrow + 8NH_3\uparrow + 4H_2O \end{aligned}\right\} \quad 2(a\text{-}c)$$

Cu-EP bath reactions [45]:

$$\left.\begin{aligned}
&\text{Anodic Reaction:} && 2CH_2O + 4OH^- \rightarrow H_2\uparrow + 2HCOO^- + 2H_2O + 2e^- \\
&\text{Cathodic Reaction:} && Cu\left[NH_3\right]_6^{2+} + 2e^- \rightarrow Cu^o + 6NH_3\uparrow \\
&\text{Overall Reaction:} && Cu\left[NH_3\right]_6^{2+} + 2CH_2O + 4OH^- \rightarrow \\
& && \quad Cu^o + 2HCOO^- + H_2\uparrow + 6NH_3\uparrow + 2H_2O
\end{aligned}\right\} \quad 3(a\text{-}c)$$

The membrane support, MPSS substrates (316L SS discs, 1 inch diameter, 0.062 inch thickness with an average pore size of 0.2 μm) were obtained from Mott Metallurgical Corporation (Farmington, CT). Prior to the sensitization and activation processes, the substrate surface was thoroughly cleaned in three steps. The substrate was cleaned by dipping it into an alkaline cleaning solution (composition is given in Table 1) for 40 to 60 minutes at 333 K in an ultrasonic bath followed by a thorough cleaning with de-ionized water until the pH of the substrate surface reached to 7. Finally, the substrate was dipped into an isopropanol solution (Fisher Scientific) for 10 minutes, and dried for 2 hours at 393 K.

The sensitization and activation solutions were prepared using reagent grade $SnCl_2$ and $PdCl_2$. The substrate surface was sensitized and activated sequentially by dipping it into $SnCl_2$ and $PdCl_2$ solutions, respectively. The substrate was rinsed with de-ionized water between the sensitization and activation steps. The composition and conditions used in sensitization and activation are given in Table 2.

To fabricate Pd-Cu membrane on MPSS surface, Pd and Cu were deposited sequentially on the activated MPSS surface by the SIEP process using dodecyl trimethyl ammonium bromide (DTAB) surfactant. Similarly, Pd-Ag membrane was fabricated by sequential deposition of Pd and Ag on the activated MPSS substrate by the SIEP process using DTAB. In Table 3, composition and operating conditions of the Pd-, Cu- and Ag-EP baths used in this study are given. The DTAB concentration is expressed in critical micelle concentration (CMC). The 4×CMC concentration of the DTAB was used for all Pd- Ag- and Cu-baths in SIEP process [40, 46-48]. EP without surfactant is referred to here as conventional electroless plating (CEP).

The microstructure of the fabricated Pd, Pd-Cu, and Pd-Ag membranes was analyzed using scanning electron microscopy (SEM), energy dispersive spectroscopy (EDS), X-ray diffraction (XRD) and atomic force microscopy (AFM) techniques. The grain sizes were determined using point-to-point measurements from representative SEM images. The statistical distributions of deposited metal grains were estimated considering a minimum 500 number of

Table 1. Chemical composition of cleaning solution

Component	Supplier	Composition
$Na_3PO_4.12H_2O$ (ACS reagent grade, 99.4%)	Alfa Aesar	45 g/L
Na_2CO_3 (ACS reagent grade, ≥ 99.5%)	Alfa Aesar	65 g/L
NaOH (ACS reagent grade, 97%)	Alfa Aesar	45 g/L
Industrial detergent (Liqui-Nox^R)	Alconox	5 mL/L

Table 2. Chemical composition of sensitization and activation solutions

Component	Supplier	Sensitization Solution	Activation Solution
$SnCl_2.2H_2O$ (ACS Reagent grade, 98%)	Sigma-Aldrich	1 g/L	-
$PdCl_2$ (ACS reagent grade, 99.9%)	Alfa Aesar	-	0.1 g/L
HCl (ACS reagent grade, 37%)	Sigma-Aldrich	1 mL/L	1 mL/L
Operating conditions			
Temperature		293 K	293 K
Time		4-6 minutes	4-6 minutes
pH		4-5	4-5

Table 3. Chemical compositions and operating parameters of Pd-, Cu-, and Ag-baths

Name of Chemicals	Supplier	Pd-bath	Cu-bath	Ag-bath
Pd $(NH_3)_4Cl_2.H_2O$ (≥ 99.99%)	Sigma-Aldrich	4 gm/L	-	-
$CuSO_4.5H_2O$ (≥98.0%)	Alfa Aesar	-	1.22 gm/L	-
$AgNO_3$ (≥ 99.99%)	Alfa Aesar	-	-	0.519 gm/L
Na_2EDTA (≥ 99%)	Acros Organics	40.1 gm/L	10.05 gm/L	40.1 gm/L
NH_4OH (29.17%)	Fisher Scientific	198 mL/L		198 mL/L
NaOH (97%)	Alfa Aesar	-	10 gm/L	-
N_2H_4 (1.0 M)	Sigma-Aldrich	5.6 mM		5.6 mM
DTAB (~ 99%)	Sigma-Aldrich	4 CMC	4 CMC	4 CMC
Formaldehyde (37% in aq. soln)	Alfa Aesar	-	280μL	-
2, 2'- Bipyridine (> 99%)	Alfa Aesar	-	2.5g/L	-
Operating conditions				
Time		1 hr	20 min	1 hr
Temperature		333 K	333 K	333 K
pH		10-11	12-13	10-11

grains in a constant cross-section area. The membranes were cut into pieces to analyze the cross-section across the thickness of the Pd-Cu and Pd-Ag alloy films after the permeability studies. The cross-sections were studied in terms of metal diffusivity from Pd-Ag and Pd-Cu film to substrate, as well as from substrate to film using EDS mapping and line scanning at multiple location across each cross-section. All the Pd- and Pd-alloy membranes on MPSS substrate were tested in our permeability measurement set-up for helium gas-tightness and H_2-permselectivity [49]. The diffusion cell used in this permeability study is a custom-built cell.

RESULTS AND DISCUSSIONS

Pd Membranes by CEP and SIEP

Pd membranes were fabricated by SIEP and CEP methods. The fabrication technique, bath parameters and operating conditions, and substrates surface roughness have great influence on the microstructure of Pd membrane. In the SIEP method, DTAB was used along with the same bath parameters such as composition and operating conditions used in CEP method to demonstrate the role of surfactant in grain size, grain agglomeration, microstructure of Pd-film and long term thermal cycling of Pd membrane. The helium gas-tightness test was performed for the membranes at a trans-membrane pressure drop of 20 psi at 298 K. Helium was chosen since it is a smaller molecule (2.6 Å) compared to hydrogen (2.89 Å) for gas-tightness test. The helium gas-tightness tests show that about 11μm thick metal film is required to fabricate a SIEP Pd membrane. In the CEP method, the membrane requires about 16.5 μm Pd-film. Thus, thinner and pinhole free membrane can be prepared using SIEP method. The film thickness, Sieverts' law index, and H_2-flux and selectivity data of Pd membrane fabricated by both SIEP and CEP methods are summarized in Table 4. Gravimetric method and SEM analysis were used to calculate the Pd-film thickness.

Microstructure analysis Pd membranes

Pd-film microstructural analyses were carried out using SEM images at different resolutions for the Pd membranes fabricated by CEP and SIEP methods. The SEM images of the surface topology of Pd-film by SIEP at 10K, 15K, 20K and 50K magnifications are shown in Figure 1. For comparison, two SEM images at 5K and 15K magnifications of Pd-film by CEP is also presented in Figure 1 (top panel). It is evident from the images that the SIEP Pd-film structure is continuous and uniform and the film does not contain any pore. From the Figure 1, it

Table 4. Summary of Pd membranes characteristics fabricated by SIEP method

Membrane sample	DTAB (CMC)	Film thickness (μm)		Sieverts' law power index (*n*)	H_2-flux at 823K ($mol/m^2.s$)		Selectivity at 823 K (H_2-flux/N_2-flux)	
		Gravimetric analysis	SEM analysis		20 psig	100 psig	20 psig	100 psig
CEP	0	18.69	16.5	0.85	0.044	0.2202	84	35
SIEP	4	12.56	11	0.82	0.3542	1.7172	330	148

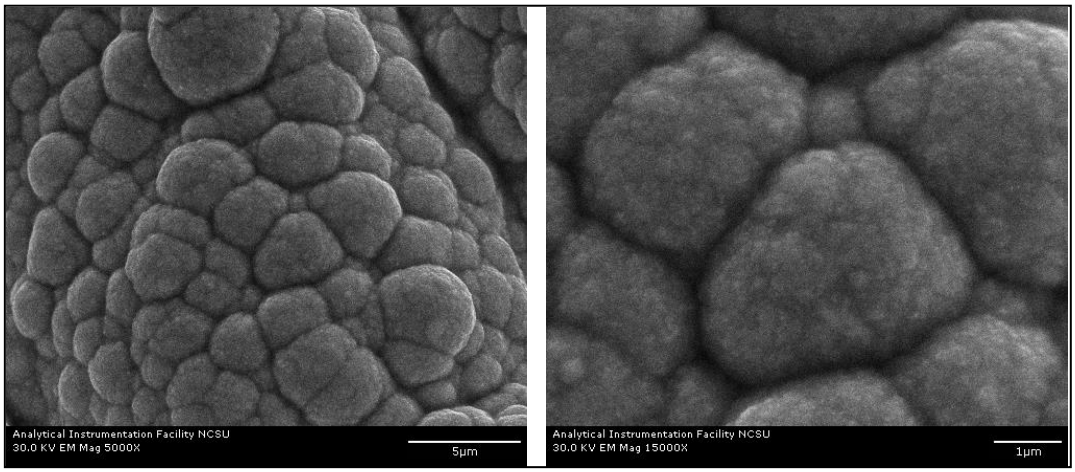

Pd at 5K (5 KV) Pd at 15K (5 KV)

CEP Pd membrane

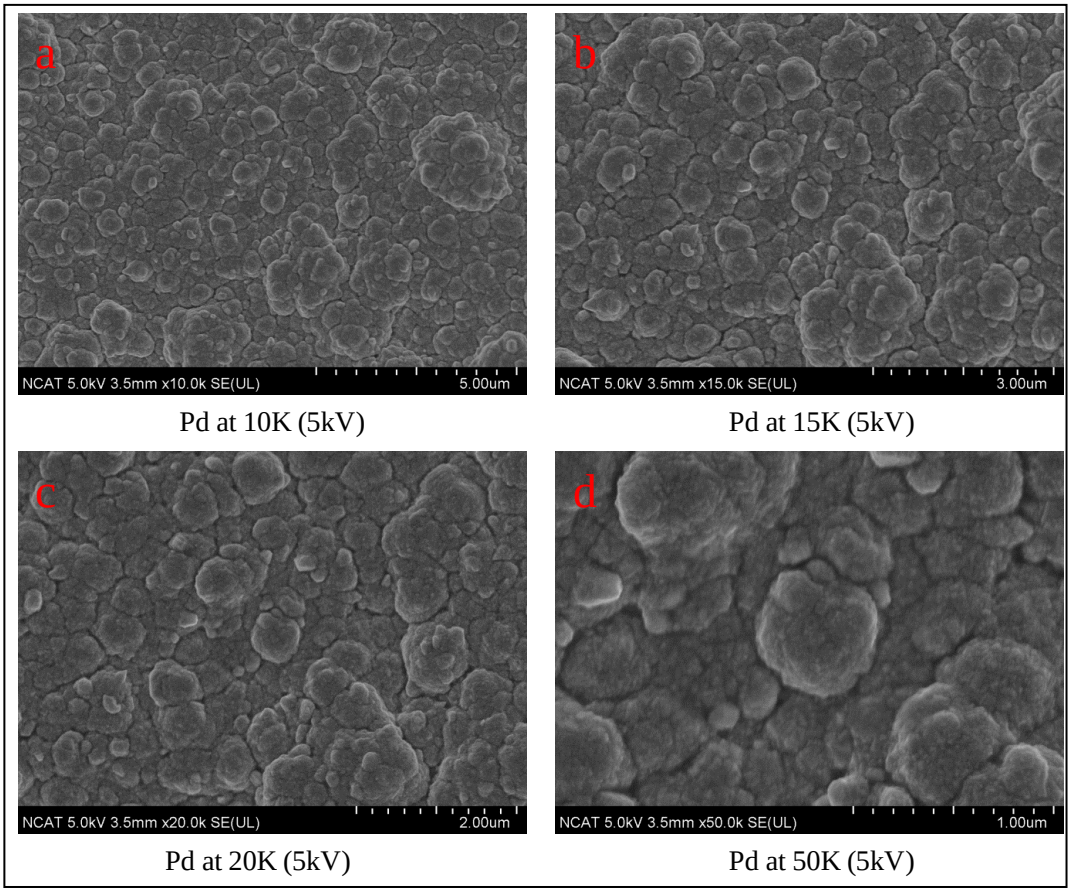

Pd at 10K (5kV) Pd at 15K (5kV)

Pd at 20K (5kV) Pd at 50K (5kV)

SIEP Pd membrane at 4×CMC DTAB

Figure 1. SEPM images of Pd membranes fabricated by CEP (top two images) and SIEP methods (bottom four images) at various magnifications.

is obvious that the Pd-film fabricated using DTAB has finer grains and the diffusion of grain boundaries results in a uniform, smooth, continuous and pinhole free surface. The particle size distribution of Pd membranes is shown in Figure 2. The average grain sizes of Pd-films by SIEP and CEP methods are 0.47 and 8 μm respectively. This result clearly suggests that the use of surfactant DTAB conclusively reduces the grain size considerably.

The Pd membrane fabricated by SIEP method was studied by SEM after annealing (heat treatment - HT). SEM images at 1K and 5K magnifications in Figure 3(a-b) and (c-d) show the Pd membrane surface morphology at pre-HT and post-HT conditions, respectively. Upon annealing, Pd grains cluster fuses intimately with small grain boundaries and a great extent of grain agglomeration is achieved after heat treatment. It is observed that smooth, continuous and uniform grain agglomeration was obtained as seen in Figure 3 (c-d). Some pinholes were formed during annealing. Repair deposition was needed to perform permeability test.

AFM analysis was used to study the surface topology of the Pd membrane fabricated by SIEP method. AFM images are presented in Figure 4. The Pd membrane shows cage-like structures and grains are diffused to one another with an average surface roughness of 16.59 nm. This smoother surface of Pd-film is attributed to the use of hydrophobic DTAB in the SIEP method. Surfactant DTAB helped to remove the evolved gas bubbles from the surface in EP bath reactions. Typical EDS pattern of the Pd-film fabricated by SIEP is presented in Figure 5. EDS showed intense Pd peaks. The EDS spectra did not show peak for any elements other than the palladium metal.

Typical XRD patterns for the Pd membranes fabricated by SIEP are shown in Figure 6 at pre-HT and post-HT conditions. XRD spectra show the reflection peaks of Pd in the face centered cubic (f.c.c) phase at [*111*], [*200*], [*220*], and [*311*] planes. Multiple peaks imply the deposition of polycrystalline structure throughout the surface. The 2θ & d-spacing values corresponding to the three major reflection peaks in [*111*], [*200*] and [*220*] planes are presented in Table 5. XRD spectra did not show any peak for MPSS elements such as Fe, Cr, Ni and Mn/Mo. By adding the surfactant, DTAB in the SIEP, no contamination was added to the Pd-film structure as confirmed by the EDS and XRD results. After 18 hours (h) of HT, the reflection peaks become sharper and more intense as shown in Figure 6. Pd crystals become well organized due to annealing.

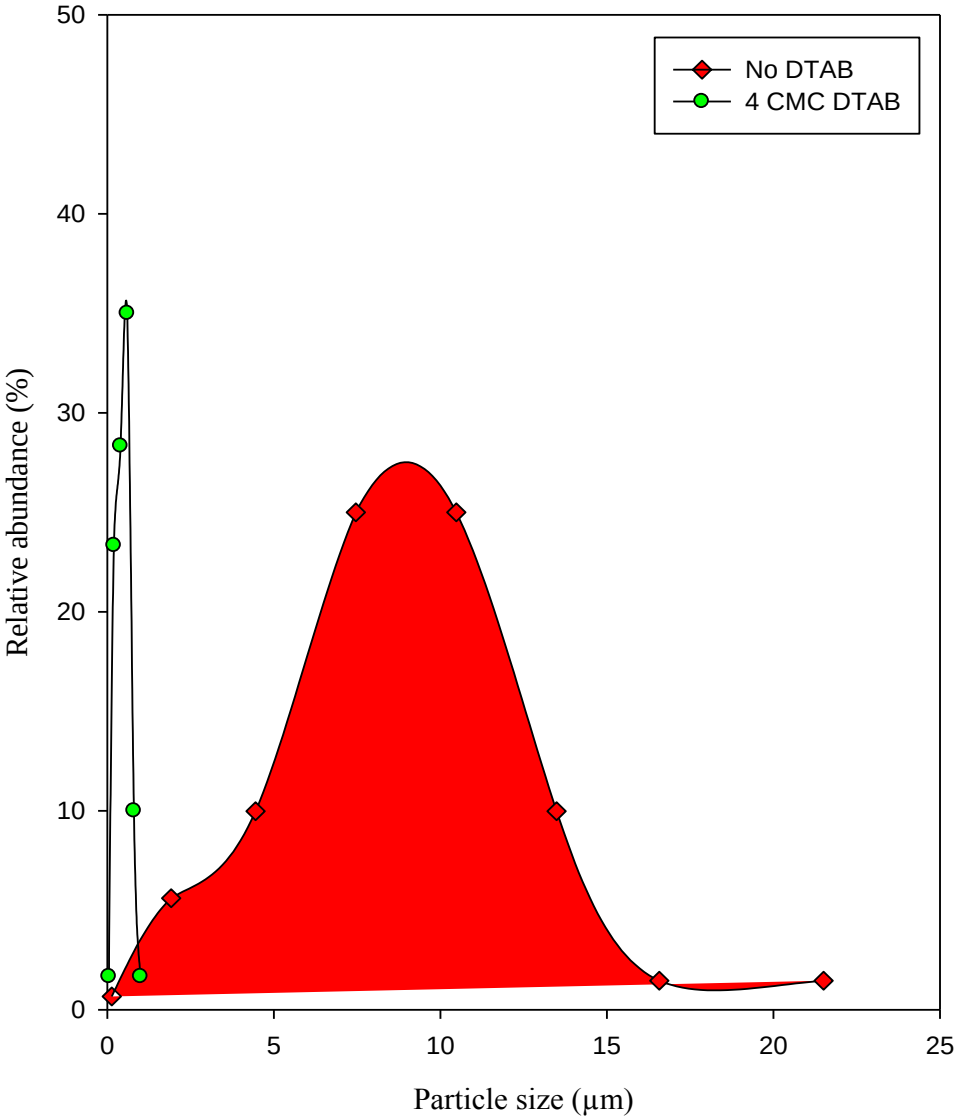

Figure 2. Grain size distribution of Pd membrane fabricated by CEP (no DTAB) and SIEP (4×CMC DTAB).

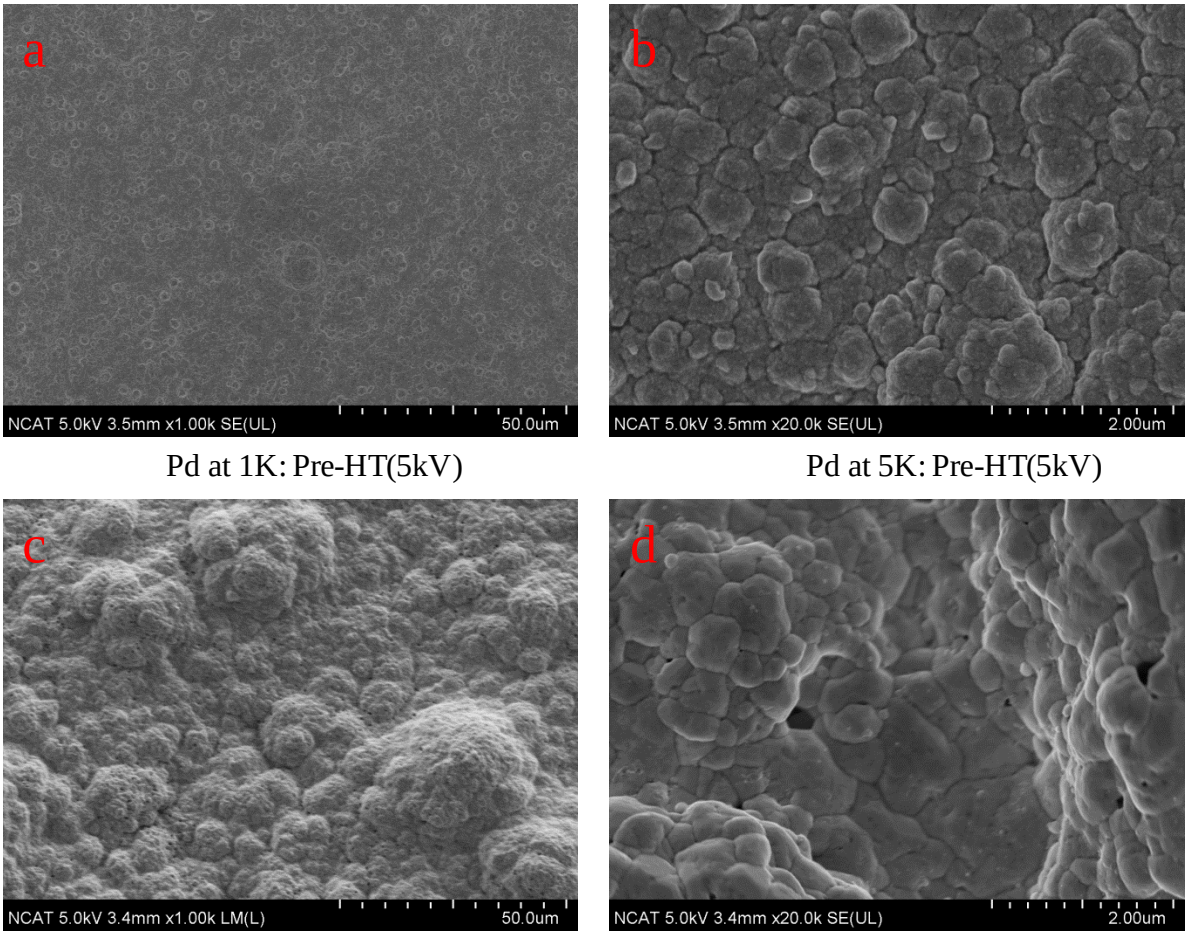

Figure 3. SEM images of top surface of Pd membrane fabricated by SIEP method at pre- and post-HT (heat treatment) conditions.

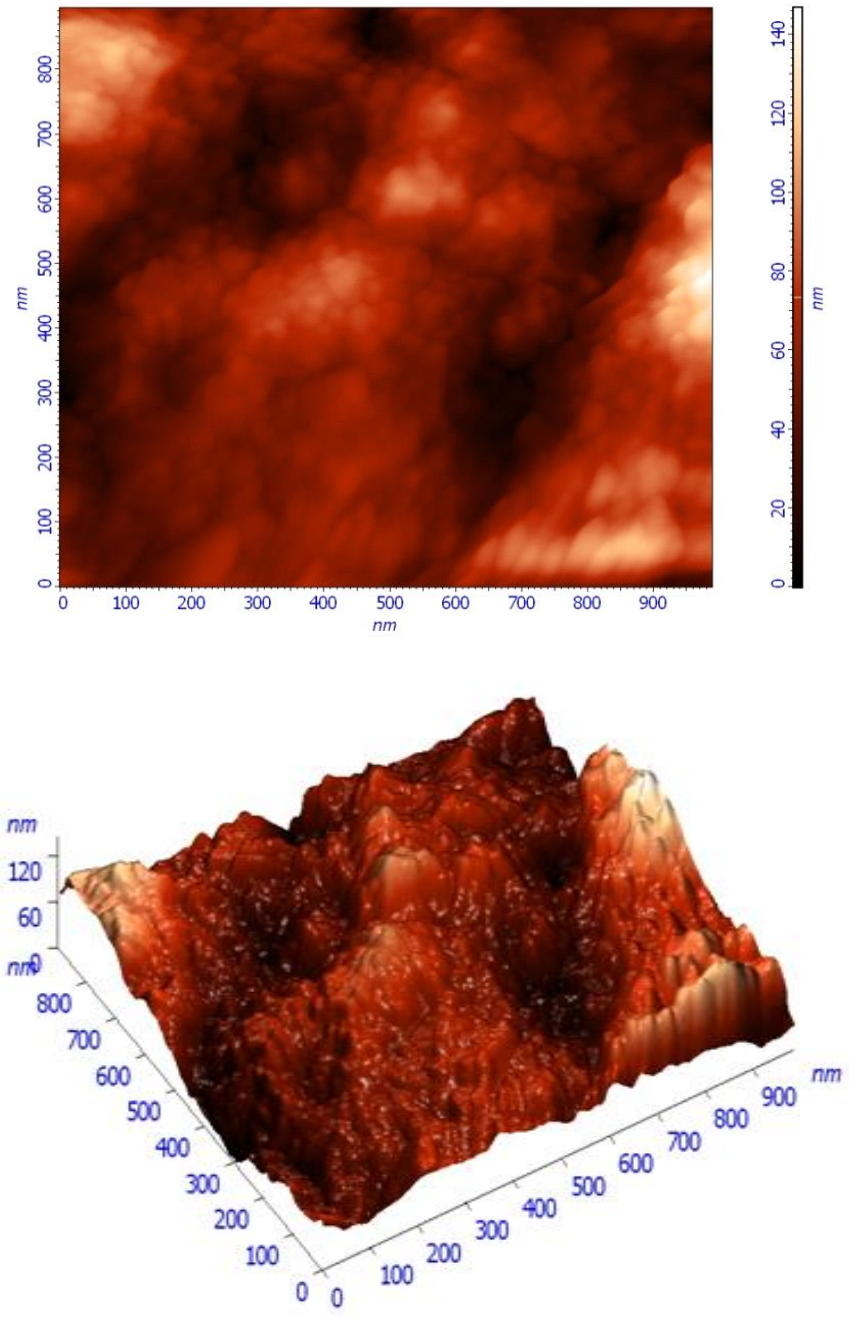

Figure 4. AFM images of solid Pd surface aggregation onto typical MPSS substrate.

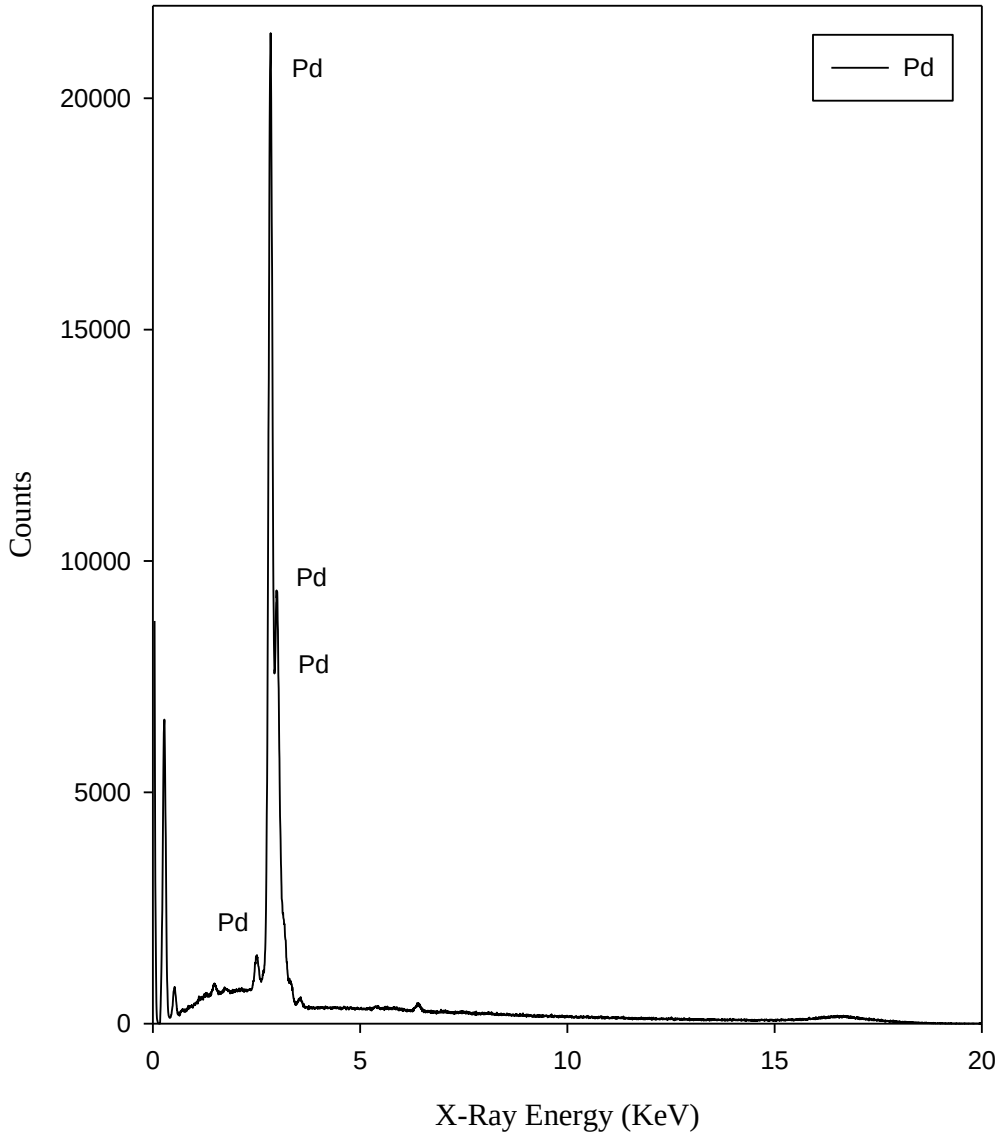

Figure 5. Typical EDS spectra of Pd membrane by SIEP shows the presence of polycrystalline Pd deposition.

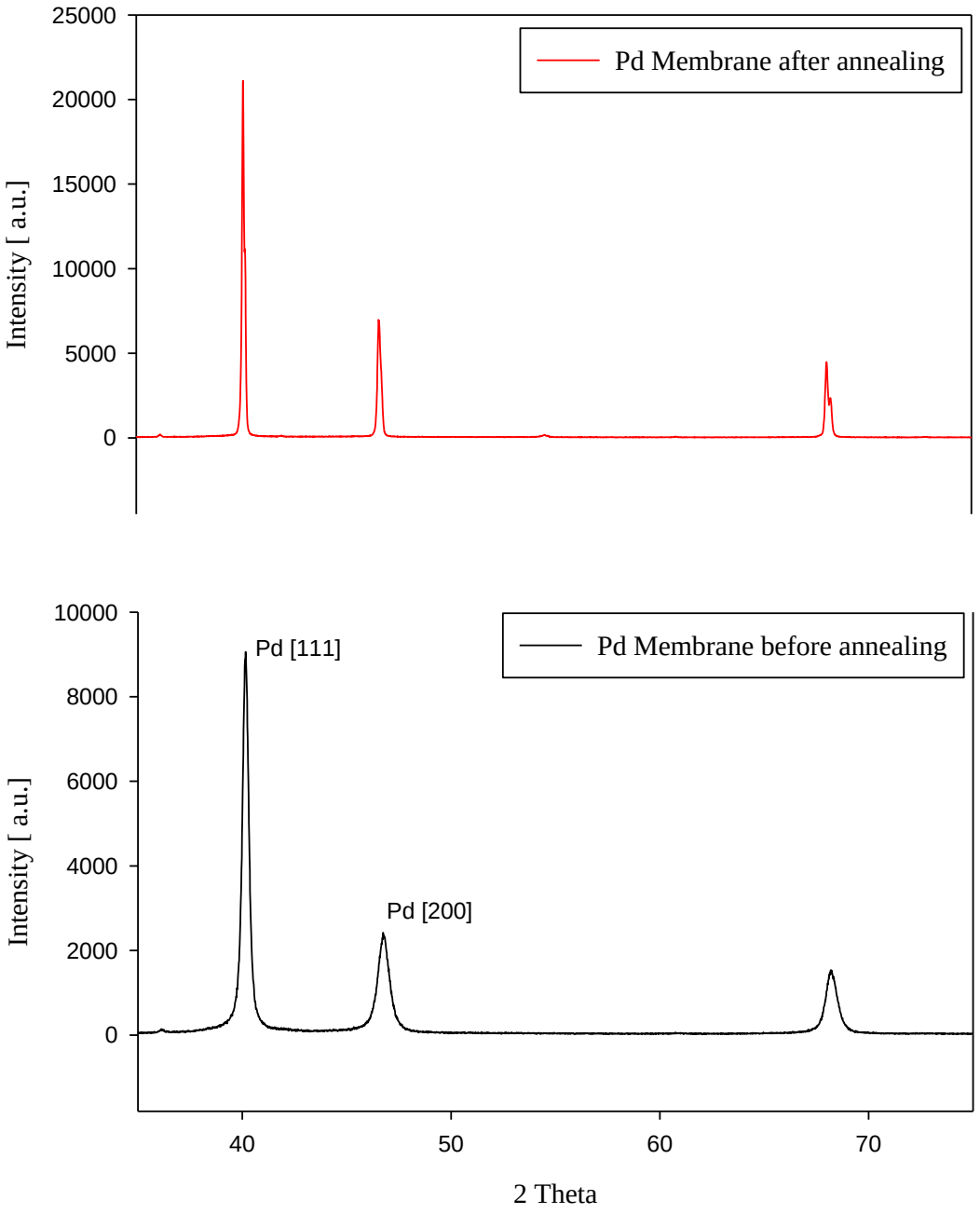

Figure 6. XRD patterns of Pd membrane fabricated by SIEP method at pre-and post-heat treatment conditions.

Table 5. Comparison of high angle XRD reflection peaks of Pd-film fabricated by SIEP method

	Bravais Lattice	Pd (pre-annealed)	Pd (post-annealed)
2-theta	111	40.159	40.26
	200	46.924	46.693
	220	68.231	68.121
	311	82.212	81.981
d-spacing	111	2.2444	2.23885
	200	1.935	1.94428
	220	1.37378	1.37589
	311	1.171945	1.17472
Lattice parameter, a		3.8826	3.8885
Lattice Structure		FCC	FCC

To understand the Pd deposition in the pores and on the substrate surface, the cross-section of the Pd membranes by SIEP was examined using EDS. In Figure 7, the line scanning carried out from the pore mouth to a distance of 35 μm deep inside the pore is shown. Fe and Cr diffused into the Pd-film and Pd diffused into the stainless steel substrate to some extent as shown in Figure 7.

Permeability studies of Pd membranes

The H_2-permselectivity test was carried out for the Pd membranes fabricated by CEP and SIEP methods. To obtain a uniform and agglomerated Pd-film, the membranes were annealed at 773 K and one atmospheric pressure under hydrogen environment for 18 hours prior to perm-selectivity test. The diffusion of atomic hydrogen through the metal films of dense metallic membranes (≥10 μm) is the rate-controlling step [49]. Hydrogen transports through Pd membrane via solution diffusion mechanism. H_2-flux is described by Sieverts' law as [50]:

$$J_{H_2} = \frac{Q_H}{t}\left(P_H^n - p_H^n\right) \tag{4}$$

where, Q_H is the hydrogen permeability, t is the membrane thickness or film thickness, and P_H and p_H are the partial pressures of hydrogen on the high and low pressure sides, respectively. The exponent n depends on the limiting transport mechanism. When the diffusion of atomic hydrogen through the Pd membrane controls the permeation of hydrogen, n becomes 1/2. On the other hand, if the gas resistance or dissociative adsorption of hydrogen molecules on the membrane surface is rate limiting in hydrogen transport, n approaches to unity [51-57].

Two membranes fabricated by SIEP and CEP methods were tested for H_2- permeability. The flux data were analyzed using Equation 4. The power indexes were estimated to be 0.82 and 0.85 for the SIEP and CEP membranes, respectively (Table 4). The power indexes indicate that both bulk diffusion and surface process dominate the hydrogen permeation. The lower value of power index (n) of the membranes fabricated by SIEP method suggests that these membranes offer hydrogen atoms more diffusion through bulk metals compared to the membranes fabricated by CEP method. The H_2-flux data for SIEP and CEP membranes are presented in Figure 8(a-b). The hydrogen permeability measurements were carried out in our permeation measurement set-up using pure hydrogen in the temperature range of 523-823 K with trans-membrane pressure of 20-100 psi. The measured data as a function of pressure difference $\left(P_H^n - p_H^n\right)$ are presented in Figure 8. The membrane selectivity of hydrogen over nitrogen is defined as:

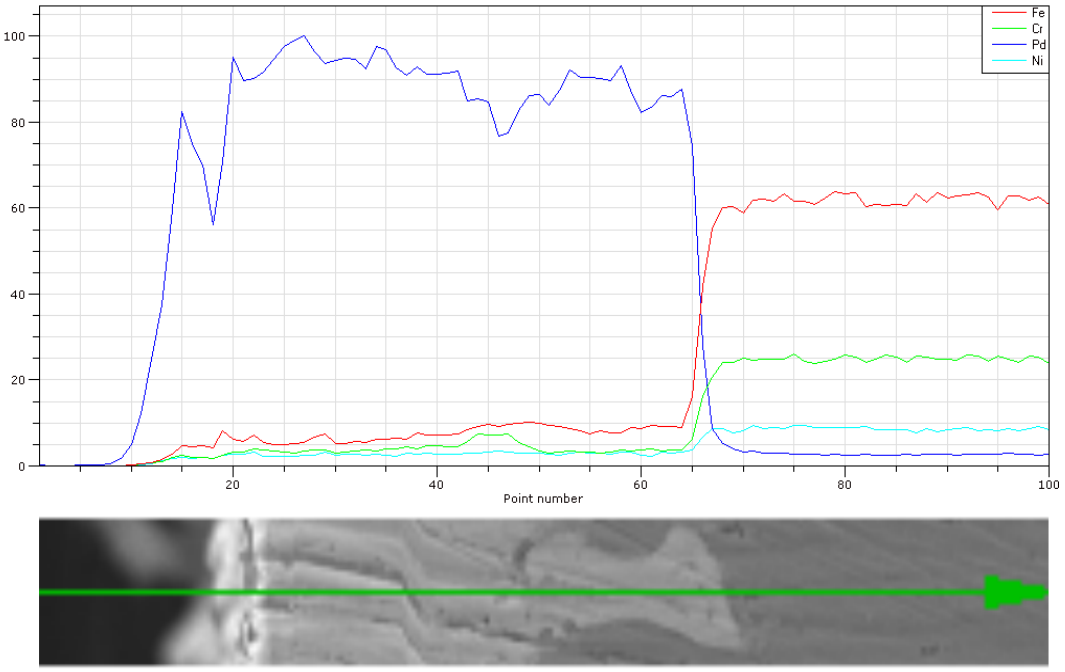

(a)

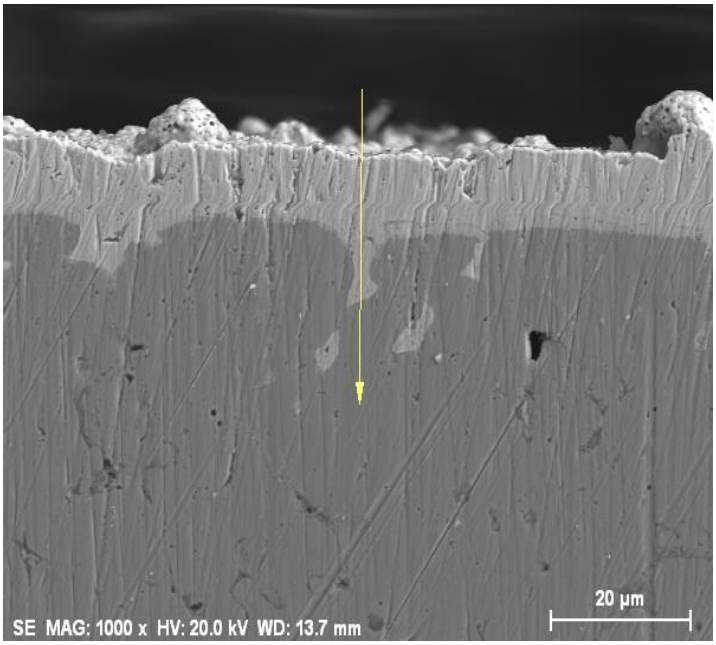

(b)

Figure 7. EDS line scanning of Pd-film cross-section (scanning length 35 µm).

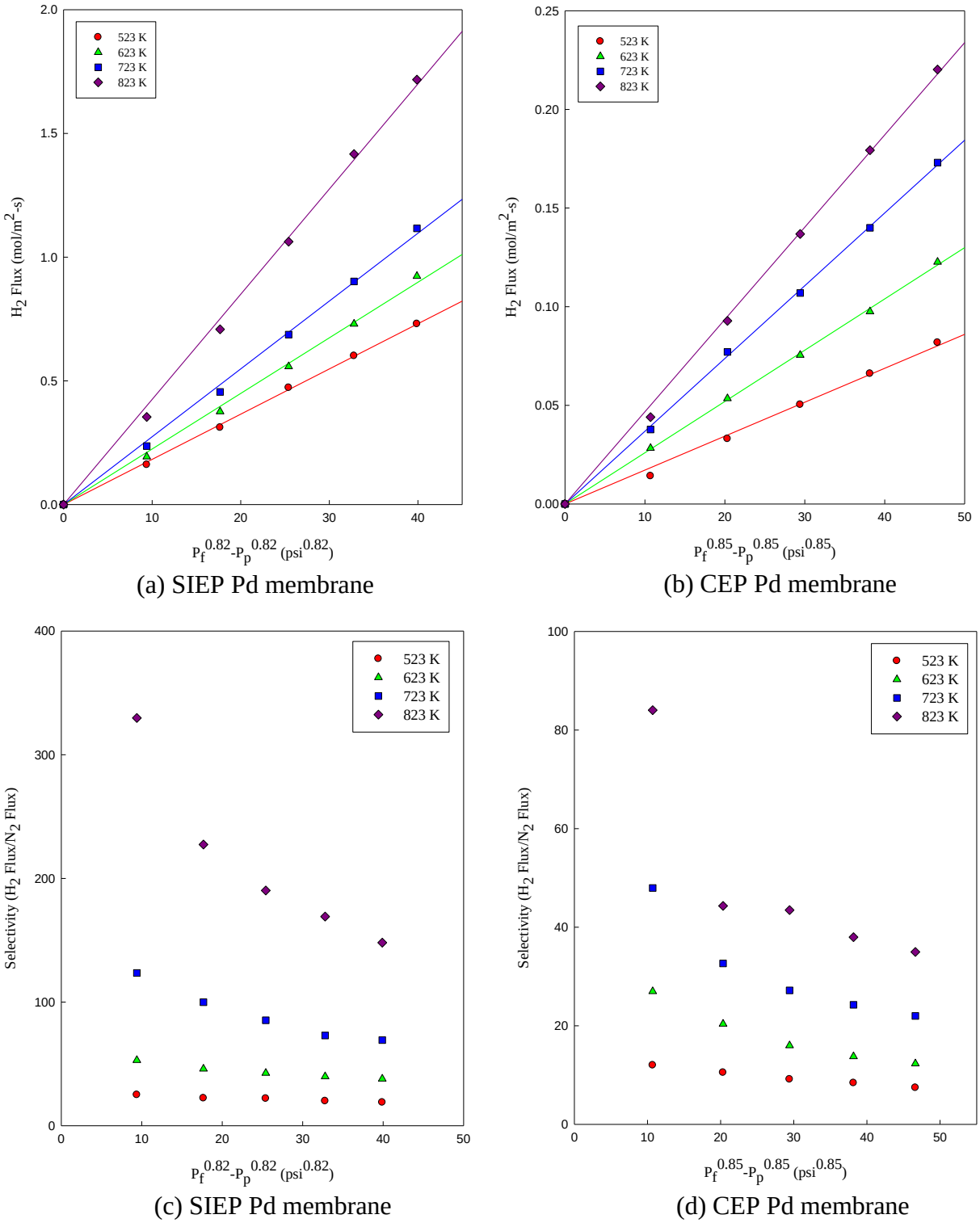

(a) SIEP Pd membrane

(b) CEP Pd membrane

(c) SIEP Pd membrane

(d) CEP Pd membrane

Figure 8. Hydrogen flux and H_2/N_2 selectivity data of Pd-membrane fabricated by SIEP and CEP methods.

$$\alpha_{H_2/N_2} = \frac{J_{H_2}}{J_{N_2}} \tag{5}$$

where, J_{H_2} and J_{N_2} are flux of H_2 and N_2, respectively. The selectivity of hydrogen over nitrogen is presented in Figure 8(c-d) for SIEP and CEP membranes, respectively as a function of $\left(P_H^n - p_H^n\right)$. Both membranes exhibited higher selectivity at higher temperature, whereas the selectivity decreases with increasing pressure. However, SIEP membrane showed higher permeability and selectivity compared to the CEP membrane. The highest H_2-flux for both membranes was observed at 823 K and 100 psi pressure. The measured H_2-flux of SIEP and CEP membranes were 1.7172 and 0.2202 mol/m^2.s, respectively. SIEP membrane exhibited about eight-fold higher H_2-flux at 823 K and 20 psi pressure than CEP membrane. We observed the highest selectivity at 823 K and 20 psi pressure. The selectivity of SIEP and CEP membranes were 330 and 84, respectively. This implies that SIEP membrane exhibited about four-fold higher selectivity at 823 K and 20 psi pressure than CEP membrane.

Long-term performance of Pd membranes

The long-term stability of Pd membrane fabricated by SIEP method was examined in H_2 and N_2 gases as a function of temperature. One Pd SIEP membrane sample of 11.6 μm thickness (Pd1) was subjected to thermal cycling to check its performance. For a period of 1200 h, H_2-flux of the membrane was recorded under thermal cycling of 573 – 723 – 573 K, and at 15 psi pressure in our permeability test set-up. On each day of testing, the membrane underwent a couple of thermal cycles. During the 1200 h test period, nitrogen leak test was carried out periodically (in about every 72 h) by switching hydrogen to nitrogen gas to check the integrity of the membrane. The H_2- and N_2-flux data are presented in Figure 9(a). The H_2-fluxes at 573 K and 723 K were 0.0150 and 0.0215 mol/(m^2.s), respectively at the beginning of operation. The H_2-flux was increasing till about 800 hours. The increase in H_2-flux up to 800 hours operation is attributed to the peeling off certain layer of the Pd-film. This peeling off made the Pd-film thinner, resulting in increasing H_2-flux. Over the period of 1200 hours of operation, there was no leakage of nitrogen which indicates that H_2/N_2 perm-selectivity was infinite. However, after 1200 hours, the N_2-flux became 0.00215 mol/(m^2.s), and the selectivity came down to about 18, based on the H_2-flux, 0.0365 mol/(m^2.s) at 450 °C. The Pd1 membrane was stable over the whole operation period.

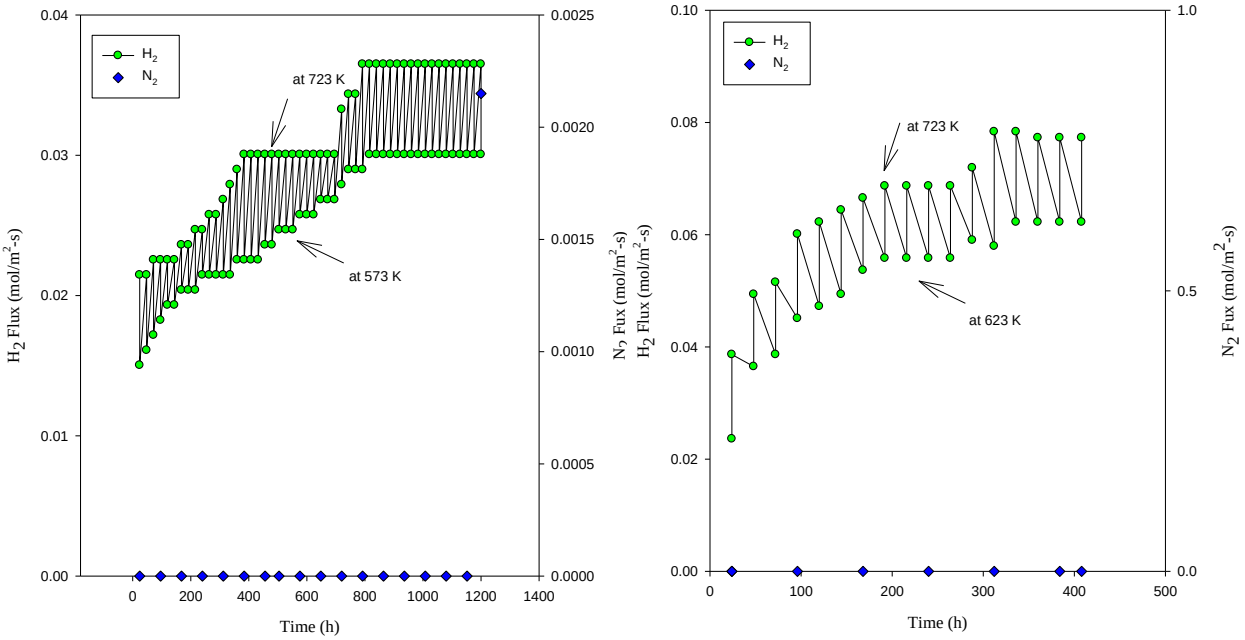

(a) Pd1 SIEP membrane (b) Pd2 SIEP membrane with diffusion barrier

Figure 9. H_2- and N_2-flux data of Pd1 and Pd2 membranes fabricated by SIEP method under thermal cycling at 15 psi trans-membrane pressure.

Another Pd membrane of 13.49 μm thickness was fabricated by SIEP method (Pd2), but an oxide layer as an intermetallic diffusion barrier was introduced on the substrate surface prior to the application of the dense hydrogen selective Pd skin layer. For the oxide layer, the cleaned stainless steel substrate was heated at 873 K for 12 h in presence of air. The Pd membrane needed thicker Pd-film to be helium gas tight due to having rougher oxide surface on the substrate surface. After heat treatment, membrane was tested for thermal cycling to check its performance and thermal stability. For a period of 408 h, H_2-flux of the membrane was recorded under thermal cycling of 623 – 723 – 623 K, and at 15 psi pressure in our permeability set-up. H_2- and N_2-flux data of Pd2 membrane are placed in the Figure 9(b). The H_2-fluxes at 623 K and 723 K were 0.062 and 0.0773 mol/(m^2.s), respectively after 408 h as shown Figure 9 (b). Over the 408 h testing period, N_2-flux was found to be zero. So, the Pd2 membrane performed thermal cycling for 408 h with infinite selectivity. As of 408 h of permeability test, the membrane remained stable. Though the thickness of the Pd2 membrane is higher than that of the Pd1 membrane, the H_2-flux of membrane Pd2 is about double than membrane Pd1. Because Pd2 membrane had an oxide film as a diffusion barrier on the substrate what prevented the diffusion of the elements such as Fe, Cr or Ni of stainless steel into the Pd-film during annealing at 723 K temperature under hydrogen atmosphere. From Figure 9(a) and 9(b), it can be observed that both Pd membranes have shown similar behavior in permeability and selectivity during the long-term thermal stability test.

Post-process characterization of Pd membranes

The tested membranes were examined by SEM analysis. Post-process characterization shows a considerable grain growth and micro-strain relaxation in the Pd membrane after the prolonged permeation experiment. The formation of pinholes is identified as the main source of the N_2 leakage during the testing at higher temperature.

SEM images of the surface topology of Pd1 membrane after 1200 h performance and thermal stability test at different magnifications are shown in Figure 10(a). It is seen from the SEM images taken after 1200 h of operation that there are some pinholes on the surface of the membrane. In Figure 10(a), the morphology of the tested membrane shows that pinhole formation is not a localized phenomenon but affects the whole surface. The pinholes have the average diameter about 0.67 μm. From the SEM images, it is seen that all of the pinholes did not penetrate the Pd-layer with same diameter. Although selectivity came down all of a sudden, it is

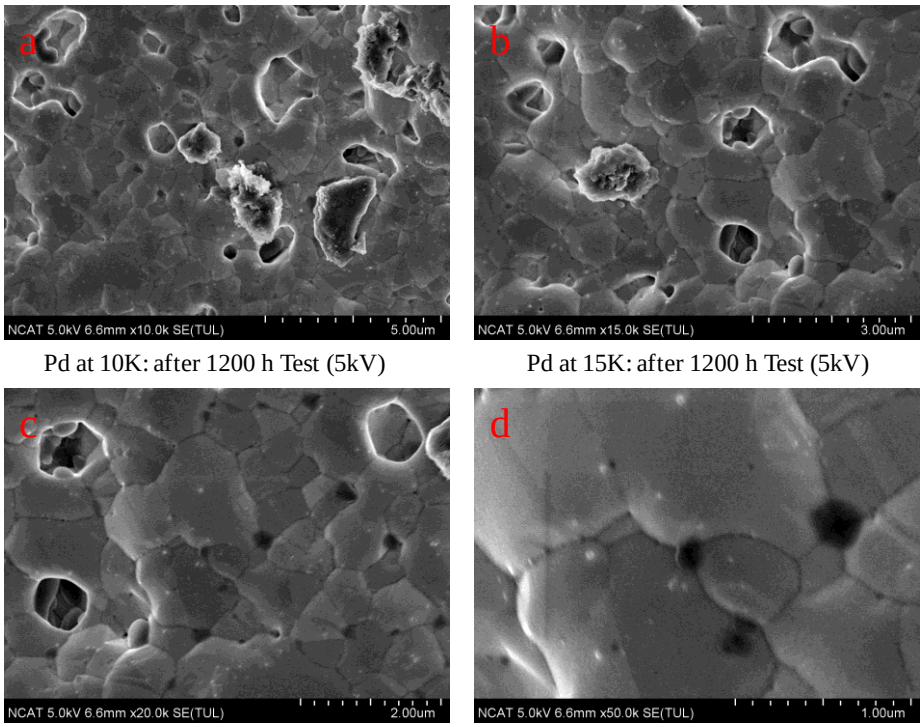

Pd at 10K: after 1200 h Test (5kV) Pd at 15K: after 1200 h Test (5kV)

Pd at 20K: after 1200 h Test (5kV) Pd at 50K: after 1200 h Test (5kV)

(a) Pd1 SIEP membrane

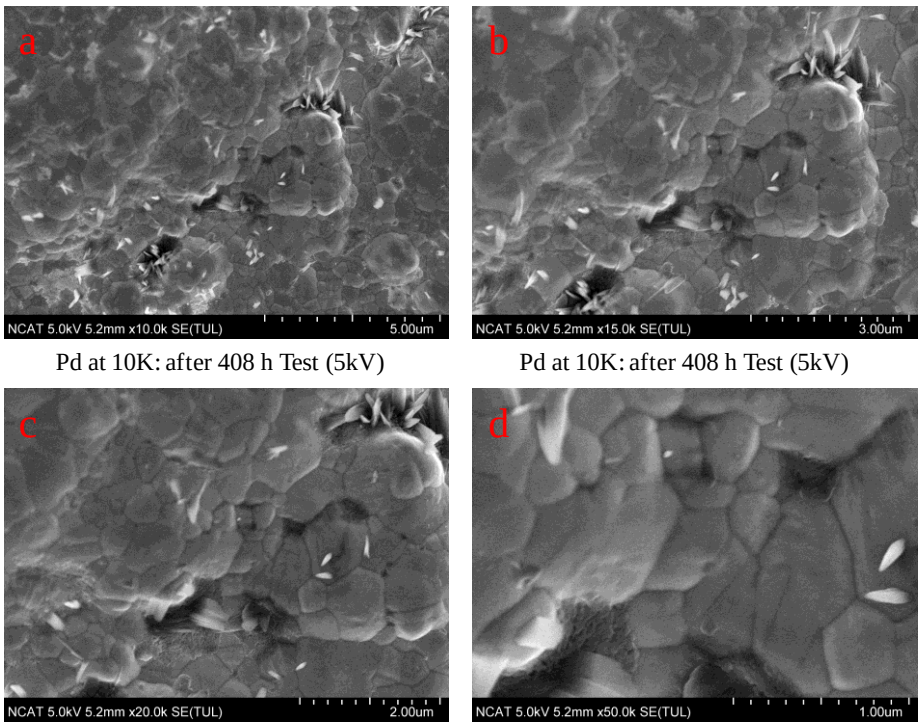

Pd at 10K: after 408 h Test (5kV) Pd at 10K: after 408 h Test (5kV)

Pd at 10K: after 408 h Test (5kV) Pd at 10K: after 408 h Test (5kV)

(b) Pd2 SIEP membrane with diffusion barrier

Figure 10. SEM images of Pd1 and Pd2 SIEP membranes after thermal cycling.

clear from the SEM image that all of the pinholes have not been created suddenly but these pinholes did not penetrate through the Pd-film. Peeling of the Pd-layer occurred during the thermal cycling. The peeling made the Pd-film thinner. After 1200 hours of operation, some spots of the peeled off area passed through the Pd-film and became pinholes. Since 0.2 – 0.4 times of the melting point of nanocrystalline metal is the sintering temperature, sintering plays an important role in the formation of leak and leak growth [58]. Pd cluster sintering is one of the reasons for leak formation. Increased surface roughness is observed by SEM for which there may be several possible causal roots; lattice stress relaxation, bcc/fcc phase transition in the Pd alloy, Pd grain coalescence, or Pd grain sintering. Some grains of the membrane top surface took shape of cauliflower as shown in Figure 10(a). It appears that the cauliflower shaped Pd grain was about to peel off the membrane surface. Further study is needed to understand the underlying causes for this behavior.

SEM images at different magnifications of the surface topology of Pd2 membrane at post 408 h performance and thermal stability test are shown in Figure 10(b). No significant number of pinholes has been created in the Pd-film of the membrane as shown in Figure 10(b). Pd membrane permeating hydrogen gas is prone to have pinholes or defects operated below 623 K temperature. Since Pd2 membrane was not operated below 623 K temperature, pinholes could not form. This result is in agreement with the nitrogen gas leak test at the end of the 408 h testing period. The Pd2 membrane contains infinitesimal sized and white colored spots over the whole surface area and some black spots in the agglomerated and clustered Pd grain boundaries. The reasons for the presence of these spots could not be ascertained. These spots might come from impurities present on the Pd-layer.

Pd-Cu Membranes by CEP and SIEP

Helium gas-tightness and film thickness analysis of Pd-Cu membranes

Pd-Cu membranes on MPSS substrate were fabricated by SIEP and CEP methods. As discussed earlier, the microstructure of the Pd-alloy membranes depends on a number of factors, such as substrate surface roughness, pore dimension, fabrication technique, bath composition and operating conditions. In this work, all these parameters (bath composition, and operating parameters) were kept constant in order to understand the role of surfactant on the microstructure of the Pd-Cu films.

The membranes were tested for helium gas-tightness in the permeability measurement set-up at a transmembrane pressure drop of 20 psi at room temperature (~298 K). In Figure 11, helium gas-tightness results are presented for two sample membranes fabricated by SIEP (S2 and S3), along with two samples fabricated by CEP (C1 and C2) methods. The results show that, in order to obtain a gas-tight Pd-Cu membrane, we need about 15 μm thick metal film by the SIEP method. In the CEP method, this thickness is over 19 μm. Thus, we observed that using DTAB we can reduce the membrane film thickness with improved gas-tightness.

Electroless plating time, film thickness, metal composition, H_2 flux and selectivity data of Pd and Pd-Cu membranes fabricated by the SIEP and CEP methods are summarized in Table 6. The film thickness of the Pd-Cu membrane was calculated using a gravimetric method and SEM analysis for SIEP membranes. For CEP membranes, only a gravimetric method was used to calculate the film thickness of the Pd-Cu membrane. From Table 6, it is evident that Pd-Cu membranes fabricated by the SIEP process are thinner compared to Pd-Cu membranes fabricated by the CEP process. The average thickness of the Pd-Cu film fabricated by the SIEP process is 15.38 μm, whereas, that of Pd-Cu film fabricated by the CEP process is 19.68 μm. In our previous study, we found that the film thickness of the pure Pd membrane fabricated by the SIEP process was 7.68 μm and the film thickness of the Pd-Ag membrane fabricated by the SIEP process was 12.63 μm [46, 47]. It should be noted that Pd-Cu films are considerably thicker than the Pd film due to Cu-plating bath kinetics. The results presented in Table 6 indicate that thinner Pd-Cu membranes can be fabricated in shorter time using DTAB in the SIEP method compared to the CEP method.

Microstructure analysis of Pd-Cu membranes

The microstructure of the Pd-Cu film was studied using SEM images at 5K, 10K, 20K and 50K magnifications. For example, in Figure 12 SEM images of a Pd-Cu membrane fabricated by SIEP reveal two different particles with differing sizes. The larger and smaller particles are mostly identified as Pd and Cu metal clusters, respectively. The particle size distribution of this Pd-Cu membrane as determined from SEM image analysis is shown in Figure 13. The particle size distribution of Pd and Cu shows two sharp peaks with average particle size of 1.01 and 0.65 μm, respectively.

The Pd-Cu membranes fabricated by CEP and SIEP methods were also examined by SEM after annealing (heat treatment-HT). In Figure 14, the SEM images of Pd-Cu membranes

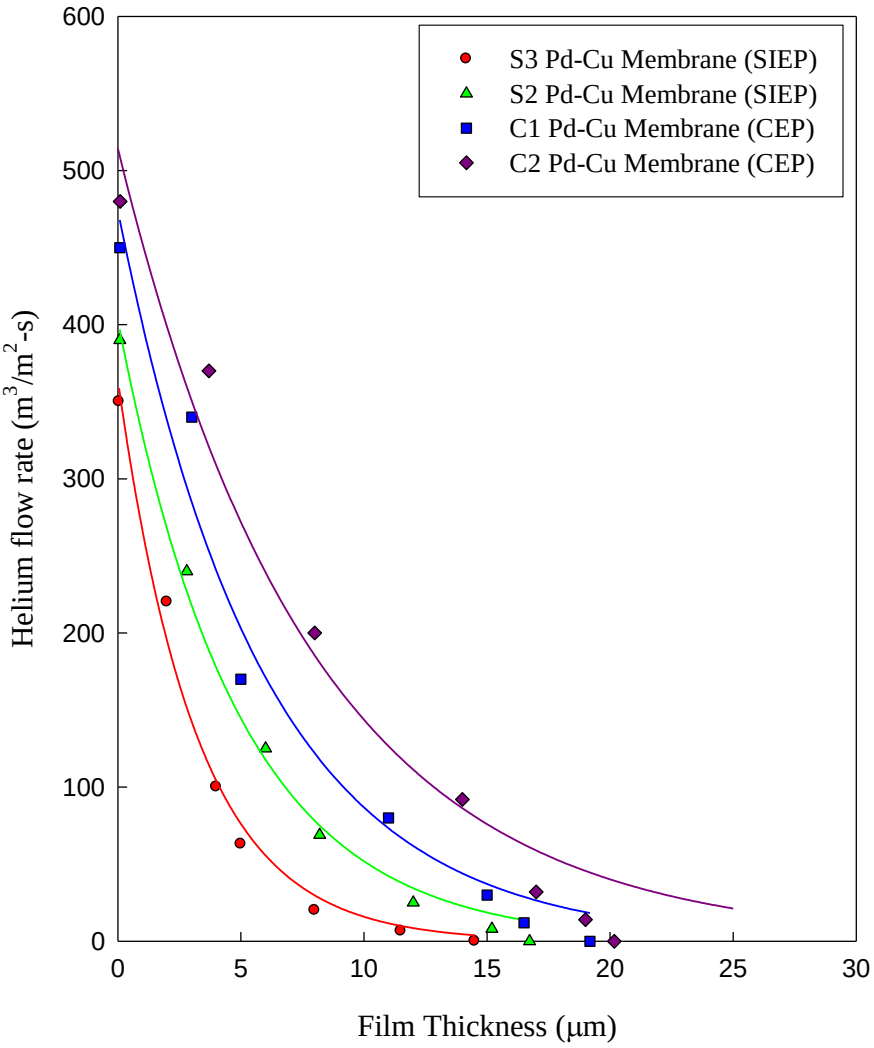

Figure 11. Helium gas-tightness of Pd-Cu membranes as a function film thickness fabricated by CEP and SIEP methods.

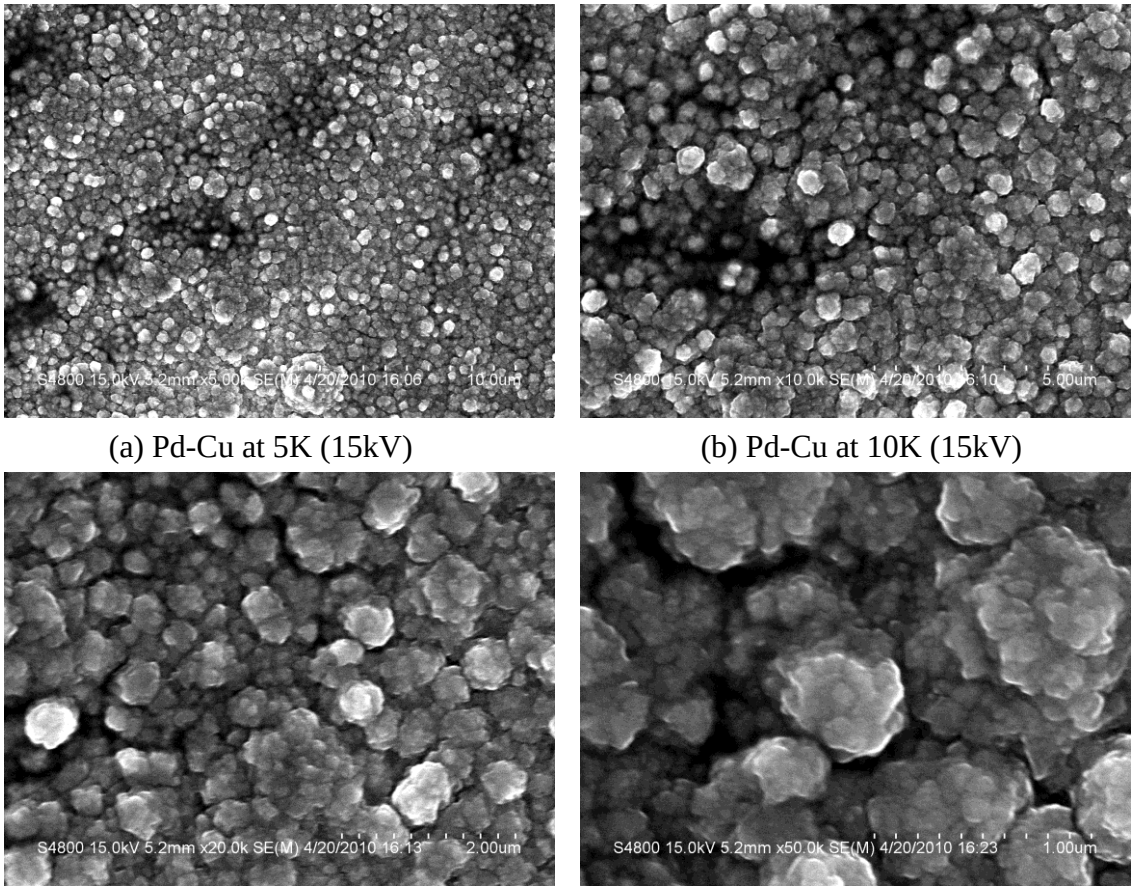

(a) Pd-Cu at 5K (15kV)

(b) Pd-Cu at 10K (15kV)

(c) Pd-Cu at 20K (15kV)

(d) Pd-Cu at 50K (15kV)

Figure 12. SEM images of Pd-Cu membrane film top surface fabricated by SIEP method.

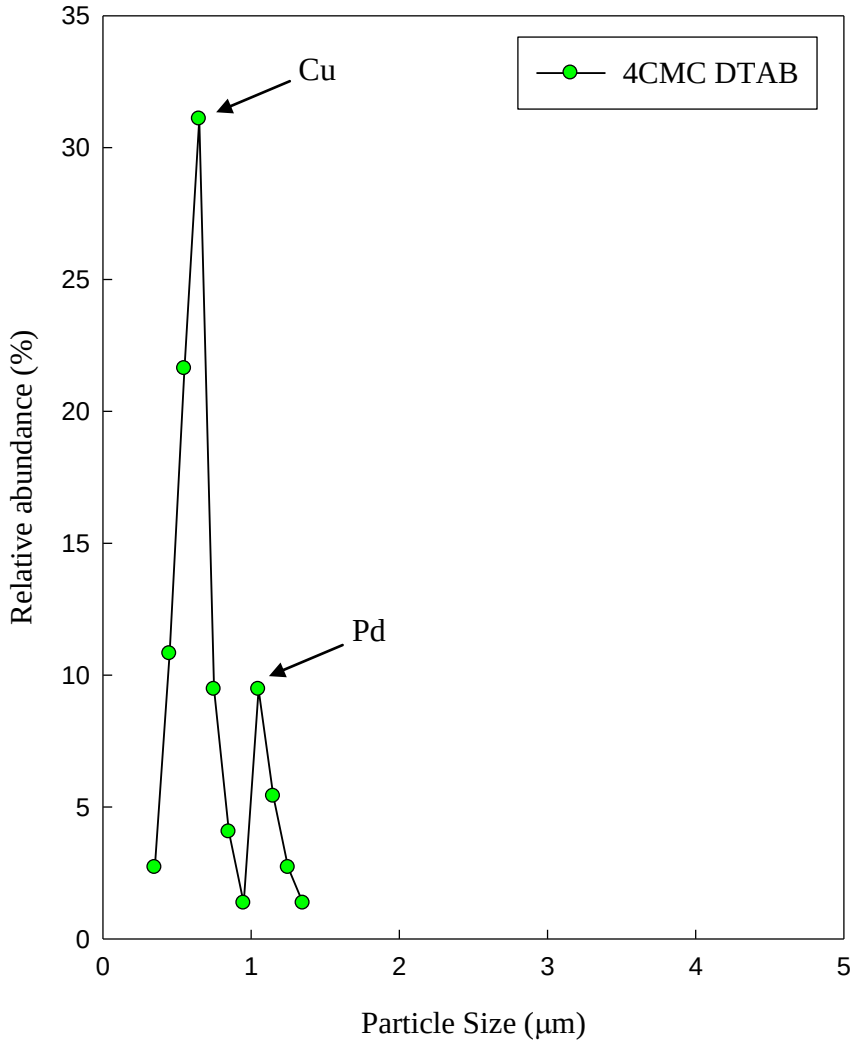

Figure 13. Cu and Pd grain size distribution in Pd-Cu membrane fabricated by SIEP method with 4×CMC of DTAB surfactant.

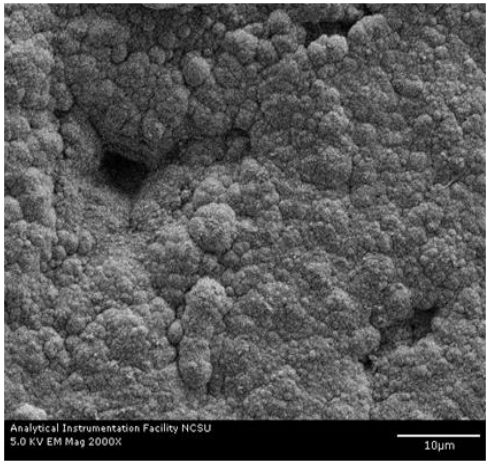

(a) Pd-Cu (CEP) at 2K: Pre-HT

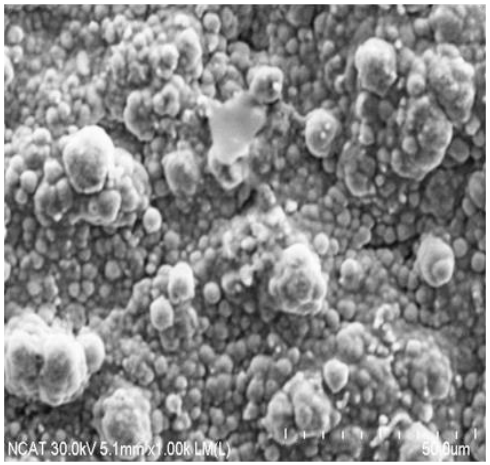

(c) Pd-Cu (CEP) at 1K: Post-HT

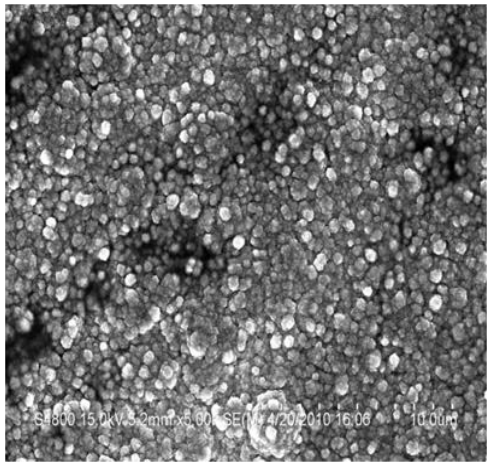

(e) Pd-Cu (SIEP) at 5K: Pre-HT

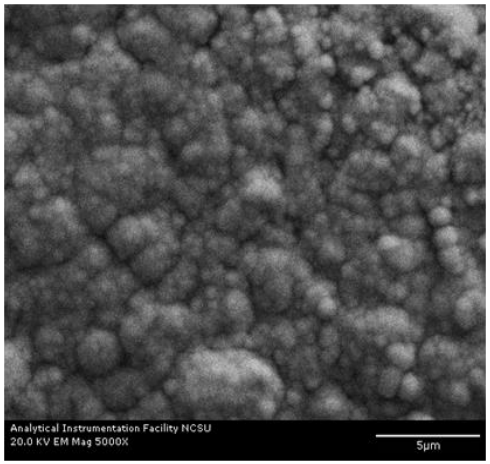

(b) Pd-Cu (CEP) at 5K: Post-HT

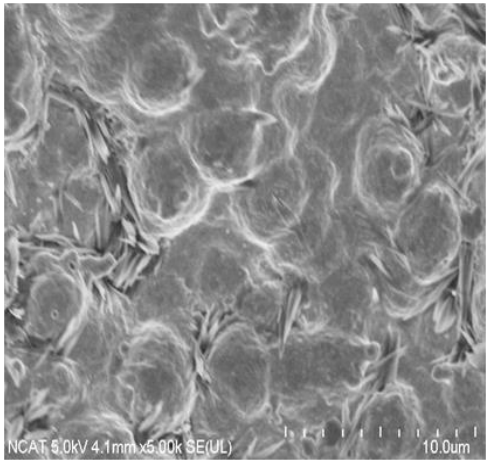

(d) Pd-Cu (CEP) at 5K: Post-HT

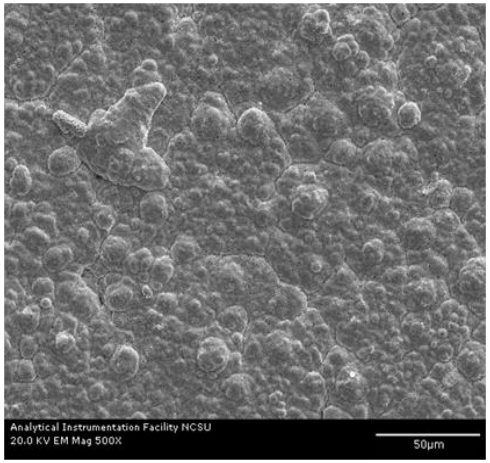

(f) Pd-Cu (SIEP) at 5K: Post-HT

Figure 14. SEM images of top surface of Pd-Cu membranes fabricated by CEP and SIEP methods at pre- and post-HT (heat treatment) conditions.

Table 6. Permeation characteristics of Pd and Pd-Cu membranes fabricated by SIEP and CEP methods

Membrane sample	Deposition time (hr)	Film thickness (μm)		Film composition (% of Cu)	Sieverts' law power index (*n*)	H_2 flux at 723 K (mol/m^2-s)		Selectivity at 723 K (H_2 flux/N_2 flux)	
		Gravimetric analysis	SEM analysis			20 psi	100 psi	20 psi	100 psi
S1 Pd-Cu	26.8	15.6	-	-	-	-	-	-	-
S2 Pd-Cu	33.8	16.73	-	35.8	0.8	0.145	0.54	123	49
S3 Pd-Cu	31.4	14.5	13.34	44.69	0.79	0.156	0.55	110	43
S4 Pd-Cu	27.8	14.7	13.61	25.8	-	-	-	-	-
C1 Pd-Cu [a]	34.3	19.18	-	36.7[c]	0.92	0.094	0.43	19	7.42
C2 Pd-Cu [a]	35.7	20.17	-	33.4[c]	0.91	0.097	0.44	17	8
Pd 4CMC	10	7.68	7.68	-	0.61	0.28	0.81	250	-
Pd 0CMC	28	28.5	27.5	-	-	-	-	-	-

[a] Membranes fabricated by CEP

fabricated by CEP (a-d) and SIEP (e-f) methods are shown. SEM images in Figure 14(a-b) and 14(c-d) show the Pd-Cu membrane (CEP) surface morphology at pre-HT and post-HT conditions, respectively. Pre- and post-HT SEM images of the Pd-Cu (SIEP) membrane are shown in Figure 14(e-f). If we compare SEM images of the CEP membrane (a and b) at pre-HT condition with that of the SIEP membrane Figure 14(e), we observe that the SIEP membrane has superior surface grain structure with uniformity. Upon annealing (post-HT), we observe smooth grain agglomeration with continuity as seen in Figure 14(f). However, the CEP membrane show poor agglomeration with a needle-like structure popping out of the surface as given in Figure 14(d). However, the grain agglomeration and size of particles are much bigger in size and shape compared to those of Pd-Cu membranes fabricated by SIEP process, which is clear in Figures 14(e) and 14(f). Thus, we observe that by introducing suitable surfactant in the EP, grain size and structure can be tailored and cotrolled to fabricate a better Pd-Cu film.

The surface topography of Pd-Cu membranes fabricated by SIEP and CEP methods was examined by AFM analysis and is presented in Figure 15. The Pd-Cu membrane fabricated by SIEP show cage-like structures (Figure 15a) and the grains are diffused to one another due to the presence of both Pd and Cu atoms with average surface roughness of about 1.122 μm. For the CEP Pd-Cu membrane (Figure 15b), AFM analysis shows non-uniform grain agglomeration with surface roughness of about 2.275 μm which is significantly higher than that of the SIEP membrane. This notable improvement in the Pd-Cu film structure is attributed to the hydrophobic DTAB used in the SIEP method. Surfactant DTAB played an important role in removing evolved gas bubbles from the surface in EP bath reactions. Tail groups of DTAB appear to be aligned around the gas-liquid interface and form various spherical or cylindrical cage-like structures. It also tends to form various meta-stable structures (spherical, cylindrical or circular) at the solid-liquid interface that inherently help finer grain formation and subsequent coarsening of the deposited film. As seen in the AFM images (Figure 15a), DTAB forms cylindrically long, repetitive chains throughout the surface. This observation is in agreement with other published work [40, 59]. DTAB may also take part in the reaction kinetics as it contains active bromide ions (Br^-) in the head group which is a strong oxidizing agent. This head group may participate in the reduction process of the complex salt and favorably take part in Pd and Cu grain formation and subsequent grain coarsening. These dual roles of DTAB appear to be very effective in thin film formation.

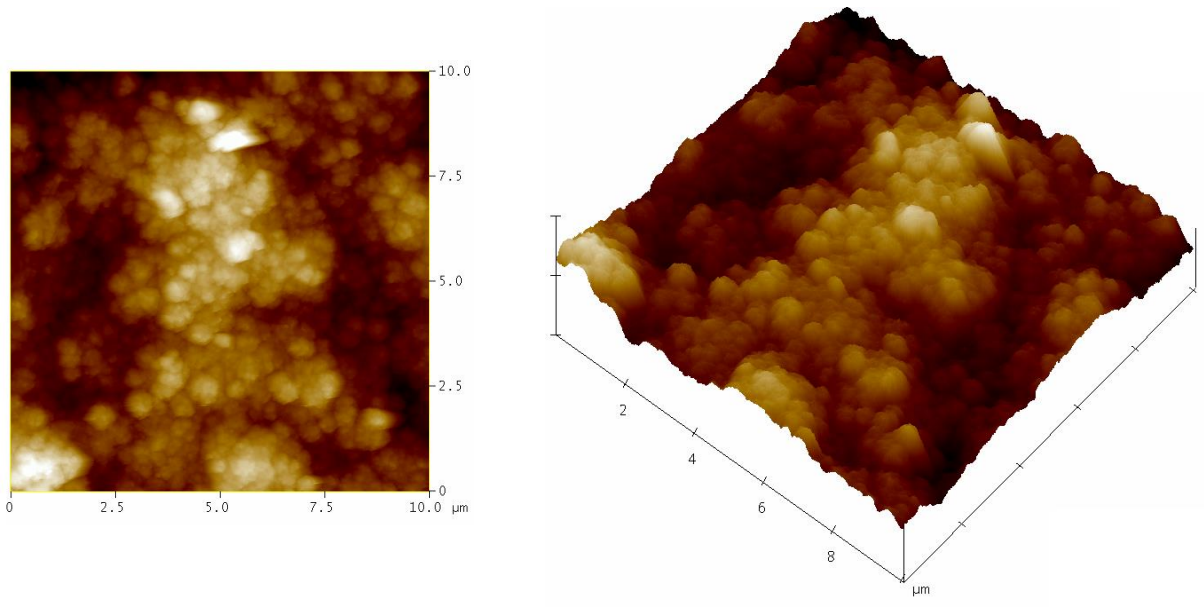

(a) Pd-Cu Membrane (SIEP)

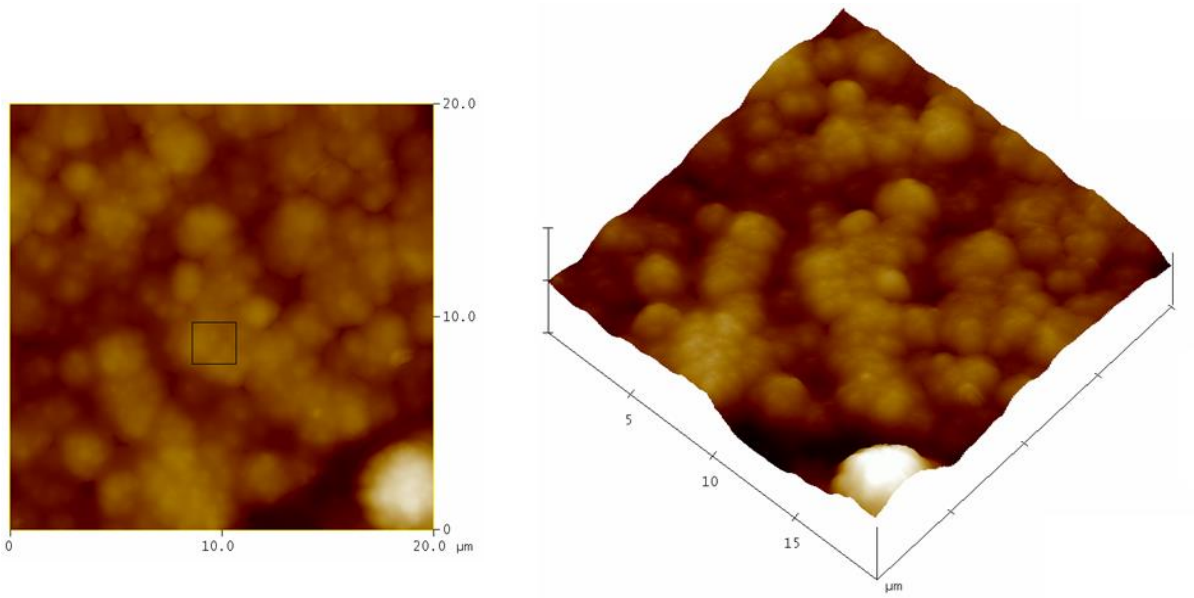

(b) Pd-Cu Membrane (CEP)

Figure 15. AFM images of solid Pd-Cu surface aggregation onto typical MPSS (SIEP and CEP).

Typical EDS pattern of Pd-Cu film fabricated by SIEP is presented in Figure 16. The EDS pattern shows two distinct peaks for Pd and Cu. The elemental compositions of Pd and Cu were found to be 55.31% and 44.69% by weight, respectively. Absence of other metal peaks in EDS spectra in Figure 16 indicates that use of DTAB in the EP baths did not introduce any kind of impurities in membrane film.

Typical XRD patterns of Pd-Cu membranes fabricated by SIEP are shown in Figure 17 at pre-HT and post-HT conditions. Pre-HT XRD spectra (Figure 17a) show the reflection peaks of Pd and Cu in the face centered cubic (f.c.c.) phase at {111}, {200}, {220} and {311} planes. Table 7 summarizes the 2θ and d-spacing values corresponding to the four major reflection peaks for pure Pd and Pd-Cu film for comparison [46, 49]. The 2θ values suggest that all of the characteristics peaks of Pd are in the same position for both Pd and Pd-Cu films. In addition, the presence of different bravais lattices signifies the formation of polycrystalline structure throughout the film. It is worth mentioning that in our XRD analysis, no reflection peaks for Fe, Cr, Ni and Mn/Mo metals were observed. The Pd-Cu membranes were annealed in a hydrogen environment at 773 K for 10 and 18 h to better understand the alloying process. In Figure 17(b), after 10 h of HT we observe that Pd and Cu in {111}, {200}, and {220} planes are merged into three distinct peaks at Pd planes. This shows formation of a Pd-Cu alloy. After 18 h of HT, as shown in Figure 17(c), the three peaks become sharper. The shifting of peaks indicates the coexistence of Pd and Cu in the deposited film and formation of Pd-Cu interstitial alloys [18, 35, 60]. Interstitial alloy formation occurs when the atoms of one component are smaller than the other, and the smaller atoms fit into the spaces (interstices) between the larger atoms. During 18 hours of annealing, we did not observe alloy formation between Pd and Cu at {311} plane. Allowing more time could result alloy formation at {311} planes.

The pores in the MPSS substrate are tortuous and interconnected. To understand the Pd-Cu deposition in the pores and on the substrate surface, we examined the cross-section of Pd-Cu SIEP membranes using EDS. As an illustrative example, in Figure 18(a), we probed four locations across a depth of 25 μm for Pd and Cu metal contents, which suggests that we were able to deposit metals deep inside the pores. The Pd and Cu metal contents in these pores are shown in Figure 18(b) by a bar graph. The Cu content inside the pores decreases across the depth, which is expected because of the sequential EP deposition of Cu over Pd. This conclusion is reaffirmed by the EDS line scanning of the Pd-Cu film cross-section, as shown in Figure 19. It

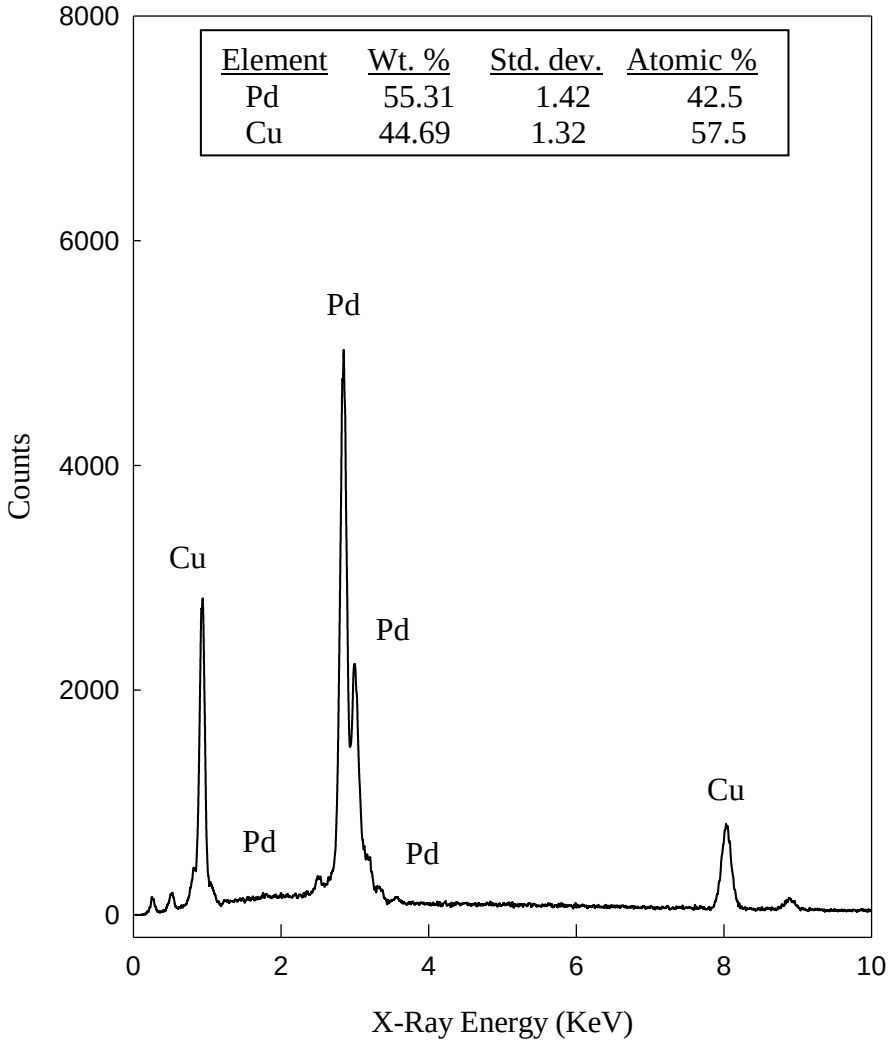

Figure 16. Typical EDS spectrum of Pd-Cu membrane shows the presence of polycrystalline deposition of Pd and Cu particles.

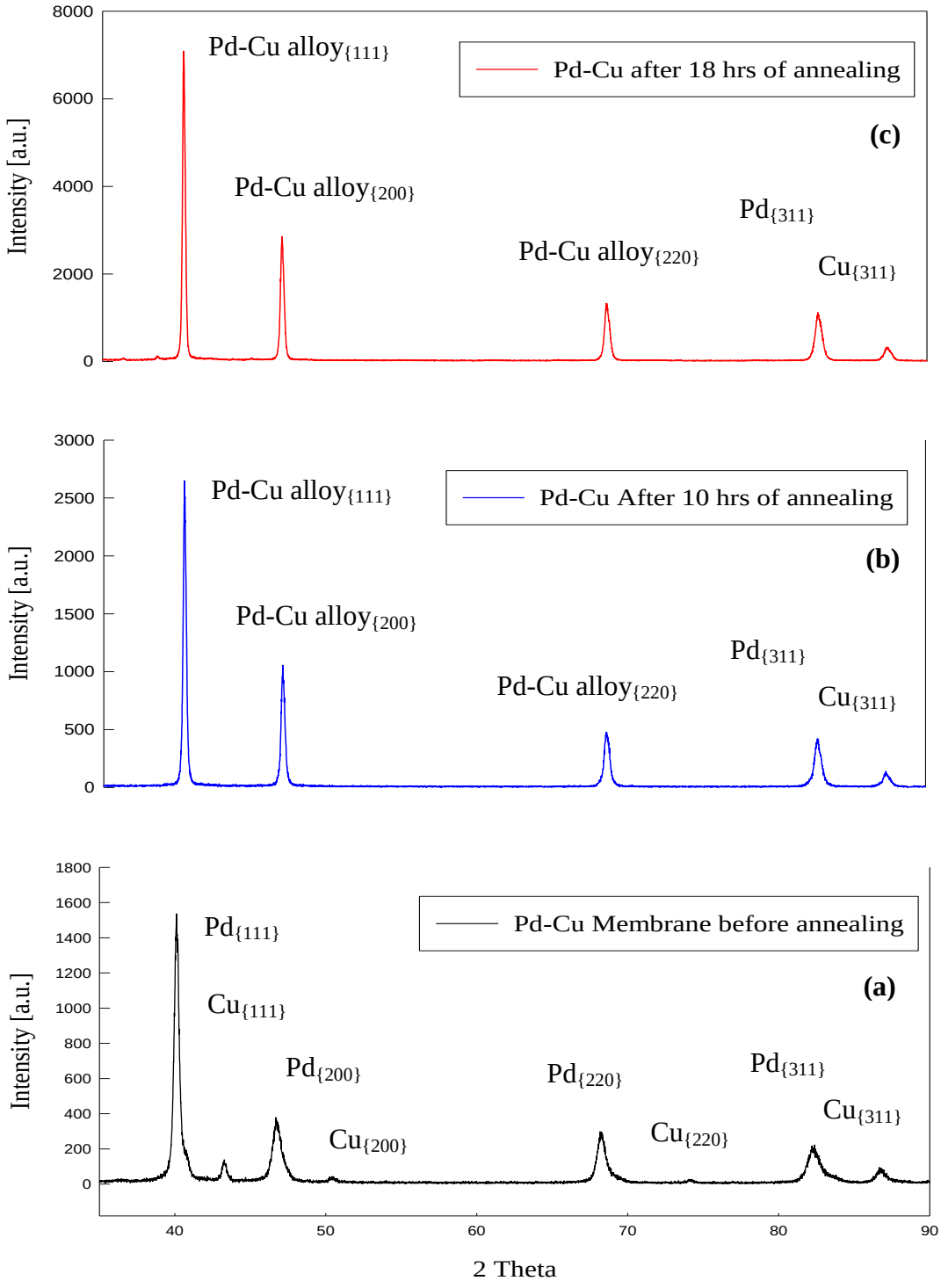

Figure 17. Effect of heat treatment on XRD pattern of Pd-Cu membrane fabricated by SIEP method.

Table 7. Comparison of high angle XRD reflection peaks of Pd and Pd-Cu film fabricated by SIEP method

	Bravais lattice	Pd-film		Pd-Cu-film		
		Pd (Pre-HT)	Pd (Post-HT)	Pd (Pre-HT)	Cu (Pre-HT)	Pd-Cu (Post-HT)
2-theta	111	40.214	40.109	40.145	43.316	40.366
	200	46.776	46.652	46.695	50.448	46.956
	220	68.303	68.107	68.176	74.125	68.585
	311	82.338	82.086	82.173	89.936	82.702
d-spacing	111	2.2407	2.2463	2.24439	2.0871	2.2326
	200	1.9405	1.9454	1.94370	1.8075	1.9335
	220	1.3721	1.3756	1.37440	1.2781	1.3671
	311	1.1701	1.1731	1.17210	1.0899	1.1659
Lattice parameter, a		3.881	3.8908	3.8874	3.6150	3.867
Lattice structure		f.c.c.	f.c.c.	f.c.c.	f.c.c.	f.c.c.

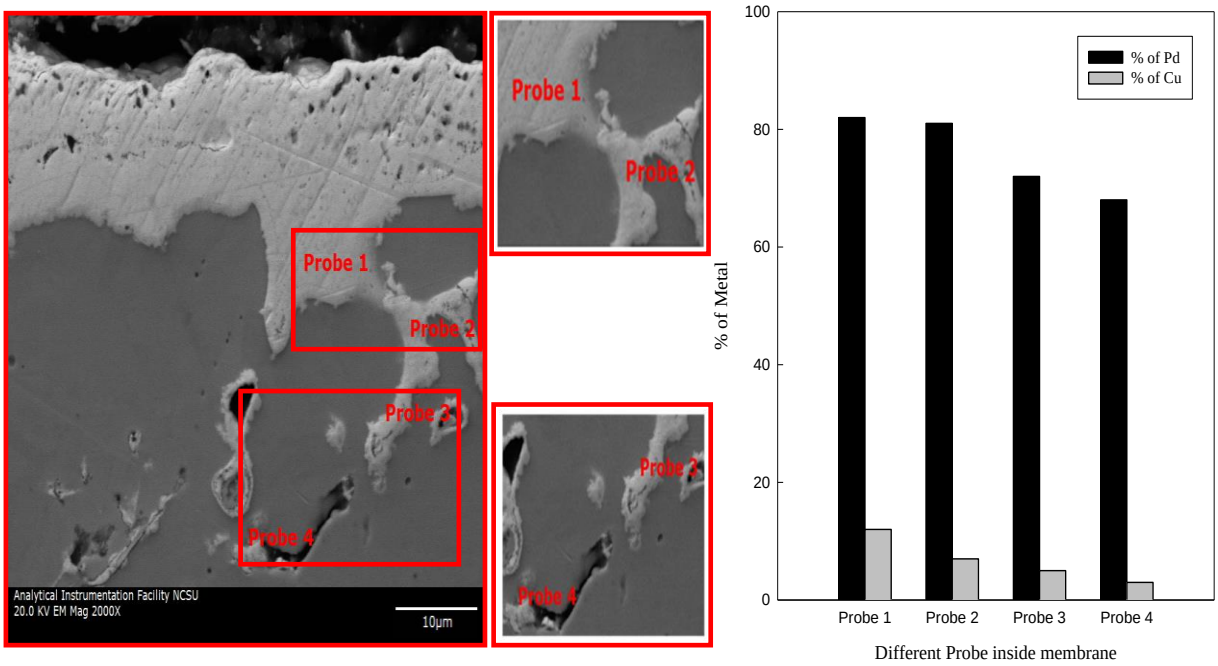

(a) Locations of pores for EDS analysis (b) Metal distribution in pores

Figure 18. SEM images of Pd-Cu film cross-section: showing the locations of pores to study Pd and Cu metal distribution by EDS analysis starting from the pore mouth to deep inside (from Probe 1→Probe 4).

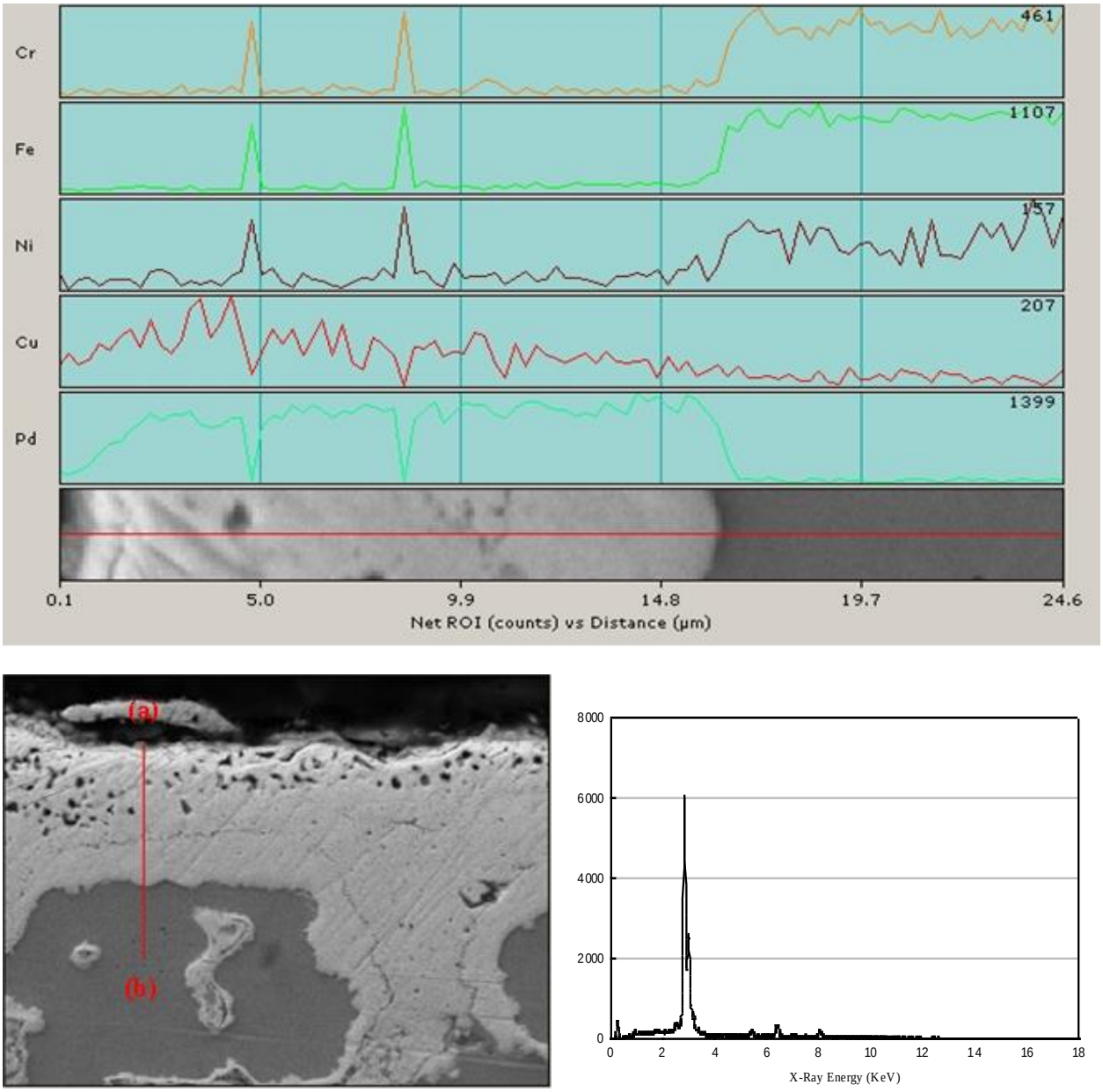

Figure 19. EDS line scanning of Pd-Cu film cross section (scanning length 25 µm, scanning direction from (a) → (b)).

may be mentioned here that in this line scanning, we did not observe Fe, Cr, and Ni metals in the Pd-Cu film. The oscillation of X-ray counts was prominent for Cu, as the Cu content is low in each deposition cycle. Being the minor constituent, Ni has the background effect and oscillates more. However, the sharp rise of peaks for Fe, Cr and Ni (sharp trough for Pd and Cu) in the middle of the Pd-Cu alloy film was observed. Indeed, these were the response from fine stainless steel particles doped in the film during metal polishing while preparing the sample.

H_2-permselectivity studies of Pd-Cu membranes

The Pd-Cu membranes fabricated by the CEP and SIEP techniques were tested for hydrogen perm-selectivity at pre-HT and post-HT conditions. As shown in Table 6 in the previous section, the SIEP membrane samples are numbered as S1 through S4 while the CEP membranes are numbered as C1 and C2. In this table, we summarized our hydrogen flux and selectivity data, along with membrane thickness.

For dense metallic membranes (≥10 μm), it is believed that the diffusion of atomic hydrogen through the metal films is the rate-controlling step [44] and in this study Sieverts' law (Equation 4) was used to analyze the H_2-flux data for Pd-Cu membranes

We tested several Pd-Cu membrane samples fabricated by the SIEP and CEP methods at pre-HT and post-HT conditions for hydrogen permeability. We observed that the power index ranged between 0.5 and 1 (Table 6). This suggests that the H_2-transport through Pd-Cu membranes not only dominated by solution-diffusion mode of transport but the gas phase resistance and/or surface reactions may be rate limiting. As an illustrative example, in Figure 20, we present hydrogen flux and selectivity data of Pd-Cu membranes fabricated by SIEP (S2) and CEP (C2) at pre-HT condition. The permeability measurements were carried out in the temperature range of 523 to 823 K with transmembrane pressure of 20 to 100 psi. The H_2-flux data is presented as a function of $\left(P_H^n - p_H^n\right)$ and from a non-linear least-square analysis we find the power index *n* as 0.85 for S2 (Figure 20a) and 0.93 for C2 (Figure 20b).The lower value of the power index (*n*) of the membranes fabricated by the SIEP method suggests that these membranes offer hydrogen atoms more diffusion through bulk metals compared to the membranes fabricated by CEP method. The selectivity of hydrogen over nitrogen of the two membranes is presented in Figure 20(c) and 20(d) for S2 and C2 membrane, respectively as a function of $\left(P_H^n - p_H^n\right)$. For both the CEP and SIEP membranes, hydrogen selectivity

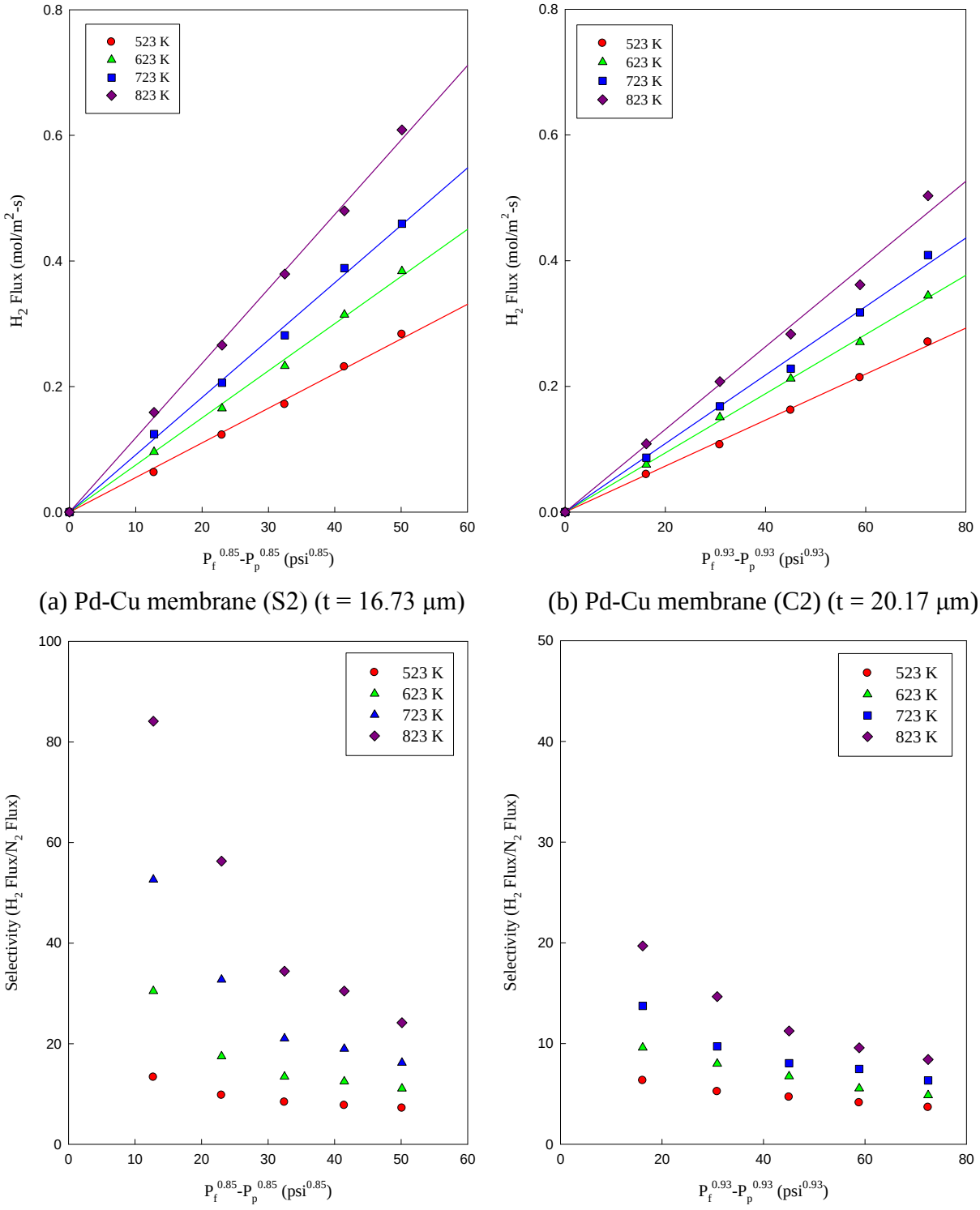

(a) Pd-Cu membrane (S2) (t = 16.73 μm)

(b) Pd-Cu membrane (C2) (t = 20.17 μm)

(c) Pd-Cu membrane (S2) (t = 16.73 μm)

(d) Pd-Cu membrane (C2) (t = 20.17 μm)

Figure 20. Hydrogen flux and H_2/N_2 selectivity data of Pd-Cu membranes fabricated by SIEP and CEP methods (pre -HT).

increases with increasing temperature, whereas the selectivity decreases with increasing pressure. However, the SIEP membrane (S2) had higher permeability and selectivity compared to the CEP membrane (C2). For the four Pd-Cu membranes (S2, S3, C1 and C2) that we tested for hydrogen perm-selectivity, we observed highest selectivity at 823 K and 20 psi pressure in pre-HT membranes. The measured selectivity was 84.1 for the S2 membrane and 19.7 for the C2 membrane. The result shows that the SIEP membrane provides significantly higher selectivity compared to the CEP membrane. In this example, the SIEP membrane had about four-fold higher selectivity at 823 K and 20 psi pressure than the CEP membrane.

The SIEP (S2 and S3) and CEP (C1 and C2) membranes were heat-treated for 18 hours in a hydrogen environment at 773 K. These membranes were then tested for hydrogen perm-selectively as before. The H_2-flux and selectivity data of the post-HT S2 and C2 membranes are presented in Figure 21 as a function of $\left(P_H^n - p_H^n\right)$. From flux data analysis, the power index was found to be 0.80 for the S2 membrane (Figure 21a). In comparison, the power index was found to be 0.91 for the C2 membrane (Figure 21b). In both membranes, hydrogen flux increased with temperature for a given transmembrane pressure. However, if we compare with pre-HT membrane fluxes, we find that the post-HT S2 membrane has significantly higher flux (Figure 21a) compared to the pre-HT S2 membrane flux (Figure 20a). In the case of CEP membranes, the pre- and post-HT C2 membrane the flux gain was found to be marginal (Figures 20b and 21b). The H_2-selectivity data of S2 and C2 membranes, presented in Figure 21(c) and 21(d), show that the SIEP membrane has significantly higher selectivity relative to CEP membrane. If we compare the selectivity of the pre- and post-HT S2 membrane, we find that the selectivity increased from 84 to 186 at 20 psi and 823 K. For the CEP C2 membrane, however, we did not observe any change in selectivity at the pre- and post-HT conditions.

To illustrate the intrinsic membrane behavior of the SIEP and CEP Pd-Cu membranes, we computed the permeability coefficients Q_H at four different temperatures using an Arrhenius plot (Q_H vs. $1/T$), shown in Figure 22. The permeability data fit very well (correlation coefficient, $r^2 = 0.98$ in both cases) to the Arrhenius equation:

$$Q_H = Q_{Ho} \exp(-E/RT) \qquad (3)$$

where, Q_{Ho} is the reference permeance, E is the activation energy, T is the absolute temperature and R is the universal gas constant. The E value of the SIEP Pd-Cu membrane (film thickness of 16.73 μm) was found to be 9.4 kJ/mol, whereas the corresponding E value of activation energy

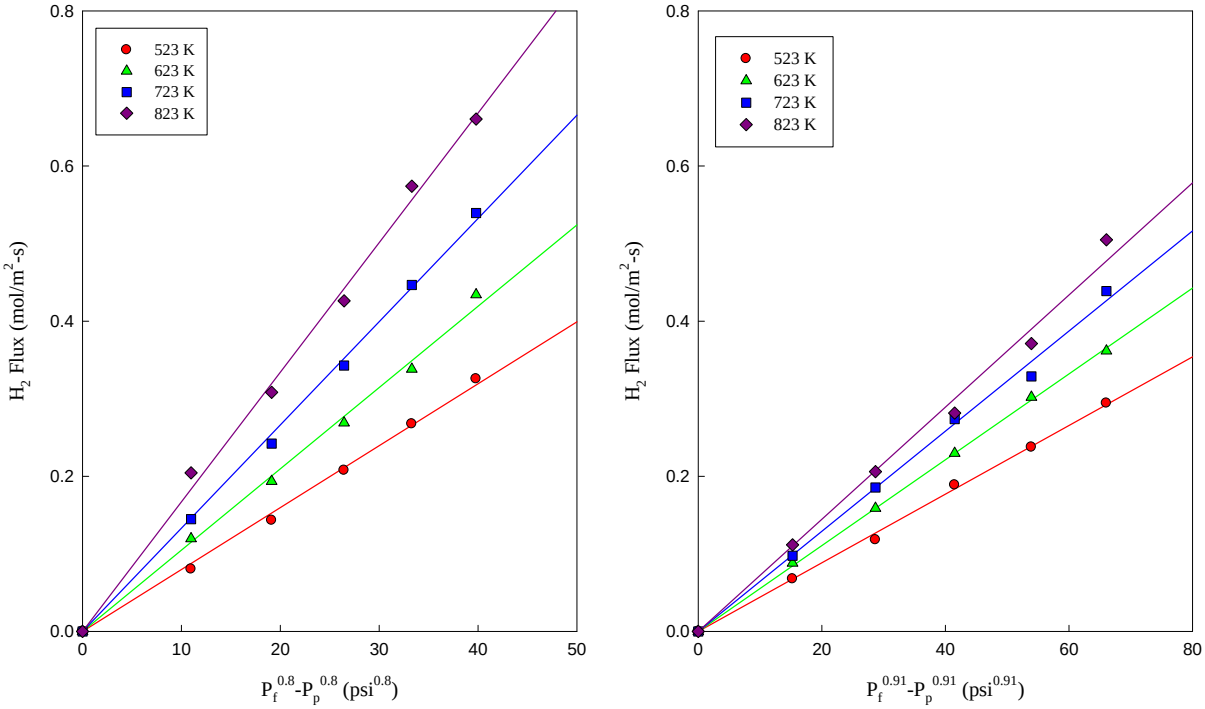

(a) Pd-Cu membrane (S2) (t = 16.73 μm)

(b) Pd-Cu membrane (C2) (t = 20.17 μm)

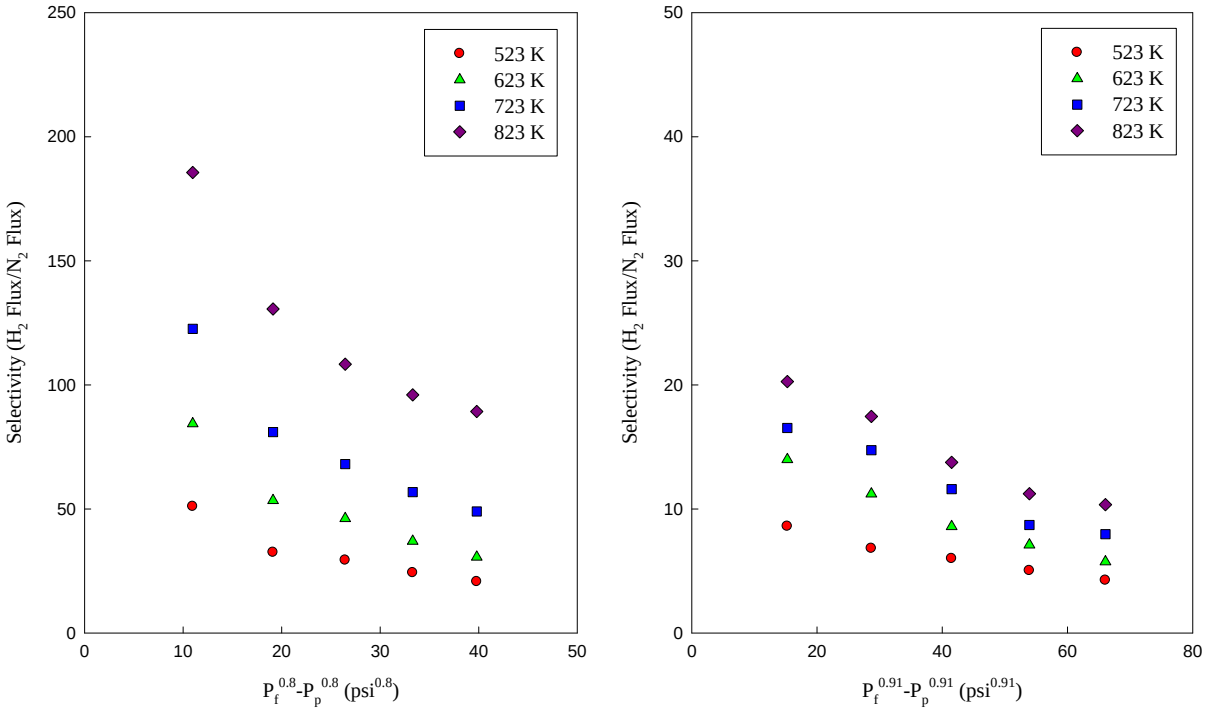

(c) Pd-Cu membrane (S2) (t = 16.73 μm)

(d) Pd-Cu membrane (C2) (t = 20.17 μm)

Figure 21. Hydrogen flux and H_2/N_2 selectivity data of Pd-Cu membranes fabricated by SIEP and CEP methods (post -HT).

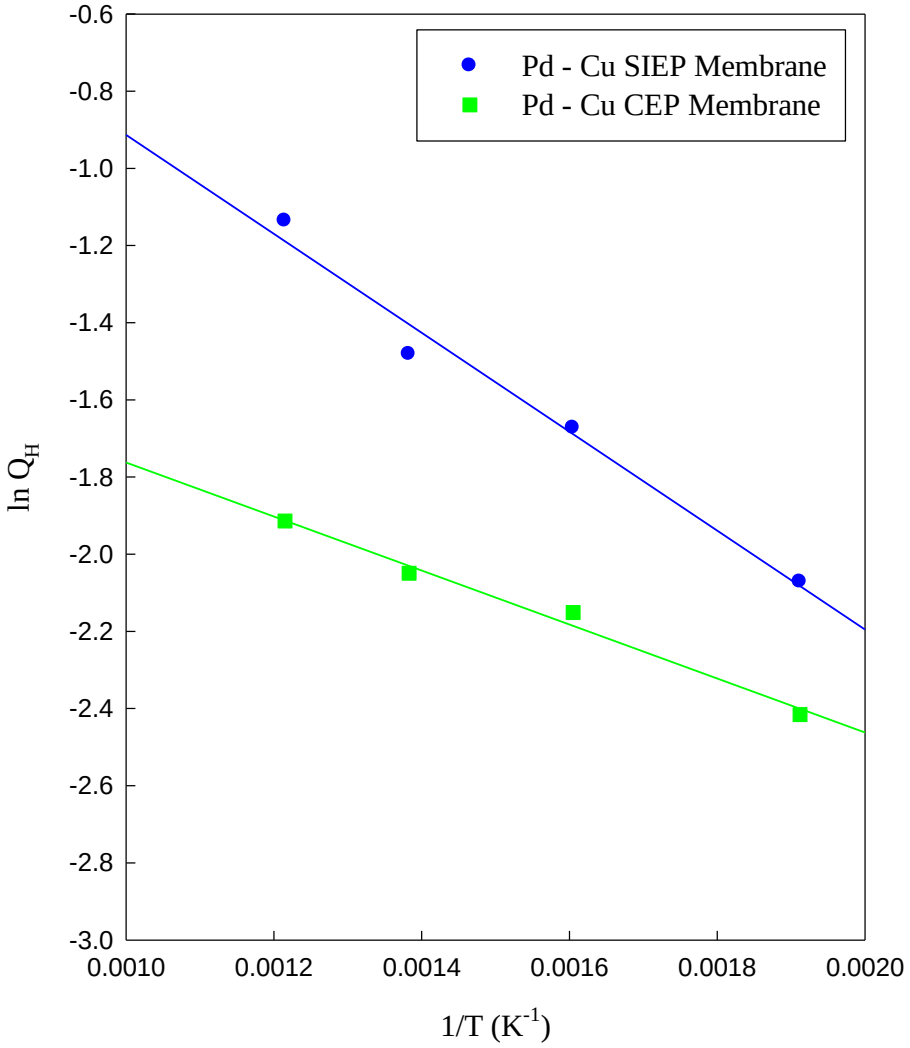

Figure 22. Arrhenius plots of H_2-permeability coefficients of Pd-Cu membranes fabricated by SIEP and CEP methods.

of the CEP Pd-Cu membrane (film thickness of 20.17 μm) was 5.82 kJ/mol. In our previous study we found the E values of the SIEP Pd membrane (film thickness of 7.68 μm) and SIEP Pd-Ag membranes (film thickness of 12.63 μm) as 16.88 and 11.93 kJ/mol, respectively [38-39]. These results are summarized in Table 8. We observed that, with increasing membrane film thickness, the activation energy decreases and consequently, the power index of Sieverts' law increases. A low value of the activation energy (<~30 kJ/mol) indicates that the surface phenomena of dissociative adsorption and recombinative desorption do not significantly influence the permeation process since they are characterized by a markedly higher activation energy (~54-146 kJ/mol) [48]. The reported activation energy may be viewed as "apparent activation energy" since the H_2-permeation in these membranes is contributed to more than one phenomenon.

The Pd-Cu membranes prepared by SIEP method were subjected to thermal cycling to check their performance. For a period of 90 days, H_2-flux of the membrane was recorded under thermal cycling of 573 - 873 - 573 K, at 10 psi pressure in on and off mode (8 to 10 h a day) in our permeability measurement setup. On each day of testing, the membrane underwent a couple of thermal cycles, and the average data of H_2 flux for each day are presented in Figure 23. The fluctuation in the hydrogen flux is attributed to the Pd-Cu alloying in progress (as discussed earlier in Figure 7). In this thermal cycling test, the membrane did not deteriorate and remained stable in terms of hydrogen permeability. Our recorded average H_2-fluxes were 0.0922 mol/m^2.s (standard deviation of 1.27%) and 0.13357 mol/m^2.s (standard deviation of 1.65%) at 573 K and 873 K, respectively.

Pd-Ag membranes by CEP and SIEP

Helium gas-tightness and film thickness analysis of Pd-Ag membranes

As discussed earlier, microstructure of Pd based membranes depends on a number of factors, such as, substrate surface roughness, fabrication technique and bath parameters. The use of different reducing agent and their concentrations also affects the reaction kinetics. Hence affects the surface microstructure and grain size distribution to some extent. For this work, we kept all those parameters (bath composition, bath parameters, surfactant and its concentration) to be constant in order to elucidate the effect of surfactant on the microstructure of the Pd and Pd-Ag films. In this study, a number of membranes Pd-Ag on MPSS have been fabricated by both SIEP and CEP process.

Table 8. Comparison of values of activation energy of different membranes fabricated by SIEP and CEP methods

Membrane film	Fabrication method	Membrane film thickness (μm)	Sieverts' law power index, *n*	Activation energy, *E* (kJ/mol)
Pd	SIEP	7.68	0.61	16.88
Pd-Ag	SIEP	12.63	0.75	11.93
Pd-Cu	SIEP	16.73	0.8	9.4
Pd-Cu	CEP	20.17	0.91	5.82

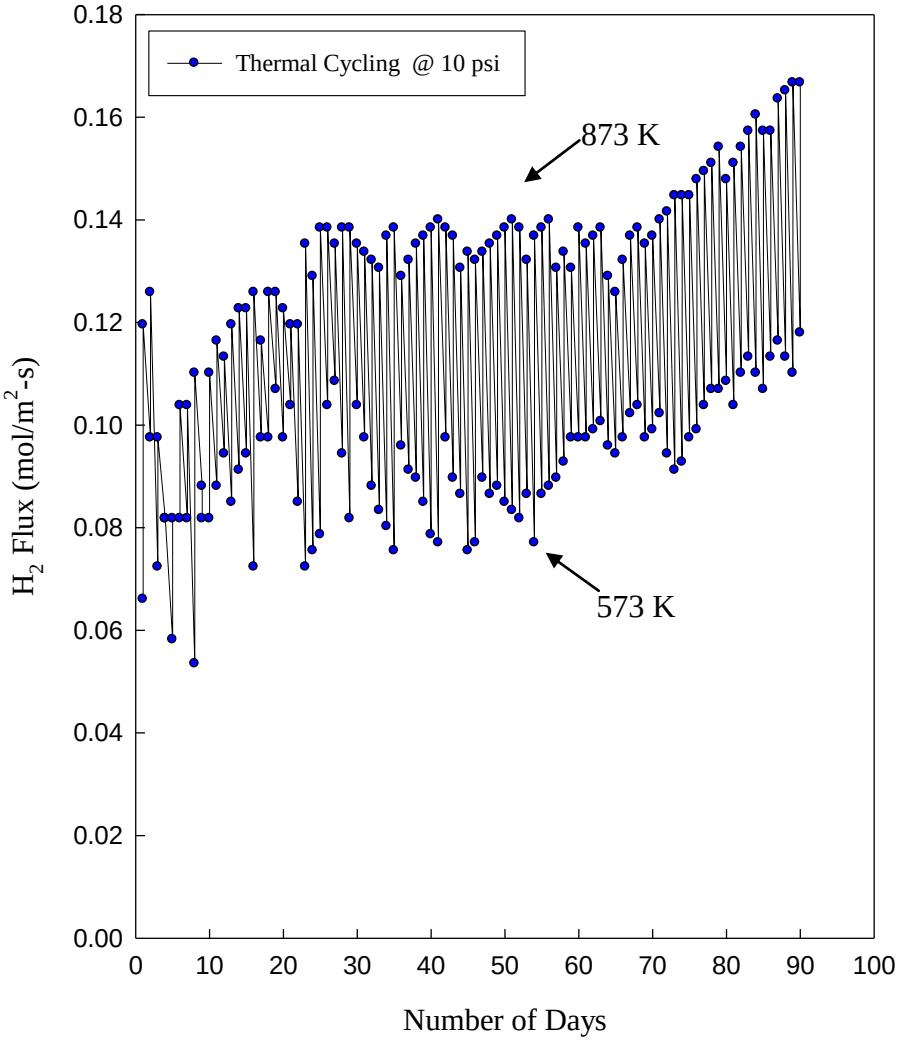

Figure 23. H_2 flux data of Pd-Cu MPSS membrane under thermal cycling fabricated by SIEP method.

Table 9 summarizes the basic characteristics of Pd and Pd-Ag membranes fabricated by SIEP and CEP process with a surfactant DTAB concentration of 4×CMC. The table provides data on electroless plating time, film thickness, metal composition, H_2 flux and selectivity for a number of Pd and Pd-Ag membranes. The membrane film thickness is calculated by both gravimetric and SEM analysis. For all these membranes, the calculated thicknesses by these two methods are very comparable. From Table 9, it is evident that the Pd membrane (SIEP) has a thinner film thickness of 7.89 µm (8.5 µm) compared to 27.5 µm (28.5 µm) prepared by CEP. This is in agreement with previous work [1]. Significant reduction in Pd-Ag film thickness (12.54 µm from 28.5 µm) was achieved with the use of surfactant. Helium leak test (Figure 24) confirmed that indeed SIEP is very effective in reducing membrane film thickness.

Microstructure analysis of Pd-Ag membranes

Pd and Ag are deposited on an activated surface by an autocatalytic SIEP process. Ag particles are being deposited on top of Pd particle layer in a sequential deposition process. The Ag particles tend to deposit on or around the Pd hills rather than depositing uniformly to the valleys. These fabrication differences along with the interaction with the dimensionally different Pd particles size make the surface rough. To investigate the particle size, surface roughness and grain boundary diffusion in detail, the SEM images were taken at magnifications of 5K, 10K, 20K and 40K as shown in Figure 25. The energy of the electron beam was chosen at 20kV and 15 kV, as lower beam energy give finer surface characteristics.

From the images, it can be inferred that two different particle sizes are dominating the grain size and the subsequent agglomeration. Higher magnification SEM images (20K and 40K) at even lower electron beam energy of 15 kV in Figure 25 shows the presence of two different size particles having two different mean grain sizes. As we gradually move to the higher magnification images, it is clear that there is similar grain boundary diffusion just beneath the top particle layer. For fabrication of Pd-Ag membrane, we followed the sequential SIEP process that ended with Ag deposition. This makes Ag to deposit only on the crest of the hills which ends up with an apparent increase in roughness of the film. Basically, for Pd-Ag film, it has a continuous grain boundaries diffused into one another just beneath the rough top layer (with different particle size). This is the combined effect of the interaction of Pd and Ag particles along with the sequential deposition mechanism.

Table 9. Summary of Pd and Pd-Ag membrane attributes fabricated by SIEP and CEP

Membrane Samples	Deposition time (hr)	Film thickness (μm)		Metal Comp. (% Ag)	H_2 Flux, mol/m^2-s at 723K		Selectivity at 723K (H_2 Flux/N_2 Flux)	
		Gravimetric	SEM analysis		40 psig	100 psig	40 psig	100 psig
Pd (A) 4CMC	14	9.3	8.35	0	0.23	0.50		
Pd (B) 4CMC	12	8.5	7.89	0	0.34	0.72	312[a]	230[a]
Pd-Ag (A) 4CMC	17	12.63	-	25±1	0.16	0.32	-	-
Pd-Ag (B) 4CMC	22	13.004	12.54	24±1	0.23	0.49	212	126
Pd-Ag (C) 4CMC	19	13.47	12.85	19±1	0.19	0.44	-	-
Pd-Ag (D) 4CMC	22	12.54	-	23±1	0.33	0.80	120	73
Pd 4CMC	10	8.5	8.5	-				
Pd 0CMC	28	28.5	27.5	-				
Pd-Ag (1) 0CMC	31	16.77	-	-	0.09	0.19	225	212
Pd-Ag (2) 0CMC	33	17.76	-	-	-	-	-	-
a. Temperature at 823 K								

21

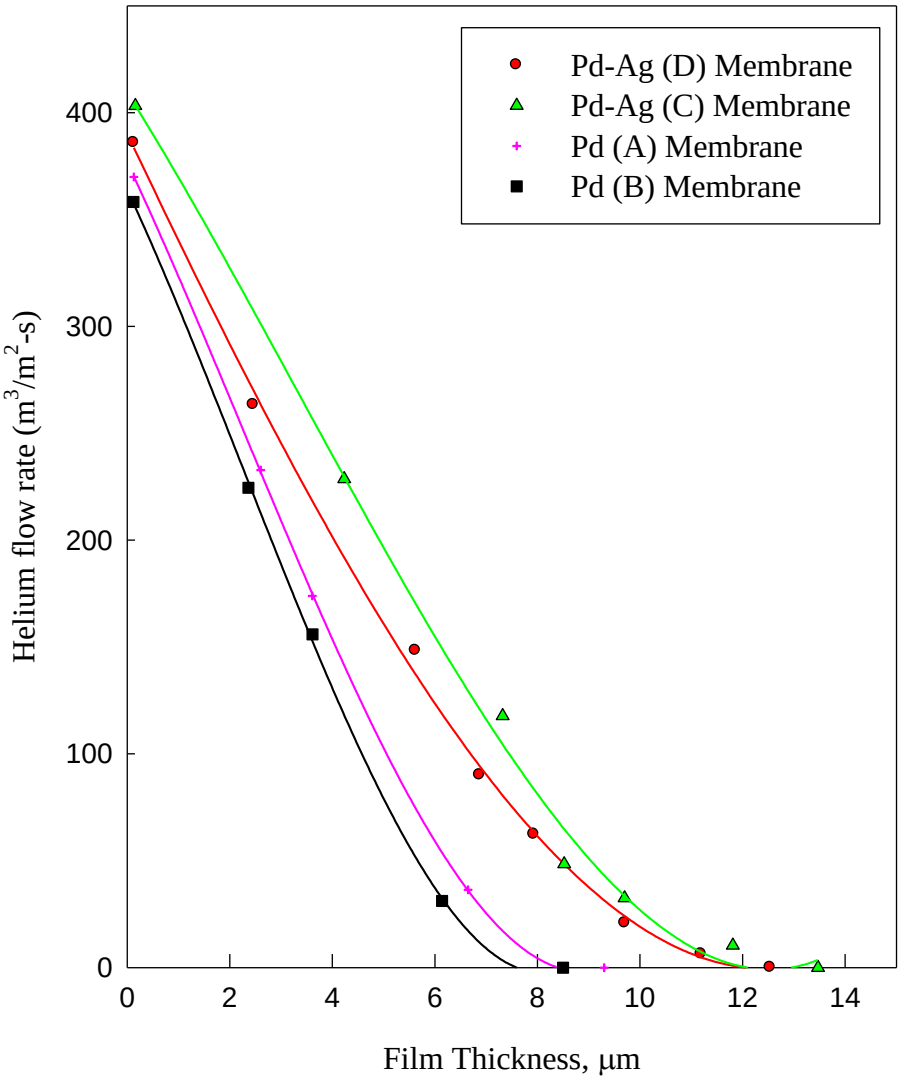

Figure 24. Helium gas-tightness as a function of membrane thickness for Pd and Pd-Ag membranes fabricated using surfactant DTAB at concentration of 4×CMC.

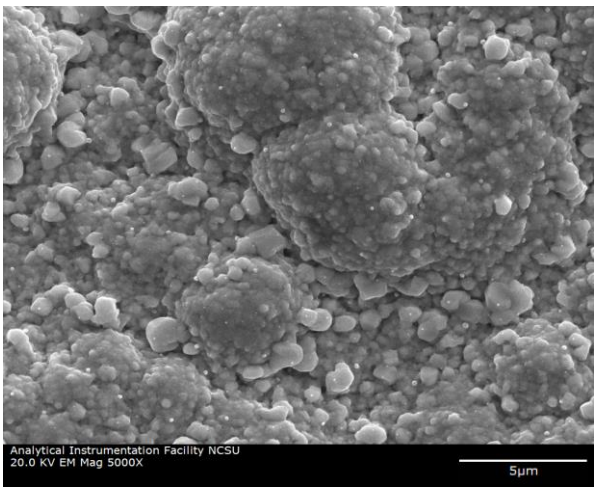

(a) Pd-Ag at 5K (20kV)

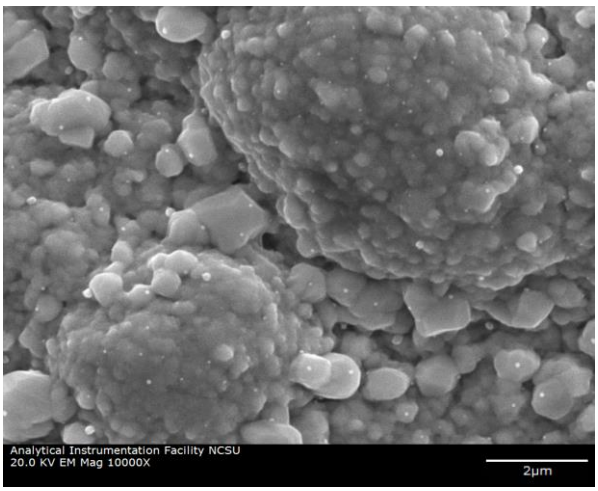

(b) Pd-Ag at 10K (20kV)

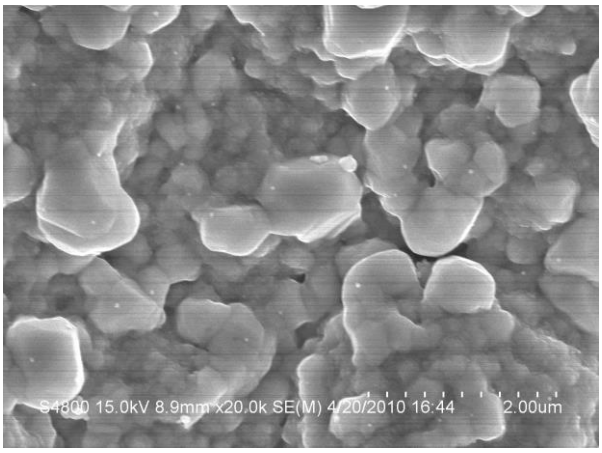

(c) Pd-Ag at 20K (15kV)

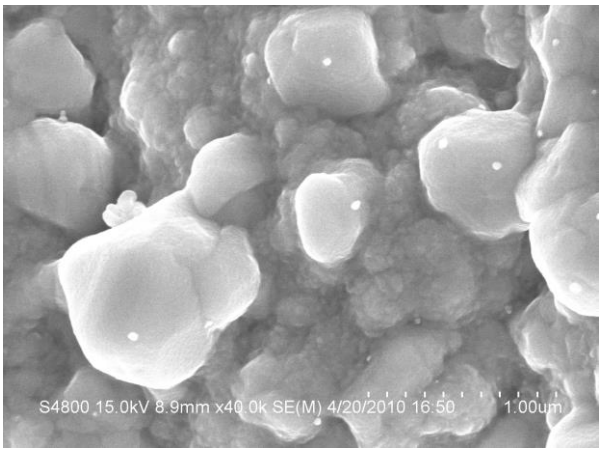

(d) Pd-Ag at 40K (15kV)

Figure 25. SEM images of Pd-Ag film top surface showing agglomerated grain growth throughout the surface just beneath the apparent rough top surface.

Figure 26 shows the grain size distribution of Pd and Ag in Pd-Ag membrane fabricated using DTAB at 4 CMC in SIEP. The average Pd grain size actually reduced to 2 μm in presence of DTAB at 4 CMC from an average particle size of 8 μm when DTAB was absent [1]. This result clearly suggests that the use of surfactant DTAB conclusively reduce the grain size considerably. In Figure 26, the particle size distribution of Pd and Ag shows two sharp peaks between 0.8 to 1.2 μm. The existence of the two peaks in Figure 26 indicates the presence of two separate process of Pd and Ag deposition in a sequential fabrication technique. Both peaks indicate the existence of two different mean size particles which is consistence with the SEM images presented in Figure 25.

In a sequential deposition cycle of Pd and Ag while fabricating Pd-Ag membrane, the cycle ends with Ag deposition. The presence of Pd particle in the earlier steps in a cycle, act as a deposition site and accelerate the Ag deposition. To control the metal composition of Ag in Pd-Ag membrane, it is required to control depositing Pd and Ag in a depositing cycle. Both Pd and Ag have to be deposited before the surface gets deactivated. That actually leaves some unused nucleation sites. Thus, Pd and Ag particles do not get enough particle aggregation into the grain to grow to its normal dimension. In Figure 26, it is evident that the mean dimension of the particles is lower in Pd-Ag membrane than that is for Pd-membrane.

After membrane fabrication, Pd-Ag membranes were heat treated in a gas tight diffusion cell. Pd-Ag membrane was heat treated for 18 h at 500 °C under H_2 environment at 1 atmospheric pressure. The temperature was chosen based on tamman temperature of Pd, Ag and substrate metal constituents. Tamman temperature for Pd and Ag are 640 °C and 345 °C respectively. For MPSS substrate it is 550-560 °C (Fe: 632 °C, Cr: 817 °C & Ni: 632 °C). To minimize Fe and other support metal diffusion into the Pd and Pd-Ag film, a temperature of 500 °C was chosen which is in between Ag and MPSS tamman temperature. This annealing temperature eventually gave us a film which was almost free from substrate constituent metals. This actually offered an opportunity to study the change in microstructure which has a minimum influence of Fe, Cr and Ni.

The SEM images of Pd-Ag membrane fabricated by SIEP method at different resolutions is presented in Figure 27 at pre-HT and post-HT conditions. From these SEM images it is quite clear, as we move to higher electron beam energy, the details of the minute surface morphology is lost. On the other hand, moving to lower energy we lost the organization of the grains and

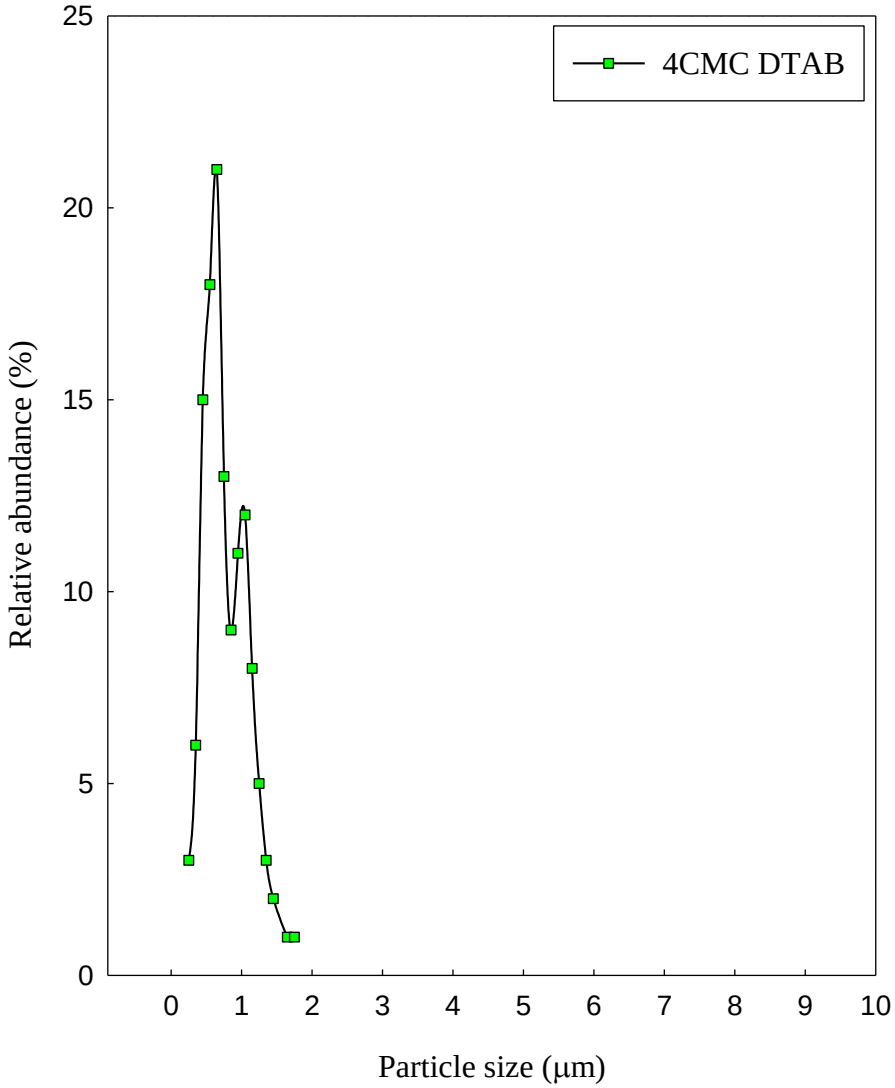

Figure 26. Pd and Ag grain size distribution observed in Pd-Ag membrane fabricated by SIEP process with 4CMC DTAB.

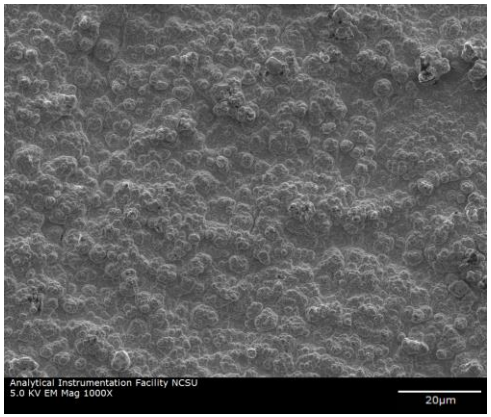

(a) Pd-Ag Pre-HT:1K (5kV)

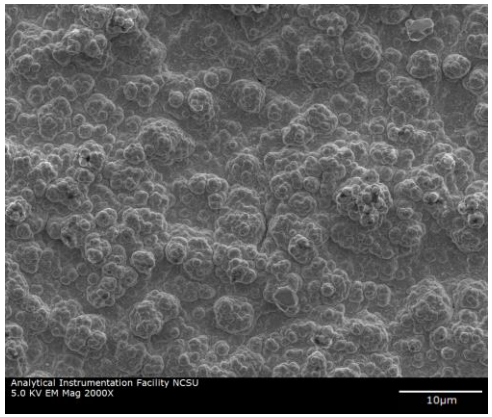

(c) Pd-Ag Pre-HT:2K (5kV)

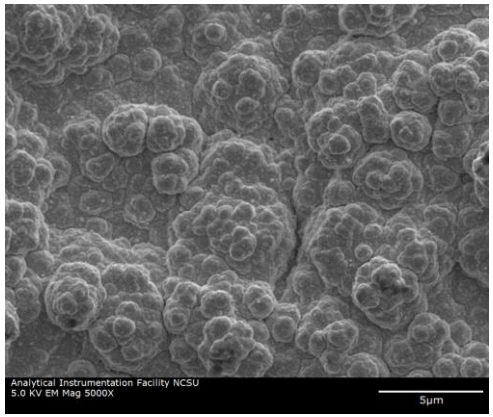

(e) Pd-Ag Pre-HT:5K (5kV)

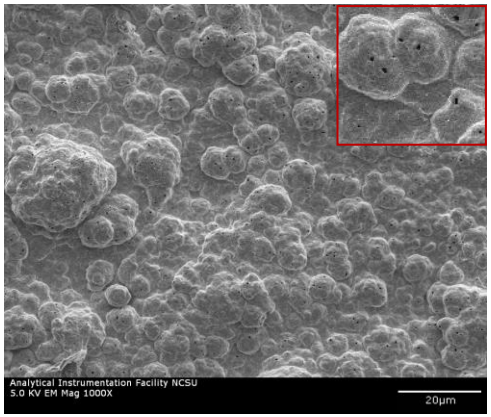

(b) Pd-Ag Post-HT:1K (5kV)

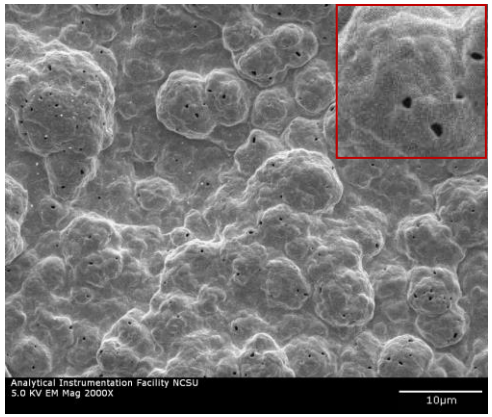

(d) Pd-Ag Post-HT:2K (5kV)

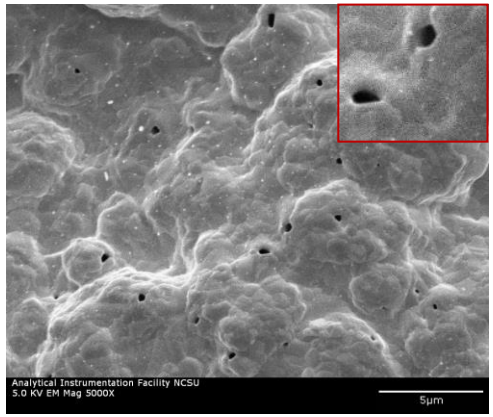

(f) Pd-Ag Post-HT:5K (5kV)

Figure 27. SEM images of top surface of Pd-Ag membranes fabricated by SIEP method a pre- and post-HT (heat treatment) conditions at different resolution showing grain agglomeration.

diffusion of grain boundaries. So for the kind of surface and the particle size that is dealt in membrane fabrication, it is a critical requirement to capture low energy (5kV) SEM images.

Figure 27 depicts a representative surface morphology for Pd-Ag membrane at pre- and post-annealing conditions. Clearly, it is recognizable from the images that the smaller grains agglomerated into forming larger grains with recognizable boundaries after annealing (Figure 3 for Pd membrane). In Pd membrane there is Pd particle only and Fe diffusion was carefully prevented into the Pd film during heat treatment. Therefore, annealing temperature helps orienting the Pd particles to form large clusters between them. As a result, a great extent of grain agglomeration is achieved after heat treatment. A similar effect is observed for Pd-Ag membrane which is shown in Figure 27. Throughout the surface, the dimension of the agglomerated grains increased by 2 to 5 times after heat treatment. During the heat treatment of the Pd-Ag film, Ag particles diffused into the Pd layers forming homogeneous alloys of larger clusters.

As stated earlier, DTAB is hydrophobic in nature and aligned them around gas-liquid interfaces and form various cylindrical and spherical cage like structure. Surfactant also tends to form meta-stable structure in the solid-liquid interfaces that helps finer grain formation and subsequent coarsening of the grain. The surface topography was examined with AFM and presented in Figure 28 for Pd-Ag-MPSS surface. The surface roughness of the Pd-Ag-MPSS was observed to be higher (160 nm) and the surface is largely agglomerated. The cage like structure in Pd-Ag-MPSS surface is hard to recognize. This may be because of the interaction of different size of particles and different deposition mechanism of the metals.

Surface elemental analysis was carried out by X-ray diffraction (XRD) and energy dispersive spectroscopy (EDS). Typical EDS pattern of Pd-Ag film fabricated using DTAB surfactant is presented in Figure 29. The EDS of Pd-Ag film shows the intense peaks for Pd and Ag. In the EDS spectrum, it is difficult to distinguish Pd and Ag peaks [3]. However, quantitative EDS elemental analysis of Pd-Ag film shows 24% Ag as presented in Figure 29. The target metal content was 23%, which means we are going to lead to a membrane composition representative to the target. As Pd and Ag are placed next to each other in the periodic table, both metals give sharp peak nearly at the same place. An escape peak for Pd at approximately 1.5 Kev X-ray energy is always observed when Pd is involved in the analysis. However, no

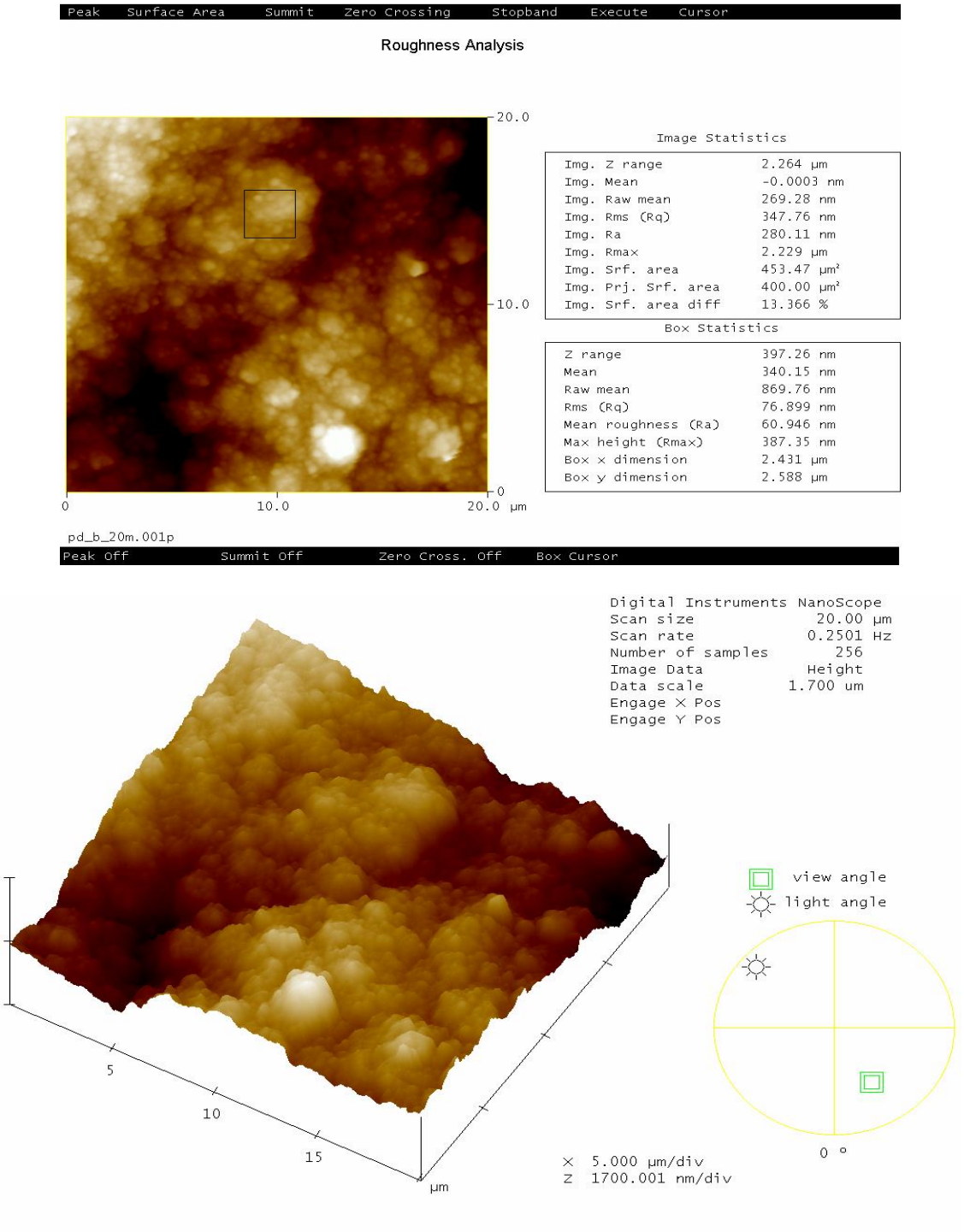

Figure 28. AFM images of solid Pd-Ag surface aggregation onto typical MPSS surface with DTAB.

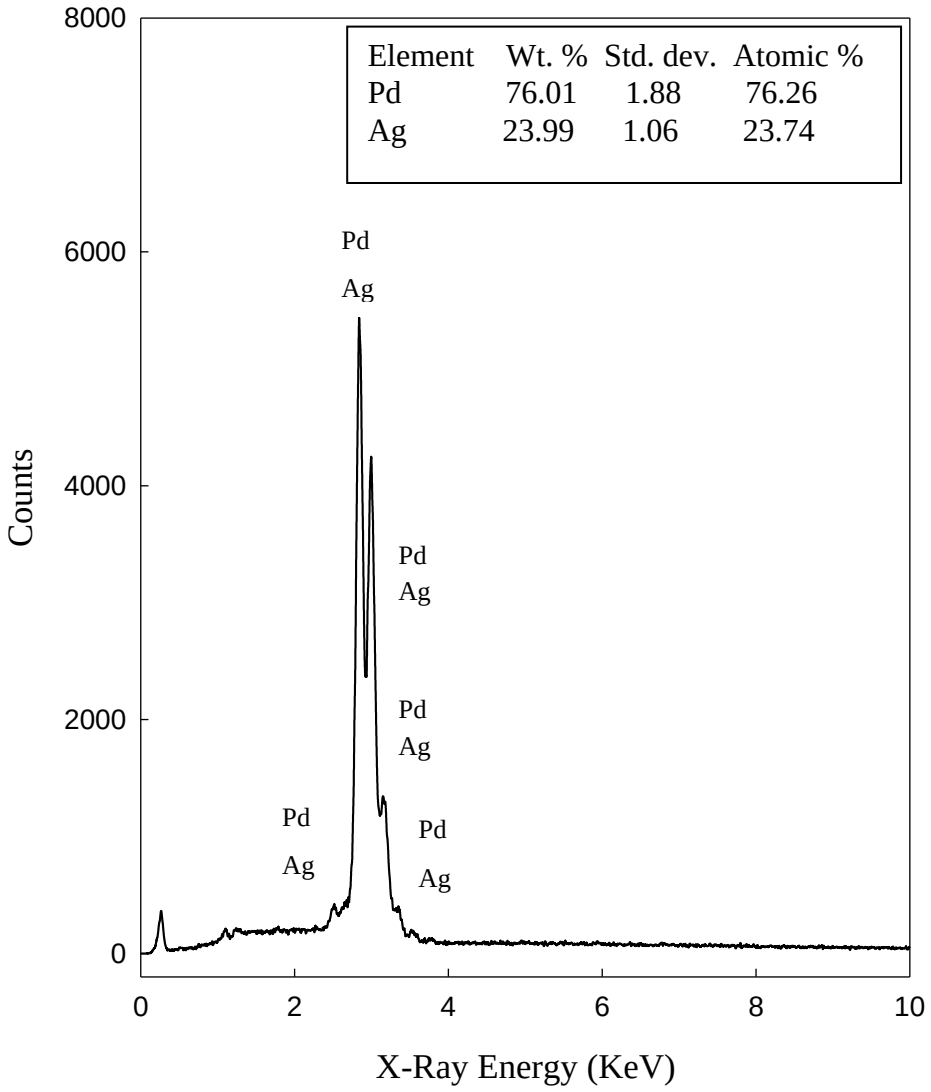

Figure 29. Typical EDS spectrum for Pd-Ag membrane shows the polycrystalline deposition of Pd and Ag particles.

impurities were observed from the EDS spectrum. The EDS patterns demonstrate a representative membrane of target composition. This also implies that the use of surfactant DTAB in the EP solution bath does not introduce any impurities in the membrane film.

In Figure 30, three XRD patterns (before annealing, after 10 h of annealing and after 18 h of annealing) are shown for Pd-Ag membrane. The XRD patterns taken after 10 h of annealing indicate that the alloying of the Pd-Ag layer is not complete (Figure 30b). Indeed Pd and Ag peaks shifts into the middle and shoulders appeared at the characteristics planes [111], [200] and [220]. These shifts of peaks and shoulder formation indicate the co-existence of pure Pd and Ag phases with a Pd rich Pd-Ag alloy phase [5, 6]. Annealing in the same condition for a total 18 h, a single phase f.c.c Pd-Ag alloy is observed at the characteristics planes (Figure 30c). However, the reflection peaks for single phase f.c.c Pd-Ag alloy is found in between pure Pd and Ag peaks at 2θ of 39.925, 46.434 and 67.767 for {111}, {200}, and {220} planes, respectively. Table 10 lists the 2θ and d-spacing values corresponding to the three major reflection peaks [111], [200] and [220]. Using Brag's law, the lattice parameter was calculated and was found 4.10 Å which was 4.08 Å for pure f.c.c Ag. Evidently this is an indication that the observed increase in the Ag cluster size was associated with the lattice expansion of the Ag metal. These results are in good qualitative agreement with the literature which indicates an annealing temperature of 500 °C or above is required to get a homogeneous alloy [7].

A detail study of the SEM cross-section of Pd-Ag-MPSS membrane by EDS analysis was carried out to understand the behavior of metal deposition deep inside the pores. The pores in MPSS substrate are interconnected and tortuous in nature. As an example, in Figure 31(a), we probed six locations across a depth of 50 μm for Pd and Ag. Metal deposition was found in the pore walls very deep inside the substrate and film interphase. The Pd and Ag metal contents in these pores are shown in Figure 31(b) by a bar graph. The Ag metal was found in pores at a distance of 20-50 μm inside the interphase. However, Ag metal content inside the pores decreases across the depth, which is expected.

To understand metal depositions, Pd-Ag film cross-section at different locations was examined by EDS line-scanning (Figure 32). As the EDS probe approaches the interface from the far side of the substrate, Pd and Ag peaks jumps to their maximum and Fe, Cr and Ni peaks drops sharply. To understand the relative amount of each metal in the Pd-Ag film, EDS elemental analysis was taken on the substrate. The composition of the substrate was found to

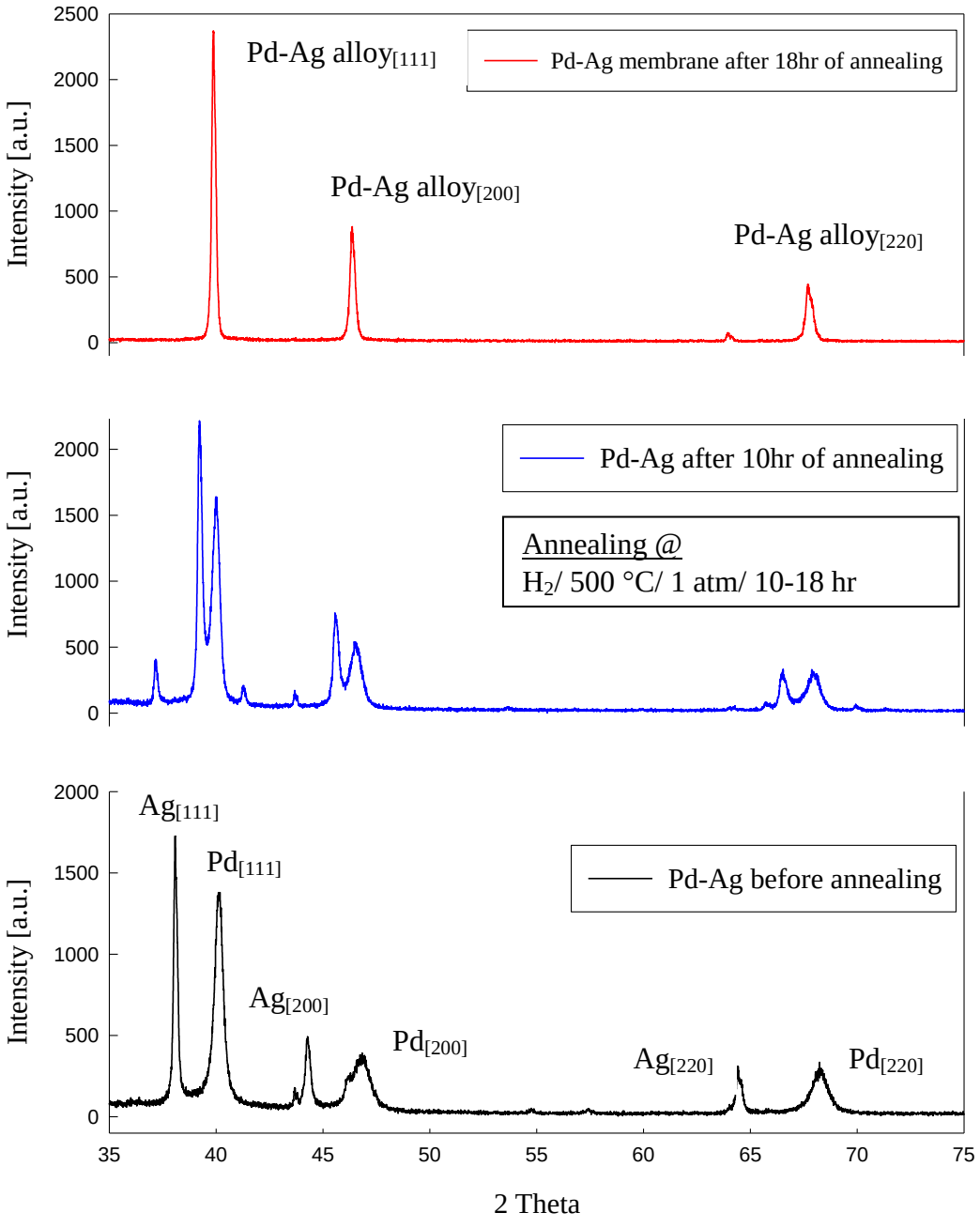

Figure 30. Effect of heat treatment on XRD pattern of Pd-Ag membrane fabricated by SIEP process.

Table 10. Comparison of high angle XRD reflection peaks of Pd- and Pd-Ag-film fabricated by SIEP process

	Bravais lattice	Pd-film		Pd-Ag-film		
		Pd (Pre annealed)	Pd (Post annealed)	Pd (Pre annealed)	Ag (Pre annealed)	Pd-Ag (Post annealed)
2-theta	111	40.214	40.109	40.119	38.115	39.925
	200	46.776	46.652	46.664	44.299	46.434
	220	68.303	68.107	68.128	64.443	67.767
	311	82.338	82.086	82.111	77.392	81.647
d-spacing	111	2.2407	2.24635	2.24578	2.35917	2.25628
	200	1.9405	1.9454	1.9449	2.0431	1.954
	220	1.37214	1.37561	1.37525	1.44469	1.38169
	311	1.17017	1.17312	1.17282	1.22204	1.17831
Lattice parameter, a		3.881	3.8908	3.8898	4.0862	3.98
Lattice structure		FCC	FCC	FCC	FCC	FCC

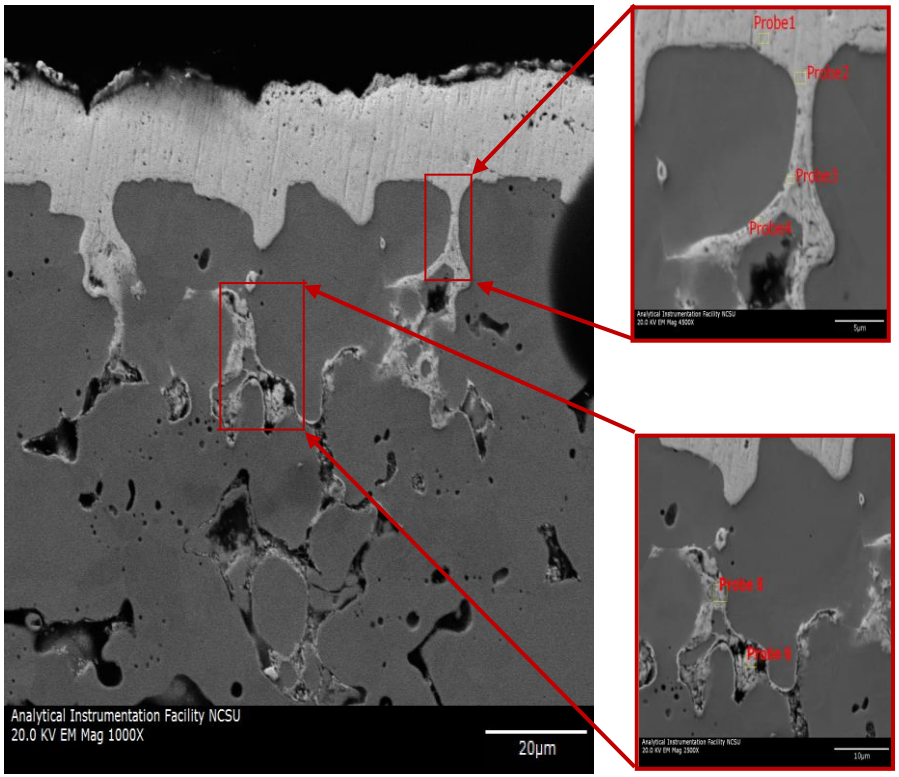

(a) Location of pores for EDS analysis

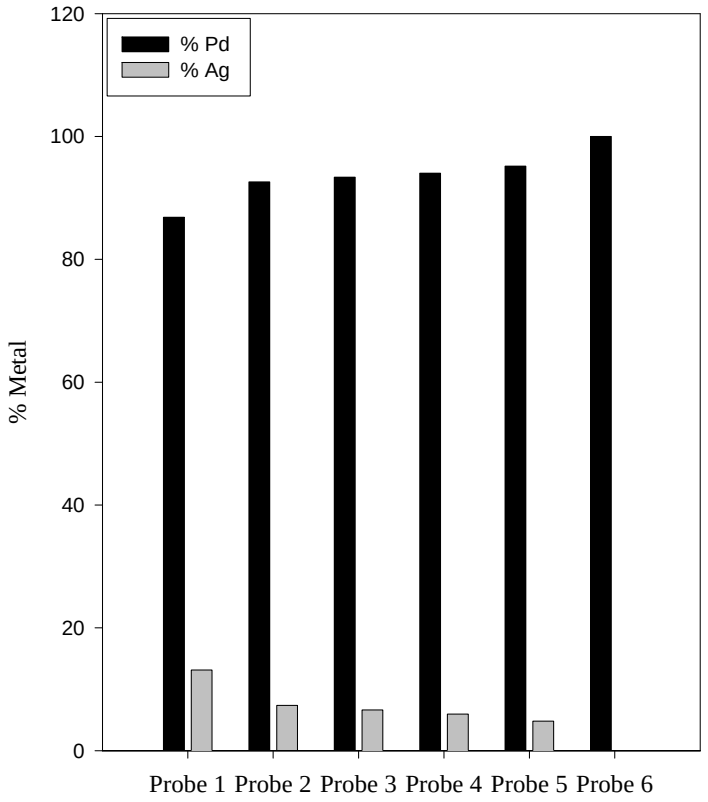

(b) Metal distribution in pores

Figure 31. SEM images of Pg-Ag film from Pd-Ag membrane cross-section: (a) showing the locations of EDS for metal deposition behavior analysis; (b) Metal (Pd and Ag) distribution during deposition in the pores starting from the pore mouth to the very deep inside (From Probe 1 →Probe 6).

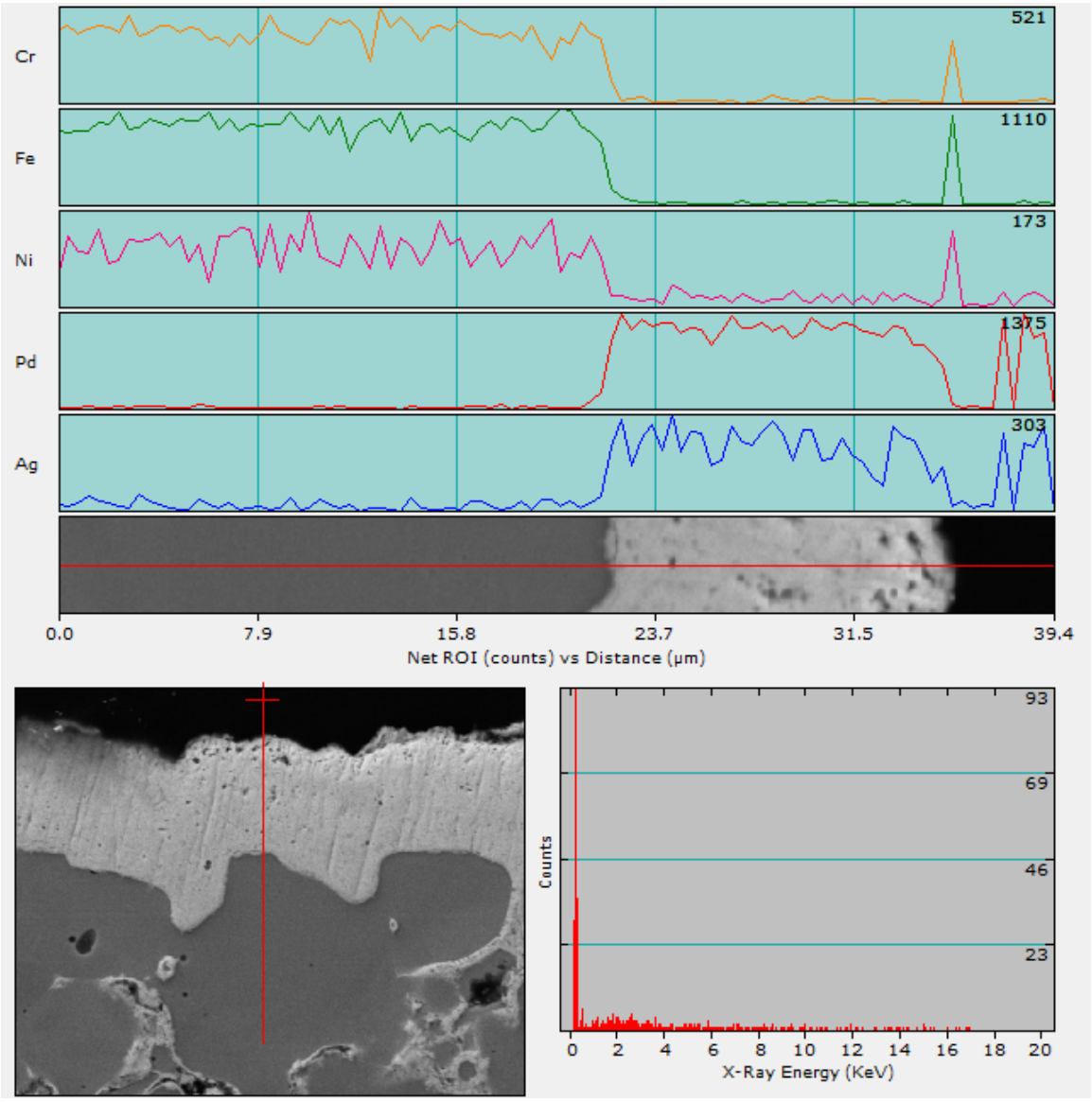

Figure 32. EDS line scanning of Pd-Ag-film cross section [Scanning length 40 µm, scanning direction from (a) → (b)].

68.73, 16.38, 11.38, 2.52 and 0.79% by weight for Fe, Cr, Ni, Mo and other trace metals, respectively. Based on the X-ray counts on the line scanning, Ag content in the film was found to be 20.5% which is little lower than the target (24% Ag). A repeated rise and fall of the X-ray counts are observed representing the sequential deposition. The oscillation of X-ray counts is prominent for Ag as the Ag content is low in each deposition cycle. Being the minor constituent, Ni has the background effect and oscillates more as confirmed by EDS mapping. However, sharp peaks for Fe, Cr and Ni (sharp trough for Pd and Ag) at the end of Pd-Ag film are observed. This could be the response from a fine SS particle which is doped in the film or in the resin where the sample was mounted for scanning. It is to be noted that during the sample preparation after cutting, membrane pieces are mounted in the resin and then the resin is dried up. The top part is polished with polishing metals to expose the membrane cross-section from the resin. As the Pd-Ag-alloy film and polymer matrix are soft, some SS particle from the substrate might get separated and are doped into the film.

H_2-permselectivity studies of Pd-Ag membranes

Pd-Ag membranes on MPSS substrate fabricated by d SIEP and CEP processes were tested for gas-tightness and hydrogen perm-selectivity in our permeability measurement set-up. The thickness of the Pd-Ag-film on MPSS support was found to be about 12.54 μm as determined by weight gain method. The gas-tightness was measured using helium as the permeating gas through the membrane. Hydrogen permeance was found to be 29 m^3/m^2.hr at 140 kPa and 450 °C for Pd-Ag membrane. Under these conditions, selectivity of hydrogen over nitrogen was about 412. This suggests that the Pd-Ag-MPSS membrane fabricated by DTAB induced SIEP was extremely gas-tight and essentially defect-free at 12.54 μm Pd-Ag film thicknesses.

Pd- and Pd-Ag-MPSS membranes fabricated by SIEP were tested for hydrogen flux in the temperature range of 250^{o}C to 550^{o}C to evaluate the transport mechanism. Hydrogen flux and selectivity for Pd-Ag membrane fabricated by CEP was also tested as a comparison. The measured data as a function of pressure difference $(P_f - P_p)$ at 250^{o}C, 350^{o}C, 450^{o}C and 550^{o}C are presented in Figure 33 for Pd- and Pd-Ag membranes fabricated by SIEP. The lines drawn in the figure are non-linear least-square fit with a power index, $n = 0.83$ for Pd-MPSS and $n = 0.85$ for Pd-Ag-MPSS membrane. These values are slightly higher than Sieverts' law index. The flux data in the Figure 33 show that with increasing temperature, hydrogen flux increases for a given

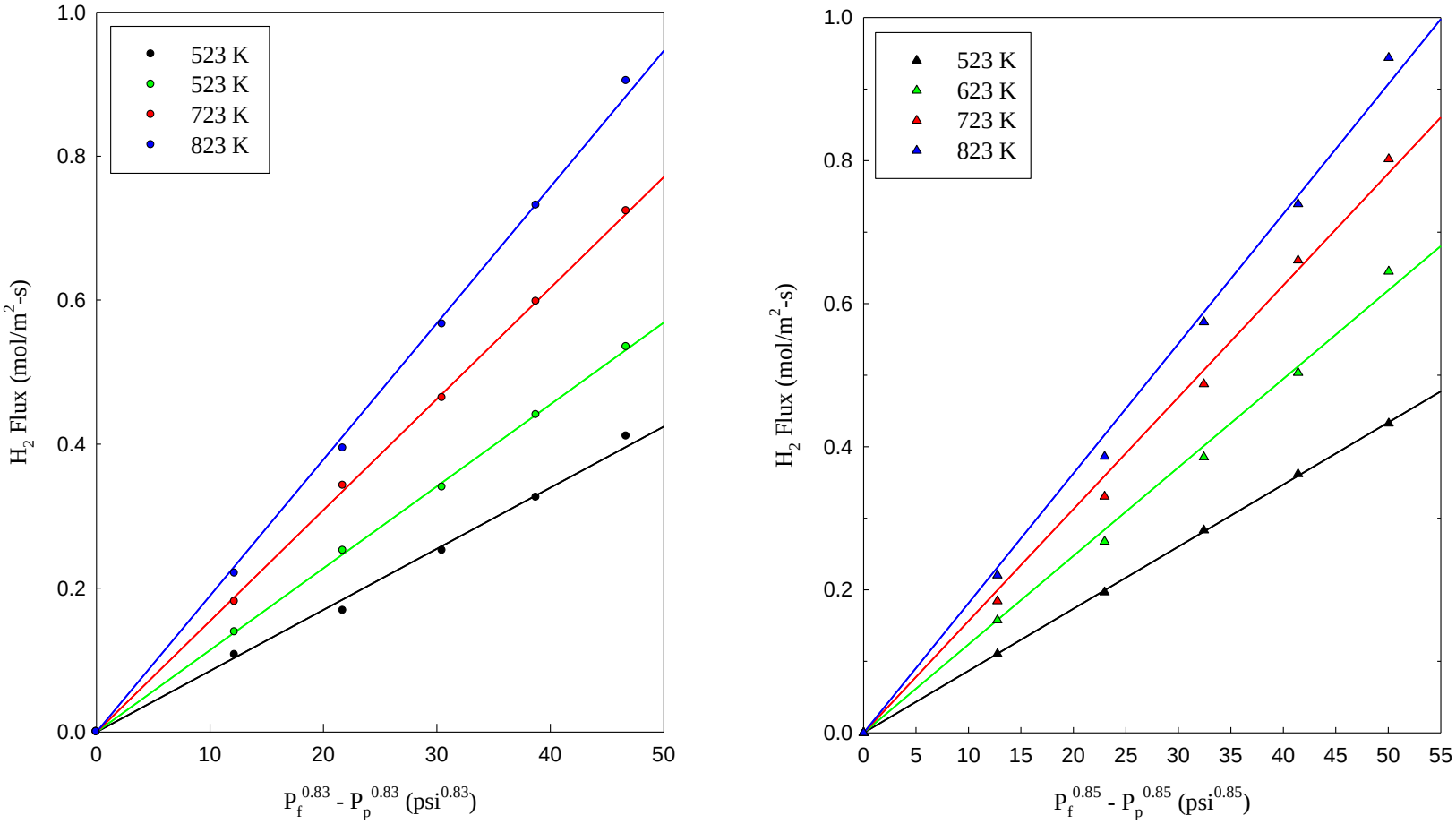

Figure 33. Hydrogen flux data of Pd and Pd-Ag-MPSS membranes fabricated by SIEP at different temperatures.

transmembrane pressure difference. Further, the hydrogen flux increases with increased pressure drop across the membrane. Figure 34 shows the hydrogen-to-nitrogen selectivity results of the same membrane.

A value of *n* greater than 0.5 may result when surface processes influence the permeation rate [16]. The hydrogen diffusivity may become dependent on concentration of dissolved hydrogen and that may contribute to n values greater than 0.5 [4]. Leakage of hydrogen through defects in the metal film or membrane seals may also increase the value of *n*. Further, small resistance of the MPSS membrane support may also slightly increase the value of *n*. The deviation in the observed flux data from the idealized Sieverts' law may be attributed to some of the contributing factors just discussed. From gas-tightness experiment, we are inclined to conclude that the Pd-MPSS (8.5 μm pd-film thickness) and Pd-Ag-MPSS membrane (12.54 μm Pd-Ag-film thickness) fabricated by DTAB induced SIEP is very much defect free. But, heat treatment produces pinholes which actually reduces the effective thickness of the perm-selective film. This might make hydrogen dissociation and adsorption a rate limiting step. Alternatively, it could result in an increase pressure exponent at high pressure.

The computed permeability coefficients (Q_H) at four temperatures are shown in Figure 35 as Arrhenius plot $(Q_H \text{ vs } 1/T)$ for Pd-MPSS and Pd-Ag-MPSS membranes. It gives an excellent fit of the data to Arrhenius equation. We found, E_{Pd} = 9.8 KJ/mol and $E_{Pd/Ag}$ = 8.85 KJ/mol. The activation energy for Pd- and Pd-Ag-film is lower than the reported results in literature. For Pd membrane, previously reported activation energy 14.45 KJ/mol for 17μm Pd film on ceramic substrate [16], 19.7 KJ/mol was reported for a different membrane [13] and 23 KJ/mol for 0.3 μm Pd-Ag film on ceramic support [17-18]. For the latter case, since the hydrogen-to-nitrogen selectivity was reported as low as 5.7, it is difficult to assess the membrane quality. Furthermore, hydrogen fluxes were studied in the temperature range of 100-250 °C. Reduction of the particle size in the film thickness and fabrication of an agglomerated microstructure may have the influence in reducing the activation energy for the membranes. As nanocrystalline palladium has almost 10 times higher diffusivity than conventional polycrystalline Pd. In small nanocrystalline metal, at least 20 to 50 % of its atom located in the grain boundaries act as a network for faster diffusion.

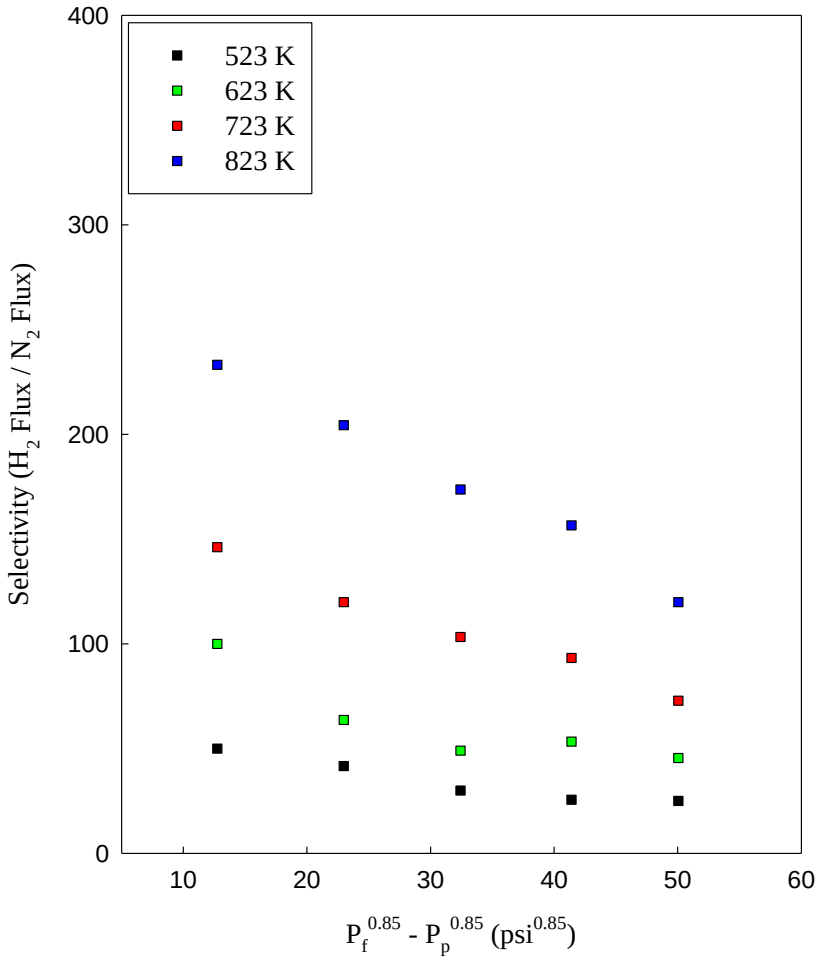

Figure 34. Hydrogen to nitrogen selectivity at different temperatures in Pd-Ag-MPSS membrane fabricated by SIEP.

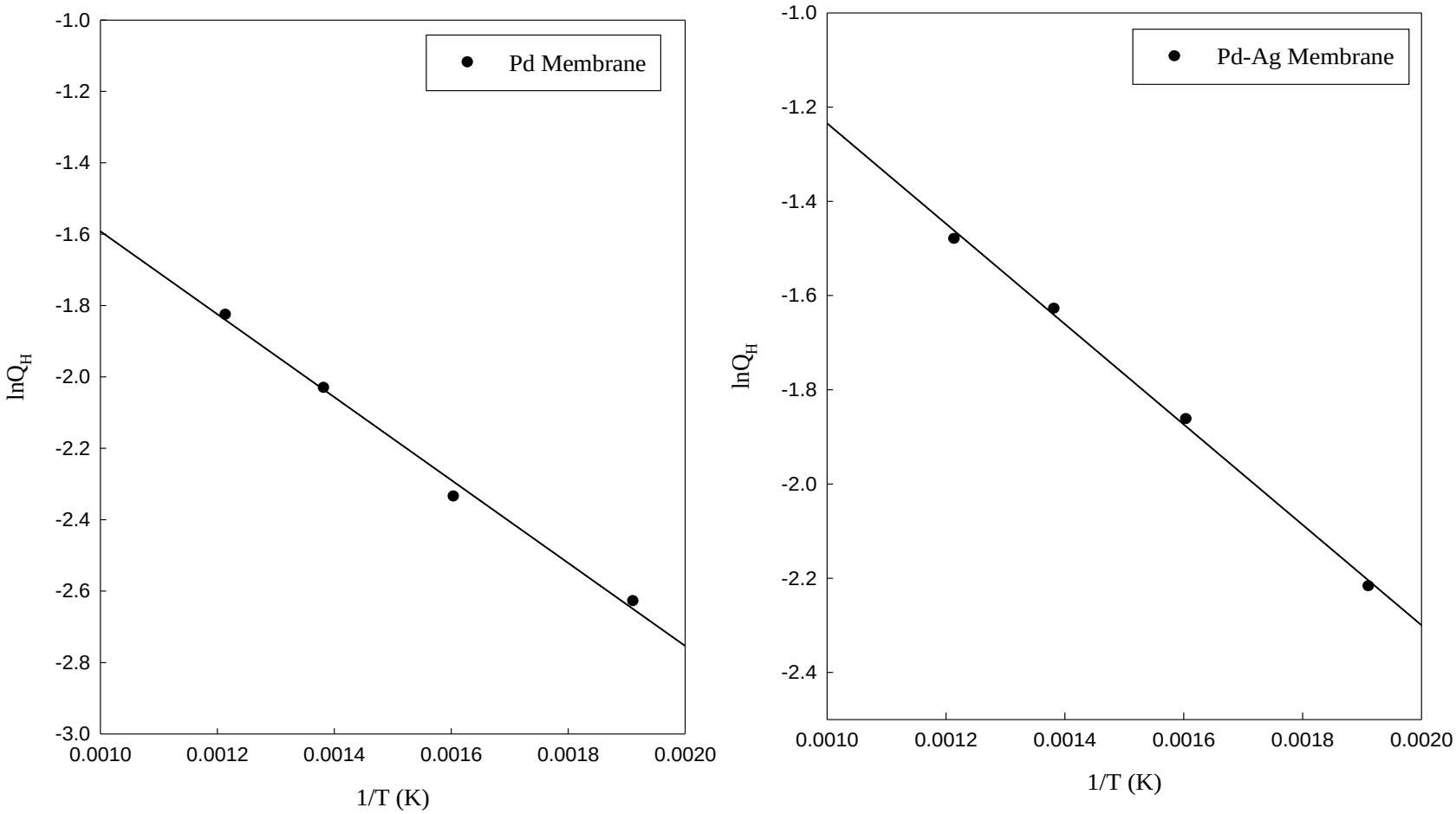

Figure 35. Arrhenius plot of H_2-permeability coefficients of (a) Pd-MPSS membrane and (b) Pd-Ag-MPSS membrane.

CONCLUSIONS

Defect free, dense and thin film Pd, Pd-Cu and Pd-Ag membrane can be fabricated by using surfactant DTAB at a concentration of 4CMC in electroless plating bath. Surfactant in effectively removes N_2, NH_3 etc gases from the substrate surface and increases the deposition rate. These two factors help uniform deposition and forms significantly reduced film thickness in a shorter time. The average grain sizes of Pd-films by SIEP and CEP methods were found to be 0.47 and 8 μm, respectively. In a sequential deposition, surfactant is capable to configure a film of grain size distribution of 0.8 to 1.2 μm for Pd-Ag membrane, while grain size distribution of Pd-Cu membrane was found to be 0.65 to 1.01 μm. Moreover, surfactant successfully protects dendrite formation and the grains are found to be largely agglomerated. Most importantly, microstructure and film thickness of similar characteristics is reproducible using SIEP. A uniform alloy of Pd-Ag and Pd-Cu is possible above 500°C under H_2 environment at 1 atmospheric pressure. The effectiveness of the surfactant DTAB over reducing the mass transfer resistance in and around the pore was confirmed by investigating the pores. Smaller particle size and grain agglomeration combined with the reduction of film thickness hugely enhances H_2 permeability. This also reduced the activation energy significantly for Pd, Pd-Cu and Pd-Ag membranes.

The membranes fabricated by the SIEP and CEP methods displayed significantly different hydrogen transport behaviors after heat treatment. Pd-MPSS membrane fabricated by SIEP under thermal cycling (573 - 723 - 573 K) at 15 psi pressure drop for 1200 hours was found to be thermally stable and retained H_2-permeability and selectivity. The H_2-flux and selectivity of the CEP Pd-Cu membrane were found to be insensitive to annealing process. On the other hand, the SIEP Pd-Cu membrane showed remarkable flux and selectivity enhancement upon heat treatment. The long-term (for a period of 90 days) thermal stability data demonstrated that the SIEP Pd-Cu membrane was very stable in rigorous exposure to low and high temperature thermal cycling.

The newly developed SIEP method is capable of fabricating defect-free, robust Pd and Pd-alloy membranes on MPSS support with favorable hydrogen perm-selectivity compared membranes fabricated by CEP method.

ACKNOWLEDGMENTS

This research was sponsored by the Pittsburgh Energy Technology Center, U.S. Department of Energy, under Award No. DE-NT0001473. Mr. Richard Dunst, NETL, Pittsburgh, PA is the DOE Project Officer. However, any opinions, findings, and conclusions, or recommendations expressed herein are those of the author and do not necessarily reflect the views of the DOE. Analytical support from the Center for Advanced Materials and Smart Structures (CAMSS) of North Carolina A&T State University is gratefully acknowledged with special thanks to Drs. Jag Sankar, D. Kumar and Zhigang Xu.

REFERENCES

[1] S.-E. Nam and K.-H. Lee, "Hydrogen separation by Pd alloy composite membranes: introduction of diffusion barrier," *Journal of Membrane Science,* vol. 192, pp. 177-185, 2001.

[2] R. Kirchheim, T. Muetschele, W. Kieninger, H. Gleiter, R. Birringer, T. D. Koble, "Hydrogen in amorphous and nanocrystalline metals," *Materials science and engineering,* vol. 99, pp. 457-462, 1988.

[3] H. Gleiter, "Nanocrystalline materials," *Progress in Materials Science,* vol. 33, pp. 223-315, 1989.

[4] S. Uemiya, Sato, N., Ando, H., Kude, Y., Matsuda, T. and Kikuchi, E., "Separation of hydrogen through palladium thin film supported on a porous glass tube," *Journal of Membrane Science,* vol. 56, pp. 303-313, 1991.

[5] S.-E. Nam and K.-H. Lee, "Preparation and characterization of palladium alloy composite membranes with a diffusion barrier for hydrogen separation," *Industrial & Engineering Chemistry Research,* vol. 44, pp. 100-105, 2005.

[6] D.-W. Kim, Y. J. Park, J.-W. Moon, S.-K. Ryi, and J.-S. Park, "The effect of Cu reflow on the Pd-Cu-Ni ternary alloy membrane fabrication for infinite hydrogen separation," *Thin Solid Films,* vol. 516, pp. 3036-3044, 2008.

[7] H. Gao, Y. S. Lin, Y. Li, and B. Zhang, "Chemical stability and its improvement of palladium-based metallic membranes," *Industrial & Engineering Chemistry Research,* vol. 43, pp. 6920-6930, 2004.

[8] X. Li, T. M. Liu, D. Huang, Y. Q. Fan, and N. P. Xu, "Preparation and characterization of ultrathin palladium membranes," *Industrial & Engineering Chemistry Research,* vol. 48, pp. 2061-2065, 2009.

[9] F. Roa, M. J. Block, and J. D. Way, "The influence of alloy composition on the H_2 flux of composite Pd-Cu membranes," *Desalination,* vol. 147, pp. 411-416, 2002.

[10] A. G. Knapton, "Palladium alloys for hydrogen diffusion membranes," *Platinum Metals Review,* vol. 21, pp. 44-50, 1977.

[11] G. J. Grashoff, C. E. Pilkington, and C. W. Corti, "The Purification of Hydrogen," *Platinum Metals Review,* vol. 27, pp. 157-169, 1983.

[12] D. L. Mckinley, "Metal alloy for hydrogen separation and purification," United States Patent 3350845 1967.
[13] M. L. Bosko, D. Yepes, S. Irusta, P. Eloy, P. Ruiz, E. A. Lombardo, and L. M. Cornaglia, "Characterization of Pd-Ag membranes after exposure to hydrogen flux at high temperatures," *Journal of Membrane Science,* vol. 306, pp. 56-65, 2007.
[14] M. E. Ayturk and Y. H. Ma, "Electroless Pd and Ag deposition kinetics of the composite Pd and Pd/Ag membranes synthesized from agitated plating baths," *Journal of Membrane Science,* vol. 330, pp. 233-245, 2009.
[15] A. Basile, F. Gallucci, A. Iulianelli, M. De Falco, and S. Liguori, "Hydrogen production by ethanol steam reforming: Experimental study of a Pd-Ag membrane reactor and traditional reactor Behaviour," *International Journal of Chemical Reactor Engineering,* vol. 6, pp. 1-16, 2008.
[16] T.-C. Huang, M.-C. Wei, and H.-I. Chen, "Preparation of palladium-silver alloy composite membranes for hydrogen permeation," *Chemical Engineering Communications,* vol. 189, pp. 1262-1282, 2002.
[17] B. K. R. Nair, J. Choi, and M. P. Harold, "Electroless plating and permeation features of Pd and Pd/Ag hollow fiber composite membranes," *Journal of Membrane Science,* vol. 288, pp. 67-84, 2007.
[18] F. Roa, J. D. Way, R. L. McCormick, and S. N. Paglieri, "Preparation and characterization of Pd-Cu composite membranes for hydrogen separation," *Chemical Engineering Journal,* vol. 93, pp. 11-22, 2003.
[19] F. Gallucci, M. De Falco, S. Tosti, L. Marrelli, and A. Basile, "Co-current and counter-current configurations for ethanol steam reforming in a dense Pd–Ag membrane reactor," *International Journal of Hydrogen Energy,* vol. 33, pp. 6165-6171, 2008.
[20] H. L. Tierney, A. E. Baber, and E. C. H. Sykes, "Atomic-scale imaging and electronic structure determination of catalytic sites on pd/cu near surface alloys," *The Journal of Physical Chemistry C,* vol. 113, pp. 7246-7250, 2009.
[21] H. Gao, J. Y. S. Lin, Y. Li, and B. Zhang, "Electroless plating synthesis, characterization and permeation properties of Pd-Cu membranes supported on ZrO_2 modified porous stainless steel," *Journal of Membrane Science,* vol. 265, pp. 142-152, 2005.
[22] J. Y. Yang, C. Nishimura, and M. Komaki, "Hydrogen permeation of $Pd_{60}Cu_{40}$ alloy covered V-15Ni composite membrane in mixed gases containing H_2S," *Journal of Membrane Science,* vol. 309, pp. 246-250, 2008.
[23] J. Y. Yang, C. Nishimura, and M. Komaki, "Preparation and characterization of Pd-Cu/V-15Ni composite membrane for hydrogen permeation," *Journal of Alloys and Compounds,* vol. 431, pp. 180-184, 2007.
[24] K. H. Muller, "Dependence of thin-film microstructure on deposition rate by means of a computer simulation," *Journal of Applied Physics,* vol. 58, pp. 2573-6, 1985.
[25] R. S. Souleimanova, A. S. Mukasyan, A. Varma, "Pd-composite membranes prepared by electroless plating and osmosis: Synthesis, characterization and properties," *Separation and Purification Technology,* vol. 25, pp. 79-86, 2001.
[26] M. E. Ayturk, I. P. Mardilovich, E. E. Engwall, and Y. H. Ma, "Synthesis of composite Pd-porous stainless steel (PSS) membranes with a Pd/Ag intermetallic diffusion barrier," *Journal of Membrane Science,* vol. 285, pp. 385-394, 2006.

[27] A. Kulprathipanja, G. O. Alptekin, J. L. Falconer, and J. D. Way, "Effects of water gas shift gases on Pd−Cu alloy membrane surface morphology and separation properties," *Industrial & Engineering Chemistry Research,* vol. 43, pp. 4188-4198, 2004.

[28] J. Y. Yang, C. Nishimura, and M. Komaki, "Effect of overlayer composition on hydrogen permeation of Pd-Cu alloy coated V-15Ni composite membrane," *Journal of Membrane Science,* vol. 282, pp. 337-341, 2006.

[29] J. Y. Yang, M. Komaki, and C. Nishimura, "Effect of overlayer thickness on hydrogen permeation of $Pd_{60}Cu_{40}$/V-15Ni composite membranes," *International Journal of Hydrogen Energy,* vol. 32, pp. 1820-1824, 2007.

[30] N. Pomerantz and Y. H. Ma, "Novel method for producing high H_2 permeability Pd membranes with a thin layer of the sulfur tolerant Pd/Cu fcc phase," *Journal of Membrane Science,* vol. 370, pp. 97-108, 2011.

[31] M. E. Ayturk, E. E. Engwall, and Y. H. Ma, "Microstructure Analysis of the Intermetallic Diffusion-Induced Alloy Phases in Composite Pd/Ag/Porous Stainless Steel Membranes," *Industrial & Engineering Chemistry Research,* vol. 46, pp. 4295-4306, 2007.

[32] M. E. Ayturk, I. P. Mardilovich, E. E. Engwall, and Y. H. Ma, "Synthesis of composite Pd-porous stainless steel (PSS) membranes with a Pd/Ag intermetallic diffusion barrier," *Journal of Membrane Science,* vol. 285, pp. 385-394, 2006.

[33] M. E. Ayturk, E. A. Payzant, S. A. Speakman, and Y. H. Ma, "Isothermal nucleation and growth kinetics of Pd/Ag alloy phase via in situ time-resolved high-temperature X-ray diffraction (HTXRD) analysis," *Journal of Membrane Science,* vol. 316, pp. 97-111, 2008.

[34] Y. H. Ma, B. C. Akis, M. E. Ayturk, F. Guazzone, E. E. Engwall, and I. P. Mardilovich, "Characterization of iIntermetallic diffusion barrier and alloy formation for Pd/Cu and Pd/Ag porous stainless steel composite membranes," *Industrial & Engineering Chemistry Research,* vol. 43, pp. 2936-2945, 2004.

[35] W.-H. Lin and H.-F. Chang, "Characterizations of Pd-Ag membrane prepared by sequential electroless deposition," *Surface and Coatings Technology,* vol. 194, pp. 157-166, 2005.

[36] V. Jayaraman and Y. S. Lin, "Synthesis and hydrogen permeation properties of ultrathin palladium-silver alloy membranes," *Journal of Membrane Science,* vol. 104, pp. 251-262, 1995.

[37] B. H. Chen, L. Hong, Y. Ma, T. M. Ko, "Effects of surfactants in an electroless nickel-plating bath on the properties of Ni-P alloy deposits," *Industrial and Engineering Chemistry Research,* vol. 41, pp. 2668-2678, 2002.

[38] R. S. Souleimanova, A. S. Mukasyan, and A. Varma, "Effects of osmosis on microstructure of Pd-composite membranes synthesized by electroless plating technique," *Journal of Membrane Science,* vol. 166, pp. 249-257, 2000.

[39] S. Ilias and M. A. Islam, "Methods of preparing thin films by electroless plating," United States Patent, 2010.

[40] M. A. Islam and S. Ilias, "Characterization of Pd-composite membrane fabricated by surfactant induced electroless plating (SIEP): Effect of grain size on hydrogen permeability," *Separation Science and Technology,* vol. 45, pp. 1886-1893, 2010.

[41] T.-C. Huang, M.-C. Wei, and H.-I. Chen, "Preparation of hydrogen-permselective palladium-silver alloy composite membranes by electroless co-deposition," *Separation and Purification Technology*, vol. 32, pp. 239-245, 2003.
[42] S. Adhikari and S. Fernando, "Hydrogen Membrane Separation Techniques," *Industrial & Engineering Chemistry Research*, vol. 45, pp. 875-881, 2006/02/01 2006.
[43] Y. S. Cheng and K. L. Yeung, "Effects of electroless plating chemistry on the synthesis of palladium membranes," *Journal of Membrane Science*, vol. 182, pp. 195-203, 2001.
[44] Y. S. Cheng and K. L. Yeung, "Palladium–silver composite membranes by electroless plating technique," *Journal of Membrane Science*, vol. 158, pp. 127-141, 1999.
[45] G. Orhan, S. Gurmen, and S. Timur, "The behavior of organic components in copper recovery from electroless plating bath effluents using 3D electrode systems," *Journal of Hazardous Materials*, vol. 112, pp. 261-267, 2004.
[46] M. M. Rahman, "Fabrication of Pd and Pd-Ag membranes by surfactant induced electroless plating (SIEP)," MS Thesis, Chemical and Bioengineering, North Carolina A & T State University, Greensboro, NC, 2010.
[47] M. A. Islam, "The development of improved electroless plating in fabricating Pd-based membrane and membrane reactor application for hydrogen separation," PhD Dissertation, Energy and Environmental Studies, North Carolina A & T State University, Greensboro, NC, 2008.
[48] M. S. Islam, "Fabrication of Pd-Cu membranes by surfactant induced electroless plating (SIEP)," MS Thesis, North Carolina A&T State University, Greensboro, NC, , 2011.
[49] M. S. Islam, "Fabrication of Pd-Cu Membranes by Surfactant Induced Electroless Plating (SIEP)," MS Thesis, Chemical and Bioengineering, North Carolina A&T State University, Greensboro, 2011.
[50] J. Okazaki, T. Ikeda, D. P. Tanaka, K. Sato, T. M. Suzuki, and F. Mizukami, "An investigation of thermal stability of thin palladium–silver alloy membranes for high temperature hydrogen separation," *Journal of Membrane Science*, vol. 366, pp. 212-219, 2011.
[51] F. C. Gielens, H. D. Tong, M. A. G. Vorstman, and J. T. F. Keurentjes, "Measurement and modeling of hydrogen transport through high-flux Pd membranes," *Journal of Membrane Science*, vol. 289, pp. 15-25, 2007.
[52] J. P. Collins and J. D. Way, "Preparation and characterization of a composite palladium-ceramic membrane," *Industrial & Engineering Chemistry Research*, vol. 32, pp. 3006-3013, 1993.
[53] S. Uemiya, N. Sato, H. Ando, Y. Kude, T. Matsuda, and E. Kikuchi, "Separation of hydrogen through palladium thin film supported on a porous glass tube," *Journal of Membrane Science*, vol. 56, pp. 303-313, 1991.
[54] A. Caravella, G. Barbieri, and E. Drioli, "Modelling and simulation of hydrogen permeation through supported Pd-alloy membranes with a multicomponent approach," *Chemical Engineering Science*, vol. 63, pp. 2149-2160, 2008.
[55] J. Okazaki, T. Ikeda, D. A. Pacheco Tanaka, T. M. Suzuki, and F. Mizukami, "In situ high-temperature X-ray diffraction study of thin palladium/α-alumina composite membranes and their hydrogen permeation properties," *Journal of Membrane Science*, vol. 335, pp. 126-132, 2009.

[56] A. Caravella, F. Scura, G. Barbieri, and E. Drioli, "Sieverts law empirical exponent for Pd-based membranes: critical analysis in pure H_2 permeation," *J Phys Chem B,* vol. 114, pp. 6033-47, May 13 2010.

[57] J. Y. Yang, M. Komaki, and C. Nishimura, "Effect of overlayer thickness on hydrogen permeation of Pd60Cu40/V–15NiPd60Cu40/V–15Ni composite membranes," *International Journal of Hydrogen Energy,* vol. 32, pp. 1820-1824, 2007.

[58] C. C. Koch, *Nanostructured materials processing, properties and potential applications*: Willian Andrew publishing, 2006.

[59] S. Manne and H. E. Gaub, "Molecular Organization of Surfactants at Solid-Liquid Interfaces," *Science,* vol. 270, pp. 1480-1482, 1995.

[60] P. P. Mardilovich, Y. She, Y. H. Ma, and M.-H. Rei, "Defect-free palladium membranes on porous stainless-steel support," *AIChE Journal,* vol. 44, pp. 310-322, 1998.

[61] M. A. Islam, "The development of improved electroless plating in fabricating Pd-based membrane and membrane reactor application for hydrogen seperation " Ph.D Ph.D Thesis, Chemical and bioengineering, North Carolina A&T State University, Greensboro, NC, 2008.

[62] M. E. Ayturk, E. E. Engwall, and Y. H. Ma, "Microstructure analysis of the intermetallic diffusion-induced alloy phases in composite Pd/Ag/porous stainless steel membranes," *Industrial and Engineering Chemistry Research,* vol. 46, pp. 4295-4306, 2007.

[63] W.-H. Lin and H.-F. Chang, "AFM, EDS and XRD microstructural characterizations of Pd-Ag/PSS membranes," *Journal of the Chinese Institute of Chemical Engineers,* vol. 37, pp. 239-247, 2006.